TECHNICAL NOTES

NATIONAL ADVISORY COMMITTEE FOR AERONAUTICS

No. 909

SOME INVESTIGATIONS OF THE GENERAL INSTABILITY OF STIFFENED METAL CYLINDERS

V - STIFFENED METAL CYLINDERS SUBJECTED TO PURE BENDING

Guggenheim Aeronautical Laboratory
California Institute of Technology

Washington
August 1943

NATIONAL ADVISORY COMMITTEE FOR AERONAUTICS

TECHNICAL NOTE NO. 909

SOME INVESTIGATIONS OF THE GENERAL INSTABILITY OF STIFFENED METAL CYLINDERS

V - STIFFENED METAL CYLINDERS SUBJECTED TO PURE BENDING

Guggenheim Aeronautical Laboratory
California Institute of Technology

This is the fifth of a series of reports covering an investigation of the general instability problem by the California Institute of Technology. The first five reports of this series cover investigations of the general instability problem under the loading conditions of pure bending and were prepared under the sponsorship of the Civil Aeronautics Administration. The succeeding reports of this series cover the work done on other loading conditions under the sponsorship of the National Advisory Committee for Aeronautics.

SUMMARY

This report summarizes the work that has been carried on in the experimental investigation of the problem of general instability of stiffened metal cylinders subjected to pure bending at the C.I.T. This part of the investigation included tests of 46 sheet-covered specimens. The most significant result was the determination of a new design parameter for the case of a stiffened metal cylinder subjected to pure bending.

INTRODUCTION

It is intended to give in this report a summary of the results of the experimental investigation of the general instability of stiffened metal cylinders sub-

jected to pure bending. The earlier work at C.I.T. on the problem of general instability of stiffened metal cylinders has been reported in references 1, 2, 3, and 4. A total of 46 sheet-covered specimens has been tested.

The investigation was planned so as to include most of the essential variables involved in the problem and was sufficient in scope to determine a suitable design parameter. Although this parameter was obtained for specimens subjected to pure bending, it is felt that it may be possible through suitable modifications to use the same parameter for combined loadings. The experimental data are also sufficient to allow a thorough check on theoretical methods for predicting general instability. A comparison of the predicted and experimental results is, therefore, included in this report.

In addition to the above results, an account is also given of the experimental studies which have been made to give a better understanding of the mechanism involved in the buckling phenomena of stiffened cylinders. The body of this report, therefore, consists of four parts; namely,

(a) Experimental investigations on the failure of metal cylinders

(b) A comparison between theoretical predicted general instability stresses and the experimental results

(c) A discussion of the mechanism involved in the buckling phenomena of stiffened cylinders

(d) A new design parameter

EXPERIMENTAL INVESTIGATION

In starting this research program, it was felt that a complete study of the pure bending phenomena would form a desirable background for the more complicated problem of bending plus shear and for the more general combined loading conditions. With this idea in mind, the research to date has been confined to a systematic investigation of cylinders subjected to pure bending.

To obtain a better understanding of the amount of

experimental research work which can now be considered as completed, it might be well to briefly review the variables involved in the problem of general instability. The variables involved may be divided into two classes - those dealing with the geometry of the structure and those involving the sectional properties of the stiffening elements as well as the sheet covering.

The geometrical variables involve:

(a) a variation of longitudinal spacing

(b) a variation of frame spacing

(c) a variation in diameter

(d) a variation in length

The second group of variables involves:

(a) a change in the section properties of the longitudinals

(b) a change in the section properties of the frames

(c) a change in the thickness of the sheet covering

The first group of variables has been thoroughly investigated inasmuch as a large number of specimens having 2.53-, 5.06-, and 10.12-inch longitudinal spacings, and 1-, 2-, 4-, 8-, and 16-inch frame spacings have been tested. Although the second group of variables is not yet completed, a sufficient number of the variables have been investigated to form a basis for the analysis of general instability. Three different frame sizes have been investigated; that is, frames F_1, F_5, and F_6 (fig. 1), and also two different sheet thicknesses, 0.010- and 0.016-inch have been used. Six specimens having a 20-inch diameter have been tested; all other specimens are 32 inches in diameter. Of the former, two had an L/D ratio of 2.6, while in all other cases the L/D ratio was 2.0. The longitudinals have not been varied. However, by varying the sheet thickness, a certain variation in the section properties of the longitudinals is obtained, since a certain effective width of sheet which varies with the sheet thickness is assumed to act with each longitudinal.

These variables which have been investigated have been

found sufficient to establish a suitable design parameter for structures subjected to pure bending. Hence, if we confine ourselves to the pure-bending phase of the investigation, it is felt that future work will only involve a number of check specimens in which the longitudinal section properties are varied. Also, an additional number of specimens should be tested to further investigate the influence of local instability of the frames. A few additional specimens will be tested to further check the length effect.

A complete list containing all the necessary data of the sheet-covered specimens which have been tested to date is given in table I. It should be noted that the maximum unit compressive deformation σ/E' at failure is tabulated rather than the compressive stress, where σ is the compressive stress and E' is the effective modulus - the reason being that in many cases the compressive stress at buckling exceeds the yield point of the material, and the difficulty involved in determining the basic stress in such cases makes it desirable to use the unit strain rather than stress. The nondimensional quantity σ/E' is also more desirable from the standpoint of determining a nondimensional design parameter.

The method of measuring the unit strain at failure was discussed in reference 4 and needs no further discussion. It might be of interest, however, to point out that the accuracy of the method is somewhat dependent on the type of failure. Until local bending occurs the method is quite accurate; but if bowing between frames takes place, then the test data must be corrected for bending and, consequently, are subject to the inaccuracies of such calculations. General instability failure usually occurs by a sudden collapse of the structure, whereas in panel instability the failure in most cases is gradual; that is, the applied bending moment will increase after buckling of the longitudinals between frames occurs. Also, as discussed in reference 4, the sheet will reinforce the longitudinals after the amplitude of the longitudinals becomes sufficiently large - thereby causing a higher and less clearly defined ultimate load. It is therefore much more difficult to determine the ultimate load as well as the longitudinal deformation of specimens which fail by panel instability.

Figures 2 to 26 indicate the unit longitudinal deformation as a function of the applied bending moment for

the sheet-covered specimens. All specimens failed either by panel or general instability with the exception of specimen 62, which failed in tension. Failure of this specimen was precipitated by a bearing failure of the sheet at the joint, thus causing the entire tension load to be carried by the longitudinals.

It was pointed out in reference 4 that no correlation could be obtained between the sheet-covered specimens and the wire-braced specimens previously tested. Hence, data pertaining to the wire-braced specimens have not been included in this report.

A number of photographs (figs. 43 to 48) showing the various types of failure are included.

THEORETICALLY PREDICTED GENERAL INSTABILITY STRESS

A detailed discussion of the analytical methods which are available for calculating the general instability stress of stiffened cylinders is given in reference 1. As pointed out, the available experimental data were too meager to indicate whether any of the methods could be satisfactorily used for the prediction of general instability. Sufficient experimental data are now available to determine the merits of each of the methods by comparing the predicted general instability stress with the experimental values. Each method will be discussed separately.

Hoff's Method

The general instability stress is given by the equation

$$\sigma = \frac{\pi^2 E_x I_x}{A_x (\lambda d)^2} \qquad (1)$$

where

E_x Young's modulus of elasticity, pounds per square inch

I_x moment of inertia of a longitudinal plus an effective width of sheet (See section on A New Design Parameter, for effective width calculations.)

A_x cross-sectional area of a longitudinal

d frame spacing

The nondimensional quantity λ is a function of the structural coefficient Λ and the number of frames m involved in the failure. The relation between λ and Λ for constant values of m is shown in reference 2. It is seen that, for a constant value of Λ, the value of λ increases as the number of frames involved per wave length increases. This increase in λ produces, according to equation (1), a decrease in the general instability stress. In applying Hoff's method to a practical design problem, it would be necessary to consider the largest number of frames which could possibly fail, hence give the lowest possible stress. However, in making the comparison between the unit deformation σ/E', as calculated by equation (1), and the test value, the actual number of frames which failed was used. A comparison of the experimental and calculated values for a large number of specimens is shown in table II. The calculated values range from 11 to 83 percent of the experimental values. If the total number of frames in the test specimen were to be used in the calculations, the calculated values would be lower. It may therefore be concluded that, although in all cases Hoff's method does predict general instability, the method is too conservative for design purposes.

Dschou's Method

Dschou obtained for the minimum general instability stress an equation of the form

$$\sigma = \frac{2E}{R t_x} \sqrt{\frac{I_x I_y}{\frac{I_x}{t_x} + \frac{I_y t_y}{t\, t_x}}} \qquad (2)$$

which can be written as

$$\frac{\sigma}{E} = \frac{2}{R} \sqrt{\frac{\rho_x^2 \rho_y^2 \frac{t_y}{t_x}}{\rho_x^2 + \rho_y^2 \frac{t_x}{t}}} \qquad (3)$$

where

ρ_x radius of gyration of a longitudinal together with the corresponding portion of the sheet covering

ρ_y same quantity for the circumferential frames

$t_x = t + \frac{A_x}{b}$, equivalent shell thickness in the axial direction

$t_y = t + \frac{A_y}{d}$, equivalent shell thickness in the circumferential direction

t sheet thickness

A_x area of a longitudinal

A_y frame area

The same equation is reproduced in Timoshenko's theory of elastic stability (reference 6).

It is not definitely stated by either Dschou or Timoshenko whether, in calculating I_x, I_y or, similarly, ρ_x, ρ_y, the total width of sheet between longitudinals and frames should be used or an effective width of sheet. Calculations have been made, using first the total width of sheet between longitudinals and frames and then using an equal effective width of sheet with the longitudinals and frames. The effective width calculations are discussed later in this report. The results of these calculations are shown in figures 27 and 28. The calculated values in all cases are considerably higher than the experimental values. It is also evident that the expression

$$\frac{2}{R}\sqrt{\frac{\rho_x^2 \rho_y^2 \frac{t_y}{t_x}}{\rho_x^2+\rho_y^2 \frac{t_x}{t}}} \qquad (4)$$

is not suitable as a parameter, since the scatter of the experimental points is much larger than can be contributed to experimental inaccuracies.

Ryder's Method

The application of this method requires the calculation of three parameters, K_2, K_3, and K_4, depending on the geometry of the structure and on the section properties. Curves of K_2 and K_3 are not available for values of $K_4 < 0.20$; hence, in all cases where K_4 was less than 0.19, it was felt that the curves in which $K_4 = 0.20$ would no longer be valid, and these specimens were therefore not considered. The results of the calculations are shown in table III, where σ_{B_CR} are the calculated general instability stresses. The ratios of the calculated to the experimental values are also shown. The experimental stress in this case is not a true stress but an equivalent stress which is obtained from the measured unit deformation at failure under the assumption that the modulus of elasticity remains constant beyond the proportional limit of the material. The results indicate, with the exception of three specimens, that the calculated values are all considerably higher than the experimental values. It should be pointed out, however, that in practically all cases the value of K_2 is less than 0.2, which makes it extremely difficult to obtain the value of t_e/ρ_s from the curves since in this range the value of t_e/ρ_s is very sensitive to a small change in K_2.

Taylor's Method

The general instability stress was calculated for a number of specimens and is shown in table IV. The calculated stresses are of the order of five to twelve times higher than the experimental values. The given calculated values are from Taylor's approximate equation. It was found that the exact equation gave values only slightly different (approx. 2 percent) from that of the approximate equation, and the simplicity of the latter makes it preferable for calculations.

A STUDY OF BUCKLING PHENOMENA OF STIFFENED CYLINDERS

In the course of the experimental investigation, it was observed that in all cases of general instability the last specimens showed a definite preference for failing

radially inward. Also in measuring the "normal restraint coefficient," it was observed that the radial deflection was a nonlinear function of the applied load. (See fig. 32.) Furthermore, if the load is applied radially outward, the slope of the load-deflection curve increases, while for a load applied radially inward the slope decreases. This simply means that the structure has greater rigidity in the outward direction than in the inward direction.

Considering the stiffened cylinder as a whole, it is immediately evident that it is anisotropic and the influence of one member upon the other is extremely difficult to determine. The most elementary concept of the problem would be that of a column supported by continuous and concentrated elastic supports - a longitudinal stiffener being the column, the sheet covering providing the continuous elastic support, and the frames the concentrated elastic support.

The problem of a column elastically supported has been discussed by H. Zimmerman for the case of concentrated supports, and by F. Engesser and others for the case of a distributed support. In all cases the investigations have been confined to elastic supports exhibiting a linear force-deflection relation.

Since the frames and the sheet have the characteristics of a nonlinear elastic support, it was felt that it would be of general interest to investigate the effect on the load-deflection relation of a column supported by a nonlinear elastic element. Inasmuch as rings or frames are known to have the desired nonlinear properties, a thin semicircular steel ring, as shown in figure 43, was used as the elastic support. For simplicity, columns having a simple, rather than a distributed, support were tested. It may be of some interest to consider first the elastic behavior of a semicircular ring. Designating the radial load by P, and the corresponding radial deflection by δ, the curves of figure 29 indicate that if the load is applied radially inward, the value of P/δ, the elastic constant, decreases with increasing deflection. When the load is directed radially outward, the value of P/δ increases with increasing deflection. Obviously, then, if an initially straight column is supported by such an element, or elements, it may be expected that it would have a tendency to buckle in the direction of decreasing P/δ or, if due to an initial deformation in the direction of

increasing P/δ the buckling starts in that direction, then at some deflection a sudden "jump" may occur in the direction of decreasing P/δ.

Tests were conducted on columns 0.090 inch thick by 0.375 inch wide and 19 inches long. These columns were cut from 24S-RT alclad sheet stock. The steel ring was in all cases 8 inches in diameter and 0.008 inch thick. The test apparatus and method of testing are illustrated in figure 43.

The results of these tests are indicated in figure 30, where the ratio of the column load to the Euler load is plotted as a function of the ratio of the normal deflection δ at the center of the column to the column length l.

Considering the results of figure 30, it is seen that the elastic support increases the buckling load of the "straight" column (upper curve) to nearly 3.5 times the Euler load. This load is reached at a relatively small deflection. As the deflection δ increases, the decrease in load is at first quite rapid, then more gradual as the deflection becomes larger, and may approach a minimum at large deflections. It was not possible to reach very large deflections because of plastic failure of both the rings and the columns. The lower curves in the same figure indicate the effect of initial deflections in which the column was rolled to approximately the form of a half-sine-wave, the maximum initial deflection being designated by δ_o. These curves show that, with increasing initial deflection, the maximum load decreases and occurs at increasingly larger deflections. In all cases the load sustained by the column tends to approach at large deflections the "minimum load" of the straight column. Thus, in case of a nonlinear support, any initial imperfections of the specimen will appreciably lower its buckling load. To illustrate the contrast between the column with a nonlinear elastic support and one with a linear elastic support (a coiled spring), a number of tests were conducted on the same type of column. As may be seen from the curves of figure 31, the columns with an initial deflection in all cases approach the maximum load of the straight column.

The most striking features of the column supported by a nonlinear elastic element are: first, as the deflection increases the load decreases; secondly, there are two or

more possible configurations of equilibrium for the same load; one corresponds to $\delta = 0$, the others to $\delta > 0$.

Since the longitudinal members in a stiffened cylinder will behave in a manner similar to the column with a nonlinear elastic support (fig. 32), the buckling characteristics of a stiffened cylinder must be similar to those of the nonlinearly supported column. Therefore, any theory which is based on the assumption of small deflections will probably give a much higher load than that actually observed, since in a test specimen initial imperfections will prevent the specimen from reaching the maximum load, and will cause it to fail at some lower load depending on the degree of imperfection present in the specimen. This expectation is verified by the comparison between the experimentally observed stresses and the predicted stresses as obtained from the theories developed by Taylor, Dschou, and Ryder, which are essentially based on small deflections and linear restraints.

A theory based on large deflections would be extremely difficult because of the nonlinear load-deflection relationship discussed in this section. This difficulty makes it desirable to attack the problem by experimental methods which would lead to the development of a suitable design parameter.

A NEW DESIGN PARAMETER

The buckling phenomena of stiffened cylinders and the attending difficulties of a theoretical solution have been discussed in the previous section. It was hoped, however, that it would be possible to obtain a design parameter which would determine the critical value of σ/E' with a satisfactory accuracy for design purposes.

With this thought in mind, a number of specimens in which only the geometry of the structure was varied were first tested. The results of these tests are shown in figure 33, where the unit strain σ/E' is plotted as a function of the longitudinal spacing b for constant values of d/b - referred to as the reinforcement aspect ratio. The curve corresponding to an aspect ratio of 1.58 was considered as the master curve and the remaining curves are an expansion of this curve; hence they fit best by changing the horizontal scale.

A log-log plot of the expansion factor as a function of d/b indicated that this factor varied approximately as $\sqrt{d/b}$. In fact, plotting the unit strain σ/E' as a function of $\sqrt{bd}$, a single curve, as indicated in figure 34, is obtained. A log-log plot of the unit strain σ/E' as a function of $\sqrt{bd}$ showed that E'/σ varied approximately as $\sqrt[4]{bd}$. This, then, gives the influence of the geometrical variables on the general instability failure.

The next question is: In what manner does the radius R and the section parameters ρ_x and ρ_y enter into the design parameter sought? By analogy - with the buckling of unstiffened cylinders - it can be expected that, for identical values of b, d, ρ_x, and ρ_y the reciprocal of the critical value of the unit strain varies linearly with R. This surmise was checked by testing specimens with two different radii (R = 16 in. and 10 in.) and was found to be correct. Hence, it was concluded from these results that the design parameter has the form

$$\frac{\sqrt[4]{bd}\,R}{f(\rho_x,\rho_y)}$$

From dimensional reasoning, it follows that the function $f(\rho_x,\rho_y)$ must have the dimension of the 3/2 power of a length. The simplest assumption for the function which determines the influence of the section parameters, ρ_x and ρ_y, is that it depends on the geometrical mean value $\sqrt{\rho_x\,\rho_y}$ only. It was found that, in the range covered by the experiments and by the use of reasonable methods for the calculation of the effective width of the sheet, this assumption appears justified. Thus the design parameter appears in the form

$$\frac{\sqrt[4]{bd}}{(\rho_x\,\rho_y)^{3/4}} \quad \text{or} \quad \sqrt{\frac{\sqrt[4]{bd}}{\rho_x\,\rho_y}}\,\frac{R}{\sqrt{\rho_x\,\rho_y}}$$

Concerning the width of sheet to be used with the longitudinals and frames, Hoff (reference 7) and Cox (reference 5) have pointed out that the effective width for stability is not the same as that based on the load-carrying ability of the sheet. In fact, Cox states that the effective width associated with buckling phenomena is proportional to the rate of increase of the apparent stress to the rate of increase of the actual stress, rather than to the chord value as illustrated in figure 3 (reference 5). Assuming that Marquerre's effective width equation

$$\frac{2w_e}{b} = \sqrt[3]{\frac{\sigma_c}{\sigma_{st}}}$$

is sufficiently accurate for our purpose, then the apparent stress σ_a is given by the equation

$$\sigma_a = \frac{w_e}{b}\sigma_{st} = \sigma_{st}\sqrt[3]{\frac{\sigma_c}{\sigma_{st}}}$$

where

σ_{st} longitudinal stress, pounds per square inch (= edge stress)

σ_c buckling stress of the sheet, pounds per square inch

The effective width for stability is then

$$\frac{2w_e}{b} = \frac{d\sigma_a}{d\sigma_{st}} = \frac{2}{3}\sqrt[3]{\frac{\sigma_c}{\sigma_{st}}}$$

In all calculations involving the effective width of sheet acting with the longitudinals, this value has been used with the exception of the calculations involving Ryder's work, since in his work the effective width is definitely specified.

The amount of sheet acting with the frames is difficult to evaluate by analytical means; trial calculations indicated that the best results were obtained when the total width of sheet between frames was used. For this reason, ρ_y was calculated assuming the entire width of sheet to be effective. The variation of I_x, I_y, ρ_x, and ρ_y as a function of the effective width is shown in

figures 38 to 41, where I_o and ρ_o is the moment of inertia and the radius of gyration of the member alone.

In some cases a further correction, which is discussed in the appendix, is to be applied to the radius of gyration.

The unit strain σ/E' at failure (general instability), plotted as a function of $\frac{R}{\sqrt{\rho_y \rho_x}} \sqrt[4]{\frac{bd}{\rho_y \rho_x}}$, is shown in figure 35; this curve is not very convenient for design purposes as the slope of the curve becomes too steep for high values of σ/E'. A more desirable presentation is to plot σ/E' as a function of $\frac{\sqrt{\rho_x \rho_y}}{R} \sqrt[4]{\frac{\rho_x \rho_y}{bd}}$. The results are indicated in figure 36. As may be seen, the experimental values lie close to a straight line with the exception of three points. Two of these points correspond to tests on the channel section frame. As these frames failed by local instability of the outstanding legs (see fig. 44), it may be expected that the results would be low for the channel does not develop the strength corresponding to the calculated value of ρ_y. This can be illustrated by considering the behavior of an open-section column subjected to an axial thrust. The critical column stress is given by the equation

$$\sigma_E = \frac{k \pi^2 E \rho^2}{l^2}$$

If the critical column stress is higher than the local instability stress, the column will fail at the lower stress. This essentially means that an effective value of ρ can be obtained corresponding to this lower stress, that is,

$$\frac{\rho_{eff}}{\rho} = \sqrt{\frac{\sigma_{failure}}{\sigma_E}}$$

It seems reasonable to assume that the frame behaves in a similar manner and that the effective radius of gyration is lower, due to the local instability failure.

This new design parameter, $\frac{R}{\sqrt{\rho_x \rho_y}} \sqrt[4]{\frac{bd}{\rho_x \rho_y}}$, is the

ratio between the radius and a quantity having the dimensions of a length defined by $\sqrt{\rho_x \rho_y} \sqrt[4]{\frac{\rho_x \rho_y}{bd}}$. Hence, it appears that this length is proportional, to some extent, to an equivalent thickness of the reinforced cylindrical structure.

The failing stress of an unstiffened cylindrical shell of radius R is given by

$$\frac{\sigma}{E'} = k \frac{t}{R} \tag{5}$$

where t is the thickness of the shell and k is an empirically determined constant. Replacing the thickness t by the radius of gyration ρ of a strip of the shell of unit width, equation (5) can be written in the form

$$\frac{\sigma}{E'} = k \frac{\sqrt{12}\,\rho}{R} \tag{6}$$

For purposes of comparison, the failing stress of the reinforced cylinders investigated can be expressed as a function of the new parameter in the form

$$\frac{\sigma}{E'} = k' \frac{\sqrt{12}\sqrt{\rho_x \rho_y}\sqrt[4]{\frac{\rho_x \rho_y}{bd}}}{R} \tag{7}$$

where k' is a numerical constant. Figure 36 shows that equation (7) covers, with a fair approximation, the cases in which general instability occurred.

By introducing the geometrical mean value $\sqrt{\rho_x \rho_y}$, it can be assumed that the influence of the anisotropy of the structure is approximately taken into account. Then, by comparison of equations (6) and (7), an effective radius of gyration can be defined as

$$\rho_e = \frac{k'}{k} \sqrt[4]{\frac{\rho_x \rho_y}{bd}} \sqrt{\rho_x \rho_y} = \varphi \sqrt{\rho_x \rho_y} \tag{8}$$

where $\varphi = \frac{k'}{k} \sqrt[4]{\frac{\rho_x \rho_y}{bd}}$ can be considered as a correction

factor to the ratio $\frac{\sqrt{\rho_x \rho_y}}{R}$. Now $\frac{d}{\rho_x}$ is the slenderness ratio of the longitudinal, taken as a column between two frames and, similarly, $\frac{b}{\rho_y}$ is the slenderness ratio of the frame taken as a column between two longitudinals. If the geometrical mean value of these two slenderness ratios is defined by λ, that is,

$$\lambda = \sqrt{\frac{bd}{\rho_x \rho_y}} \tag{9}$$

then the correction factor can be expressed as

$$\varphi = \frac{k' \quad 1}{k \sqrt{\lambda}} \tag{10}$$

It is evident that if the stiffened shell were to be considered as an equivalent shell, in which all the materials are uniformly distributed, then the only appropriate parameter to be used is $\frac{\sqrt{\rho_x \rho_y}}{R}$. The appropriate parameters which enter into the problem of buckling of a truss are the slenderness ratios which appear in the quantity $\lambda = \sqrt{\frac{bd}{\rho_x \rho_y}}$. The fact that the empirically derived relation given here involves both parameters, $\frac{\sqrt{\rho_x \rho_y}}{R}$ and λ, indicates that a stiffened cylinder cannot be treated either as an equivalent cylinder of uniform thickness or as a cylindrical truss. Therefore, the work of Dschou, Taylor, and Timoshenko, which is based upon the concept of an equivalent uniform shell, cannot be expected to give correctly the general instability stress of stiffened cylinders. The error is particularly large if the flexural rigidity is concentrated in frames of large cross-sectional area.

It is of interest to calculate the numerical value of the factor φ, using for k' the values obtained from the experiments of this report, and for k the value $k = 0.3$, which is a reasonable average value for unstiffened shells in the range of σ/E involved. The values of

$\sqrt[4]{\frac{\rho_x \rho_y}{bd}}$ vary from 0.0598 to 0.219, as shown in table V; the average slenderness ratio λ varies from 280 to 21. The values of φ corresponding to these limiting cases are $\varphi = 0.254$ and $\varphi = 0.932$. The lower limit is obtained for a structure (specimen 34) with a 10.12-inch longitudinal, a 16-inch frame spacing, and an average slenderness ratio of 280. The upper limit refers to specimen 55 with a 2.53-inch longitudinal, a 2-inch frame spacing, and an average slenderness ratio of 21.

It is seen that for structures in which the stiffening elements are widely spaced, it is necessary that a multiplying factor much smaller than unity be applied to the quantity $\sqrt{\rho_x \rho_y}$. In the case of close spacings the factor is of the order of 1.

It is realized that this discussion does not represent a complete theory of the buckling of reinforced cylindrical shells subjected to pure bending. In particular, it cannot be expected that the use of geometrical mean values will take care of the anisotropy of the structure with sufficient accuracy in all extreme cases; for example, if the cylinder is stiffened in only one direction. It is hoped, however, that the relation developed in this report will cover most of the structures occurring in practical design.

The practical application of the design parameter is relatively simple. Since the designer will have the necessary data to compute the numerical value of the parameter, the general instability stress can be immediately obtained from the curve of figure 37. In view of the fact that general instability causes a complete collapse of the structure, it is recommended that allowance be made for ample margins, and in no case should the allowable stress exceed the boundary line indicated in figure 37. As previously stated, when the frames fail by local instability the general instability stress is considerably lower than that defined by the curve of figure 37. Hence, until further data are obtained on this type of failure, the curve of figure 37 should be used with caution when local instability of the frames is likely to occur.

If a reinforced cylinder fails by panel instability, the buckling stress should in all cases be lower than the

stress necessary to cause a general instability failure. This is obvious since, in order that panel instability may occur, it is necessary that the frame be sufficiently rigid to maintain closely the shape of the structure at the frame. If the frame is not sufficiently rigid it will fail before the panel instability stress is reached and result in a general instability type of failure. A number of the test specimens failed by panel instability. The unit strain at buckling is shown in figure 37 and, as pointed out, these values should and do lie below the curve defining general instability.

Guggenheim Aeronautical Laboratory,
California Institute of Technology,
Pasadena, Calif., July 1940.

APPENDIX

CORRECTION FOR THE EFFECT OF THE TORSIONAL RIGIDITY OF FRAMES ON THE STRENGTH OF CYLINDERS

Owing to the particular method of attaching the stiffeners to the frames, it is felt that the torsional rigidity of the frames acts as an additional restraint in the bending of the stiffeners. This effect will be appreciable if a frame such as F_6, which has a large torsional rigidity, is used. It is therefore necessary to correct for this effective increase in rigidity. A physical reasoning immediately leads to the following expression for the effective moment of inertia of the stiffeners:

$$I_{s_{eff}} = I_s + k\,C \qquad (1)$$

where

$I_{s_{eff}}$ effective moment of inertia of the stiffener, in.^{4}

I_s moment of inertia of the stiffener with effective width of sheet, in.^{4}

C torsional rigidity of the frame divided by the shear modulus of the material, in.^{4}

k a nondimensional factor which gives the effectiveness of the frames in supporting the stiffeners in bending

The following analysis is an attempt to estimate this nondimensional factor k. Consider a wave of the buckled shell, as shown in figure a.

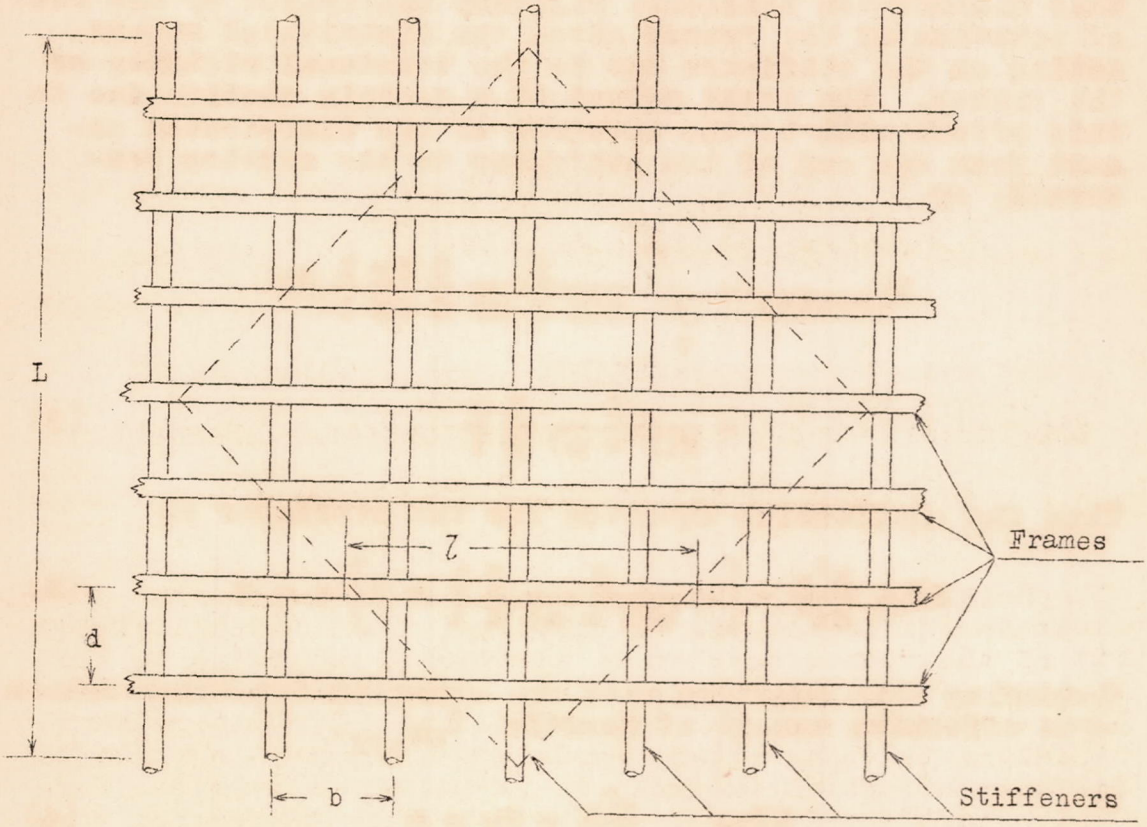

Figure a.

At the boundary of the wave the frames are not twisted by the bending of the stiffeners. At the joint with the stiffener the frames are rotated an angular amount equal to the slope of the deflection curve of the stiffener. If w is the deflection of the middle stiffener, then this angle is $\frac{dw}{dx}$ at the joint with this stiffener. As a rough estimate, let the rate of rotation of the frame be $\frac{dw}{dx}/l$ where l is the average buckled wave length of the frames.

The torsional rigidity of the frame is CG where G is the shear modulus, or $G = \frac{E}{2(1 + \mu)}$. In order to simplify the calculation, this amount of torsional rigidity is assumed to be distributed within the frame spacing d. Thus the distributed torsional rigidity is $\frac{E}{2(1+\mu)} \frac{C}{d}$. This distributed torsional rigidity multiplied by the rate of rotation of the frames gives the distributed moment acting on the stiffener due to the torsional rigidity of the frames. The total moment at a certain section due to this effect will be the integral of the distributed moment from one end of the stiffener to the section concerned; or

$$M_{torsion} = \int_0^x \frac{E}{2(1 + \mu)} \frac{C}{d} \frac{dw}{dx} \frac{1}{l} dx$$

$$= \frac{E}{2(1 + \mu)} \frac{C}{d} \frac{w}{l} \tag{2}$$

Thus the equilibrium equation for the stiffener is

$$EI_{st} \frac{d^2w}{dx^2} + \left[- \frac{E}{2(1 + \mu)} \frac{C}{d} \frac{1}{l} + P \right] w = 0 \tag{3}$$

Comparing this equation with the equation for Euler column with effective moment of inertia $I_{st_{eff}}$,

$$EI_{st_{eff}} \frac{d^2w}{dx^2} + Pw = 0 \tag{4}$$

we have

$$\frac{P}{EI_{st_{eff}}} = \frac{P}{EI_{st}} - \frac{1}{2(1 + \mu)} \frac{C}{I_{st}} \frac{1}{dl} = \frac{\pi^2}{L^2}$$

where L is the wave length of the buckle; or

$$\frac{\pi^2}{L^2} = \frac{\pi^2}{L^2} \frac{I_{st_{eff}}}{I_{st}} - \frac{1}{2(1 + \mu)} \frac{C}{I_{st}} \frac{1}{dl}$$

that is,

$$\frac{I_{st_{eff}}}{I_{st}} = 1 + \frac{1}{2(1 + \mu)\pi^2} \frac{L^2}{dl} \frac{C}{I_{st}}$$

therefore

$$I_{st_{eff}} = I_{st} + \left[\frac{1}{2\pi^2(1 + \mu)} \frac{L^2}{dl}\right] C \qquad (5)$$

Comparing this equation with equation (1), the value of the interaction factor k can be obtained as

$$k = \frac{1}{2\pi^2(1 + \mu)} \frac{L^2}{dl} \qquad (6)$$

Using the values of l and L from experimental data, it is possible to estimate the value of this factor which is found to be of the order of 1. For the majority of the frames, the value of I_{st} is much larger than C with the exception of frame F_6. Hence, the correction was only applied to the test specimens in which frame F_6 was used.

REFERENCES

1. Guggenheim Aeronautical Laboratory, California Institute of Technology: Some Investigations of the General Instability of Stiffened Metal Cylinders. I - Review of Theory and Bibliography. T.N. No. 905, NACA, 1943.

2. Guggenheim Aeronautical Laboratory, California Institute of Technology: Some Investigations of the General Instability of Stiffened Metal Cylinders. II - Preliminary Tests of Wire-Braced Specimens and Theoretical Studies. T.N. No. 906, NACA, 1943.

3. Guggenheim Aeronautical Laboratory, California Institute of Technology: Some Investigations of the General Instability of Stiffened Metal Cylinders. III - Continuation of Tests of Wire-Braced Specimens and Preliminary Tests of Sheet-Covered Specimens. T.N. No. 907, NACA, 1943.

4. Guggenheim Aeronautical Laboratory, California Institute of Technology: Some Investigations of the General Instability of Stiffened Metal Cylinders. IV - Continuation of Tests of Sheet-Covered Specimens and Studies of the Buckling Phenomena of Unstiffened Circular Cylinders. T.N. No. 908, NACA, 1943.

5. Cox, H. L.: Stress Analysis of Thin Metal Construction. Jour. R.A.S., vol. XLIV, March 1940.

6. Timoshenko, Stephen: Theory of Elastic Stability. McGraw-Hill Book Co., Inc., 1936.

7. Hoff, N. J.: Instability of Monocoque Structures in Pure Bending. Jour. R.A.S., vol. 42, no. 38, April 1938, pp. 291-346.

TABLE I

Pure Bending Tests of Longitudinal - Frame Combinations

All Longitudinals S_1

Test	Frame No.	Sheet Thick.	Long. Spacing b	Frame Spacing d	Radius	Max. Unit Strain	$\sqrt[4]{bd}$	ρ_x	ρ_y	$\sqrt[4]{(\rho_x \rho_y)^3}$	$\frac{\sqrt[4]{bd}}{(\rho_x \rho_y)^3} R$	Type of Failure
25	F_5	.010	2.53	8	15.92	.00170	2.120	.1168	.02335	.01145	2822	General Instability
26			2.53	4.		.00208	1.783	.1165	.02677	.01320	2150	" "
27			2.53	2		.00288	1.500	.1165	.02836	.01380	1730	" "
28			2.53	16		.00130	2.520	.1169	.01875	.01010	3970	Started by Panel Instability Final Failure General Instability
29			5.06	16		.00092	2.998	.1160	.01875	.01023	4660	Panel Instability
30			5.06	8		.00140	2.520	.1165	.02335	.01190	3370	General Instability
31			5.06	4		.00190	2.120	.1169	.02677	.01325	2550	" "
32			5.06	2		.00256	1.783	.1167	.02836	.01380	2060	" "
34			10.12	16		.00088	3.560	.1110	.01875	.00975	5820	Started by Panel Instability Final Failure General Instability
35			10.12	8		.00120	2.998	.1120	.02335	.01160	4120	General Instability
36			10.12	4		.00164	2.520	.1122	.02677	.01280	3135	" "
37			10.12	2		.00200	2.120	.1117	.02836	.01330	2540	" "
38			5.06	1		.00283	1.500	.1164	.02801	.01360	1755	" "
39		.010	2.53	1		.00326	1.261	.1170	.02801	.01360	1478	" "

TABLE I (CONTD.)

Test	Frame No.	Sheet Thick.	Long. Spacing b	Frame Spacing d	Radius	Max. Unit Strain	$\sqrt[4]{bd}$	ρ_x	ρ_y	$\sqrt[4]{\rho_x \rho_y^3}$	$\frac{\sqrt[4]{bd}}{\sqrt[4]{(R\rho_y)^3}} R$	Type of Failure
40	F_5	.015	2.53	16	15.92	.00104	2.520	.1175	.01723	.00955	4210	Panel Instability
41			2.53	8		.00182	2.120	.1180	.02176	.01140	2960	General Instability
42			2.53	4		.00215	1.783	.1184	.02608	.01310	2168	" "
43			2.53	2		.00280	1.500	.1184	.02879	.01410	1693	" "
44			5.06	16		.00066	2.998	.1140	.01723	.00935	5110	Panel Instability
45			5.06	8		.00146	2.520	.1150	.02176	.01120	3580	General Instability
46			5.06	4		.00167	2.120	.1151	.02608	.01285	2630	" "
47			5.06	2		.00249	1.783	.1151	.02879	.01380	2060	" "
48			10.12	16		.00048	3.560	.104	.01723	.00870	6520	Panel Instability
49			10.12	8		.00128	2.998	.1049	.02176	.01050	4540	General Instability
50			10.12	4		.00150	2.520	.1060	.02608	.01195	3360	" "
51	F_5	.015	10.12	2	15.92	.00250	2.120	.1061	.02879	.01300	2600	" "
52	F_1	.010	2.53	16	16.00	.00180	2.520	.1168	0.1288	.0430	938	Panel Instability
53			2.53	8		.00216	2.120	.1165	0.0811	.0303	1120	" "
54			2.53	4		.003732	1.783	.1168	0.0982	.03500	812	General Instability

TABLE I (CONTD.)

Test	Frame No.	Sheet Thick.	Long. Spacing b	Frame Spacing d	Radius	Max. Unit Strain	$\sqrt[4]{bd}$	ρ_x	ρ_y	$\sqrt[4]{(\rho_x\rho_y)^3}$	$\frac{\sqrt[4]{bd}}{\sqrt[4]{(\rho_x\rho_y)^3}}R$	Type of Failure
55	F_1	.010	2.53	2	16	.004775	1.500	.1168	.11000	.0378	635	General Instability
56			5.06	16		.00090	2.998	.1150	.06330	.0250	1920	Panel Instability
57				8		.00228	2.520	.1150	.08110	.0300	1345	Panel Instability
58				4		.004350	2.120	.1160	.09820	.0350	965	General Instability
59	F_1			2		.006154	1.783	.1165	.11000	.0378	742	" "
60	F_6			8		.00243	2.520	.1270	.06340	.0251	1715	Panel Instability
61				4		.004927	2.120	.1270	.06400	.0254	1245	General Instability
62			5.06	2			1.783		.06180			Tension Failure
63			2.53	4		.004045	1.783	.1278	.06400	.0255	1045	General Instability
64	F_6		2.53	2	16	.005100	1.500	.1278	.06180	.0247	905	" "
65	F_5		2.61	4	10	.003150	1.798	.1163	.02677	.0132	1362	" "
66			2.61	2		.004200	1.510	.1168	.02836	.0138	1095	" "
67			5.22	4		.002950	2.175	.1165	.02677	.0132	1650	" "
68			5.22	2		.003750	1.798	.1166	.02836	.0138	1300	" "
73			2.61	4		.003200	1.798	.1162	.02677	.0132	1365	" "
74	F_5	.010	2.61	2	10	.004400	1.510	.1164	.02836	.0138	1095	" "

TABLE II

Calculation of the General Instability Stress

by Hoff's Method

Test No.	$\varepsilon/\varepsilon_c$	I_s	I_ρ	Λ	m	Log Λ	λ	σ/E	$\varepsilon_{cal}/\varepsilon_{c\text{-}test}$
30	8.46	.0006675	.000037	447	4	2.65	2.39	.000551	0.406
31	9.75	.000658	.00003624	3,610	8	3.558	4.38	.000656	0.3455
32	9.15	.000664	.00003655	28,820	15	4.46	7.85	.000821	0.3205
35	9.2	.000815	.0000464	218	5	2.339	2.8	.000496	0.415
36	9.65	.000809	.00004625	1,740	6	3.241	3.36	.001365	0.832
37	8.04	.000823	.00004632	14,120	16	4.15	8.3	.000912	0.454
41	4.595	.000662	.00003978	826	7	2.917	3.8	.000219	0.175
42	6.155	.000643	.0000370	6,910	11	3.84	5.8	.000365	0.2115
43	6.5	.0006595	.0000367	55,450	16	4.744	8.4	.000692	0.28
45	5.84	.000795	.0000481	410	7	2.613	3.72	.0002742	0.188
46	6.30	.00079	.0000476	3,299	11	3.518	5.74	.0004575	0.274
47	6.23	.00079	.0000478	26,210	16	4.419	8.33	.00087	0.358
49	6.775	.000938	.0000586	198	7	2.297	3.61	.0003432	0.2662
50	7.83	.000928	.0000578	1,596	11	3.203	5.65	.000555	0.373
51	8.34	.0009245	.0000576	12,730	15	4.105	7.78	.001162	0.465
54	15.55	.00053	.000415	509	12	2.7065	5.85	.0002955	0.792
58	22.35	.0006245	.000485	256	*10	2.4085	4.9	.000495	0.1137
59	22.0	.0006245	.000485	2,045	15	3.311	7.5	.000848	0.1378
61	25.2	.0006245	.0003835	324	8	2.511	3.23	.00114	0.232
63	16.85	.000524	.0003315	629	8	2.7985	4.2	.000566	0.14
64	13.25	.000533	.0003355	5,050	13	3.7035	6.7	.0009075	0.178

*Obtained from test descriptions.

TABLE III

Calculations of the General Instability Stress

by Ryder's Method

Test No.	A_s	A_f	I_s	I_f	K_2	K_3	K_4	t_e/ρ_s	t_e	$\sigma_{B\text{-}CR}$	$\sigma_{BCR}/\sigma_{EXP.}$
30	.0490	.0332	.0006675	.0000282	.0205	.330	.1905	.125	.0144	5,500	.414
31	.0474	"	.000658	"	.0431	.682	.198	.375	.0433	16,530	.916
32	.0485	"	.000664	"	.0826	1.294	.193	.650	.0750	28,600	1.177
35	.0646	"	.000815	"	.0337	.501	.290	.415	.0477	18,200	1.595
36	.0640	"	.000809	"	.0678	1.012	.292	.615	.0707	27,000	1.733
37	.0658	"	.000823	"	.1335	1.965	.284	.934	.1073	41,000	2.16
38	.0496	"	.000675	"	.1625	2.60	.189	.950	.1092	41,700	1.55
45	.0604	.0352	.000795	.0000412	.0252	.284	.232	.251	.0295	11,250	.811
46	.0597	"	.00079	"	.0507	.574	.235	.469	.0551	21,000	1.325
47	.0598	"	.00079	"	.1014	1.145	.235	.756	.0888	33,900	1.433
49	.0856	"	.000938	"	.0427	.400	.328	.478	.0563	21,500	1.77
50	.0831	"	.000928	"	.0864	.826	.338	.805	.0948	36,200	2.54
51	.0822	"	.000925	"	.1735	1.670	.342	1.142	.1346	51,400	2.16
58	.0456	.0276	.000625	.000434	.676	.589	.205	1.538	.180	68,700	1.665
59	.0456	"	.000625	"	1.352	1.178	.205	1.934	.226	86,300	1.475
61	.0456	"	.000625	"	.534	1.937	.205	1.538	.180	68,700	1.47

TABLE IV

Calculations of the General Instability Stress

By Taylor's Method

Test No.	I_1	I_2	$\frac{C(J_1+J_2)}{E}$	$1/t_1$	$1/t_2$	$\frac{E}{C't}$	t_e	$\sigma_{CALC.}$	$\frac{\sigma_{CALC.}}{\sigma_{EXP.}}$
25	.0001419	.00000193	.00383	78.2	274.0	417.0	.0228	124,500	7.75
27	.0001419	.00000771	"	78.2	68.5	"	.0228	147,000	5.40
30	.0000740	.00000193	"	156.0	274.0	"	.0164	164,000	12.80
32	.0000740	.00000771	"	156.0	68.5	"	.0164	185,300	7.3
35	.0000369	.00000193	"	312.0	274.0	"	.0132	186,000	10.1
37	.0000369	.00000771	"	312.0	68.5	"	.0132	209,000	10.5

TABLE V

Values of the Factor ζ and the Slenderness Ratio λ for the Test Specimens

Test No.	ρ_x	ρ_y	$\sqrt[4]{\frac{\rho_x \rho_y}{b d}}$	ζ	λ
25	.1168	.02335	.10779	0.457	92.50
26	.1165	.02677	.1325	0.562	56.85
27	.1165	.02836	.1598	0.678	39.03
28	.1169	.01875	.0858	0.364	135.4
30	.1165	.02335	.0906	0.384	121.9
31	.1169	.02677	.11254	0.477	78.90
32	.1167	.02836	.1345	0.570	55.28
34	.1110	.01875	.0598	0.254	279.2
35	.1120	.02335	.0754	0.320	175.7
36	.1122	.02677	.0926	0.393	116.7
37	.1117	.02836	.11192	0.475	79.80
38	.1164	.02801	.1593	0.676	39.39
39	.1170	.02801	.1897	0.805	27.80
41	.1180	.02176	.10616	0.450	93.88
42	.1184	.02608	.1322	0.561	57.20
43	.1184	.02879	.1611	0.683	38.53
45	.1150	.02176	.08836	0.375	28.2
46	.1151	.02608	.11041	0.468	81.90
47	.1151	.02879	.1345	0.570	55.30
49	.1049	.02176	.0737	0.313	184.4
50	.1060	.02608	.0909	0.386	120.9
51	.1061	.02879	.11084	0.470	81.54
54	.1168	.0982	.1833	0.777	29.74
55	.1168	.110	.2193	0.932	20.80
58	.1160	.0982	.1540	0.653	42.20
59	.1165	.110	.1886	0.800	28.17
61	.116	.064	.1384	0.587	52.15
63	.1168	.064	.1648	0.699	36.80
64	.1168	.0618	.1942	0.824	26.53
66	.1168	.02836	.1587	0.673	39.71
67	.1165	.02679	.1106	0.469	81.80
68	.1166	.02836	.1334	0.566	56.19
73	.1162	.02677	.1314	0.557	57.85
74	.1164	.02836	.1586	0.673	39.74

Note: All drawings are twice actual size

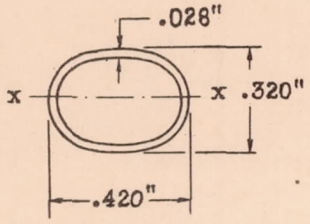

STIFFENER - S_1

AREA = .0324 I_{xx} = .000374

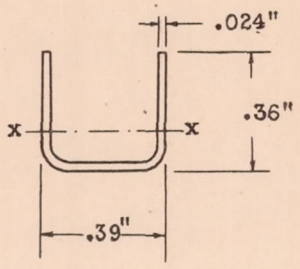

FRAME - F_1

AREA = .02355 I_{xx} = .00031194

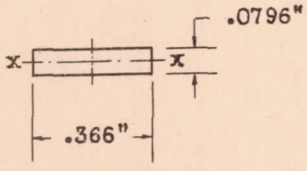

FRAME - F_5

AREA = .0291 I_{xx} = 1.537×10^{-5}

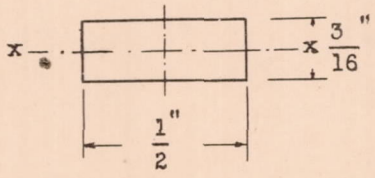

FRAME - F_6

AREA = .09365 I_{xx} = .000274

FIG. 1

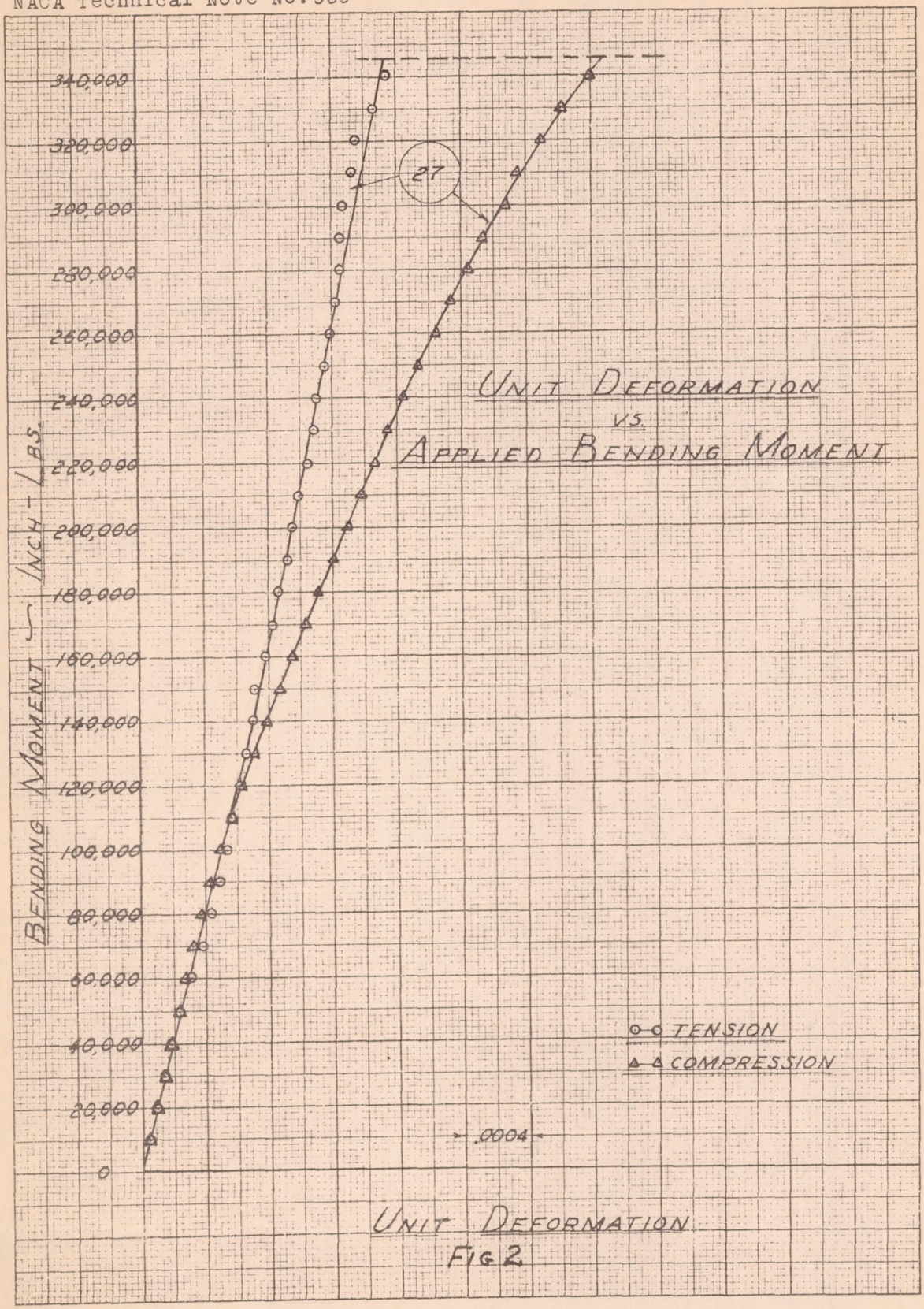
340,000
320,000
300,000
280,000
260,000
240,000
220,000
200,000
180,000
160,000
140,000
120,000
100,000
80,000
60,000
40,000
20,000
0
BENDING MOMENT — INCH - LBS.
27
UNIT DEFORMATION
VS.
APPLIED BENDING MOMENT
TENSION
COMPRESSION
-.0004-
UNIT DEFORMATION

FIG 2.

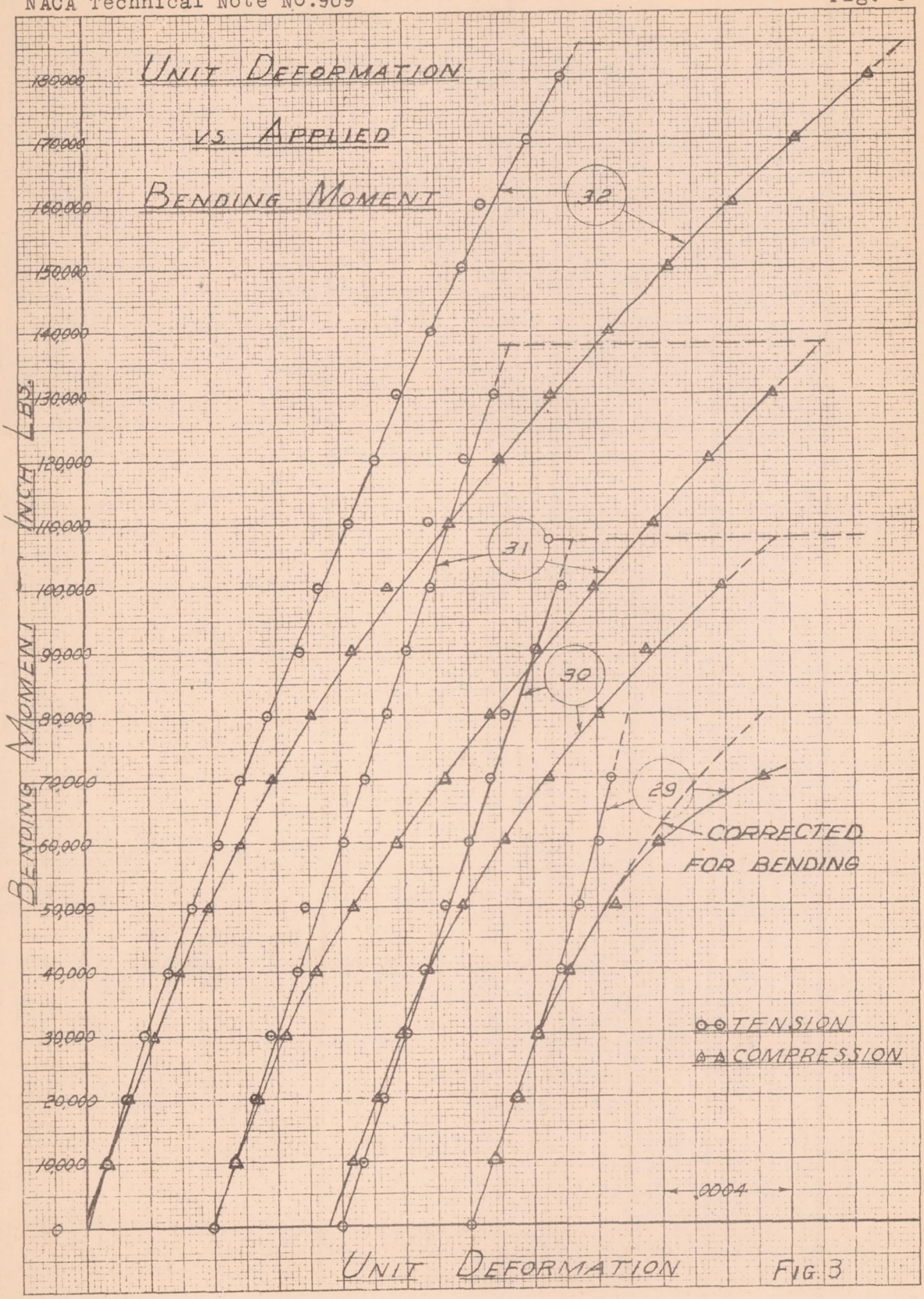
UNIT DEFORMATION
VS APPLIED
BENDING MOMENT
BENDING MOMENT IN INCH LBS.
180,000
170,000
160,000
150,000
140,000
130,000
120,000
110,000
100,000
90,000
80,000
70,000
60,000
50,000
40,000
30,000
20,000
10,000
0
32
31
30
29
CORRECTED FOR BENDING
TENSION
COMPRESSION
.0004
UNIT DEFORMATION

FIG. 3

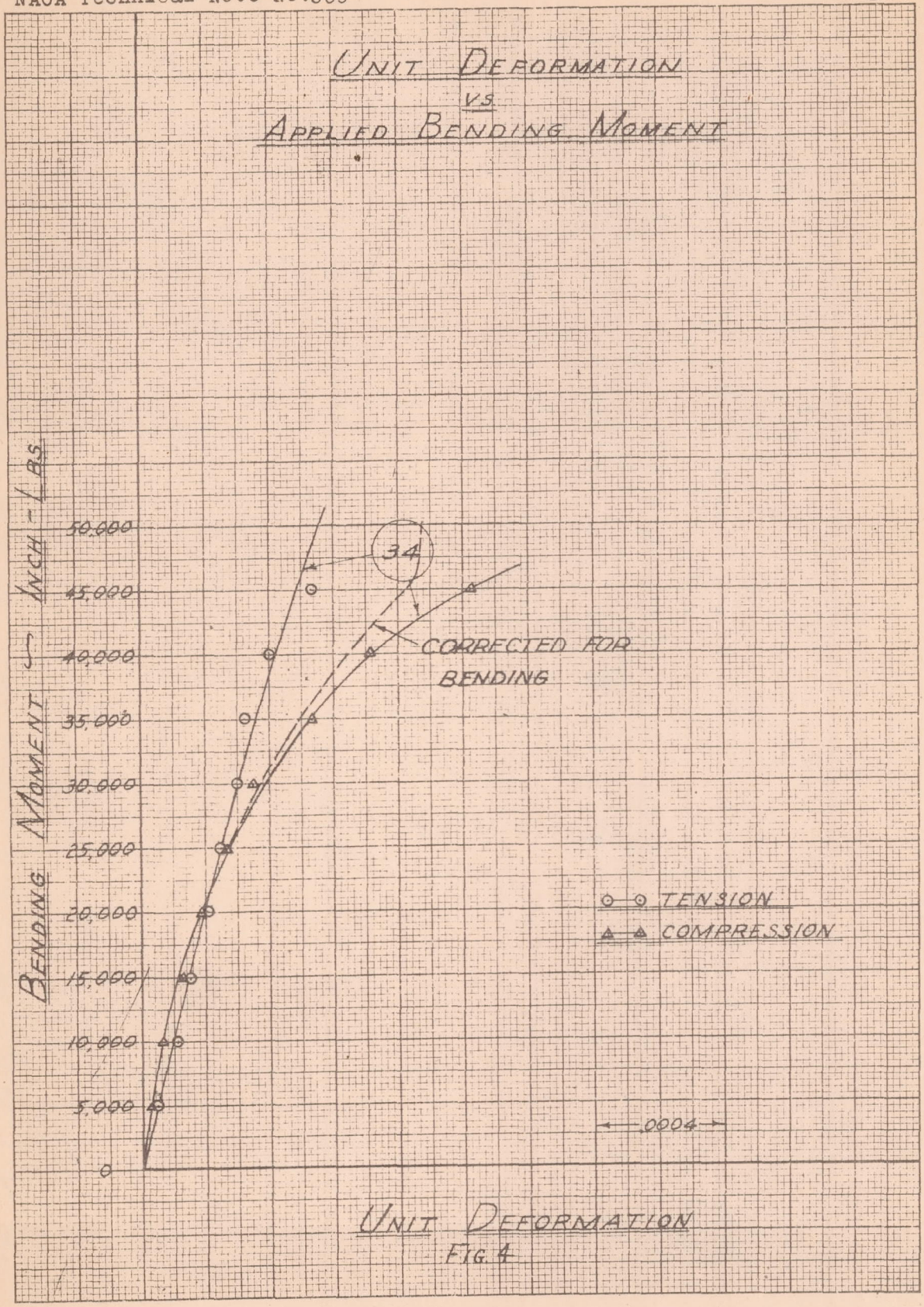
UNIT DEFORMATION
V.S.
APPLIED BENDING MOMENT
BENDING MOMENT ↔ INCH - LBS.
50,000
45,000
40,000
35,000
30,000
25,000
20,000
15,000
10,000
5,000
0
34
CORRECTED FOR BENDING
TENSION
COMPRESSION
.0004
UNIT DEFORMATION

FIG. 4

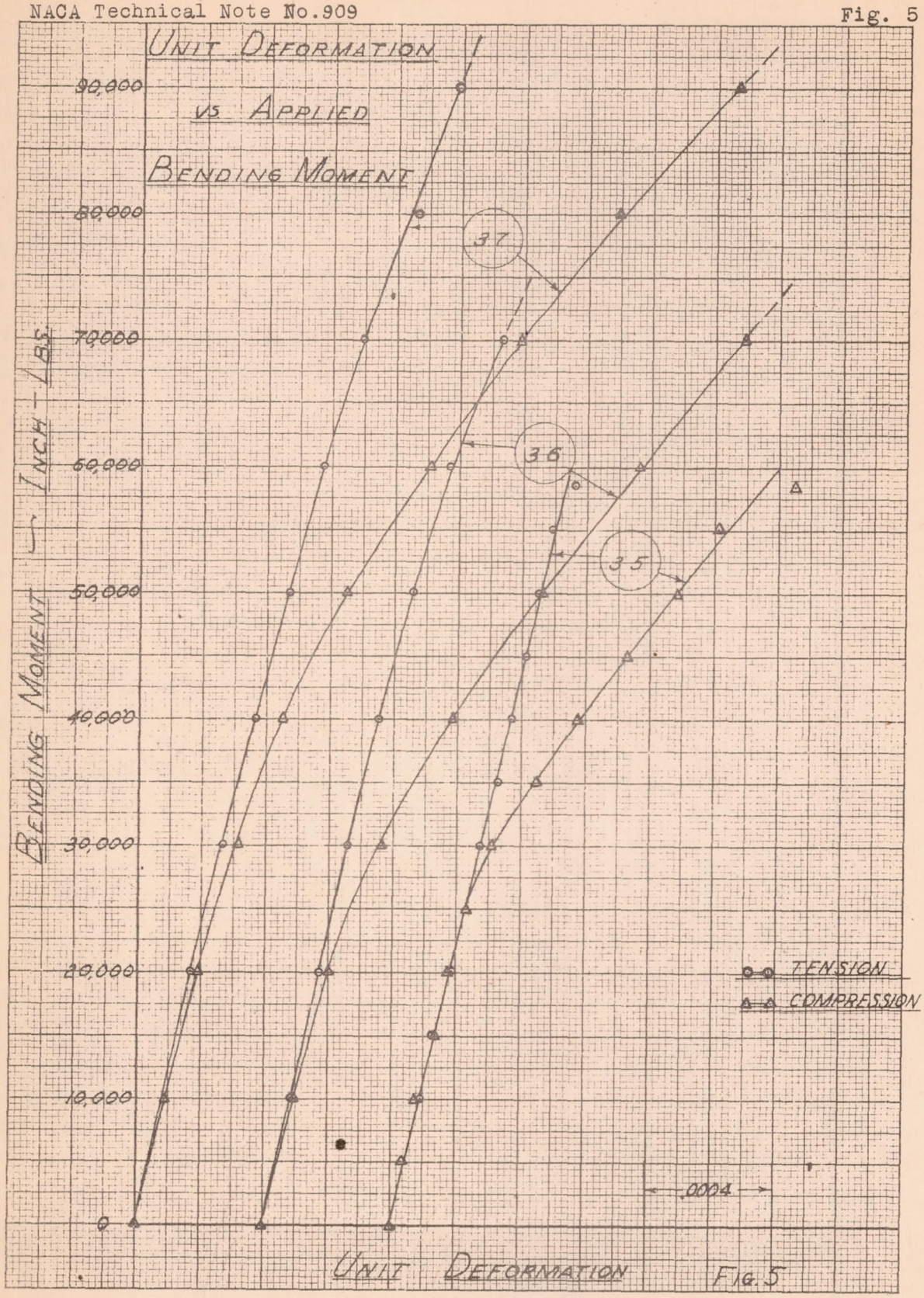
UNIT DEFORMATION
VS APPLIED
BENDING MOMENT
90,000
80,000
70,000
60,000
50,000
40,000
30,000
20,000
10,000
0
BENDING MOMENT - INCH - LBS
37
36
35
TENSION
COMPRESSION
.0004
UNIT DEFORMATION
FIG. 5

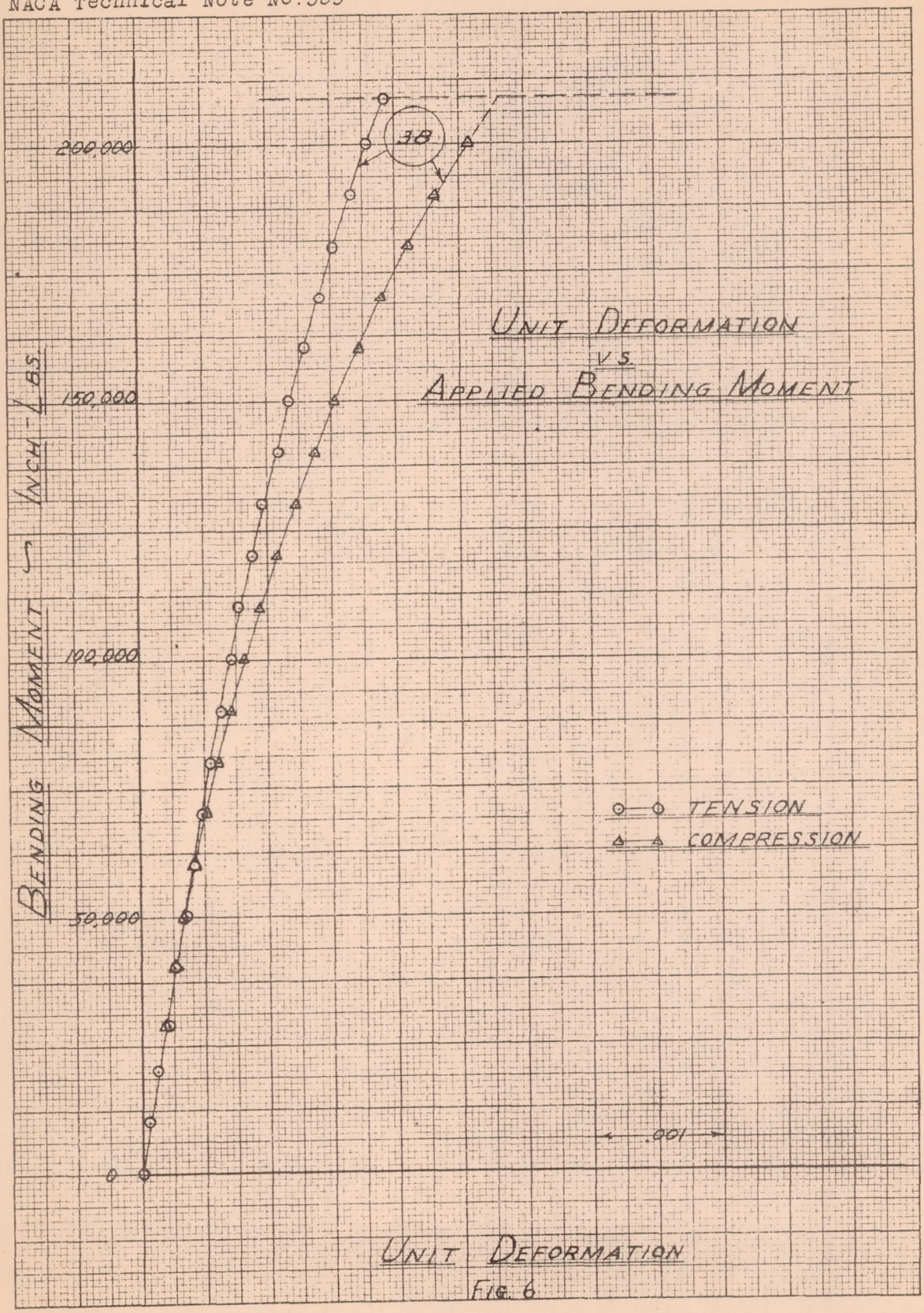
UNIT DEFORMATION
VS
APPLIED BENDING MOMENT
BENDING MOMENT - INCH-LBS
200,000
150,000
100,000
50,000
0
38
TENSION
COMPRESSION
.001
UNIT DEFORMATION

FIG. 6

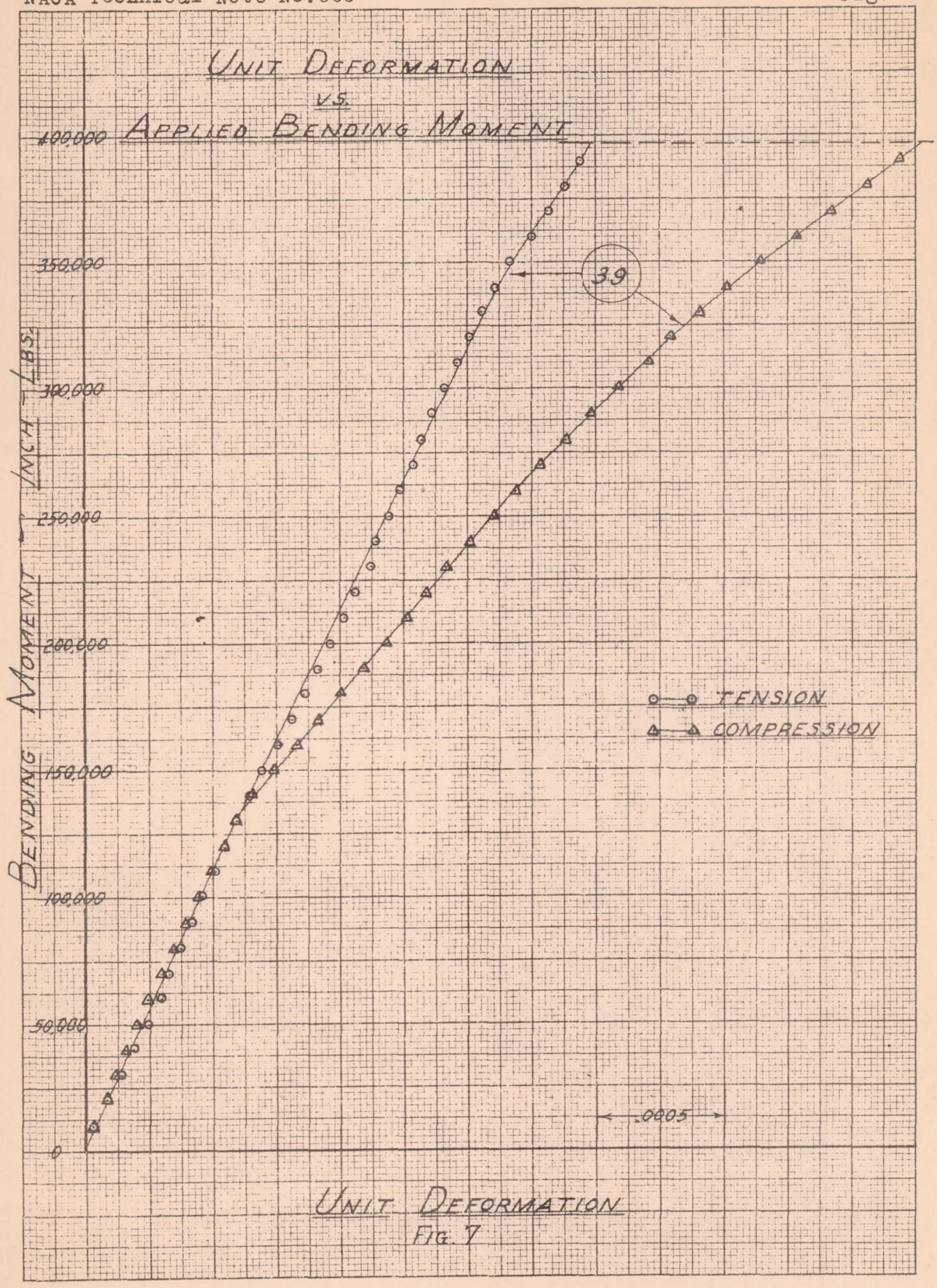
UNIT DEFORMATION
V.S.
APPLIED BENDING MOMENT
400,000
350,000
300,000
250,000
200,000
150,000
100,000
50,000
0
BENDING MOMENT - INCH - LBS.
39
TENSION
COMPRESSION
.0005
UNIT DEFORMATION

FIG. 7

Fig. 8

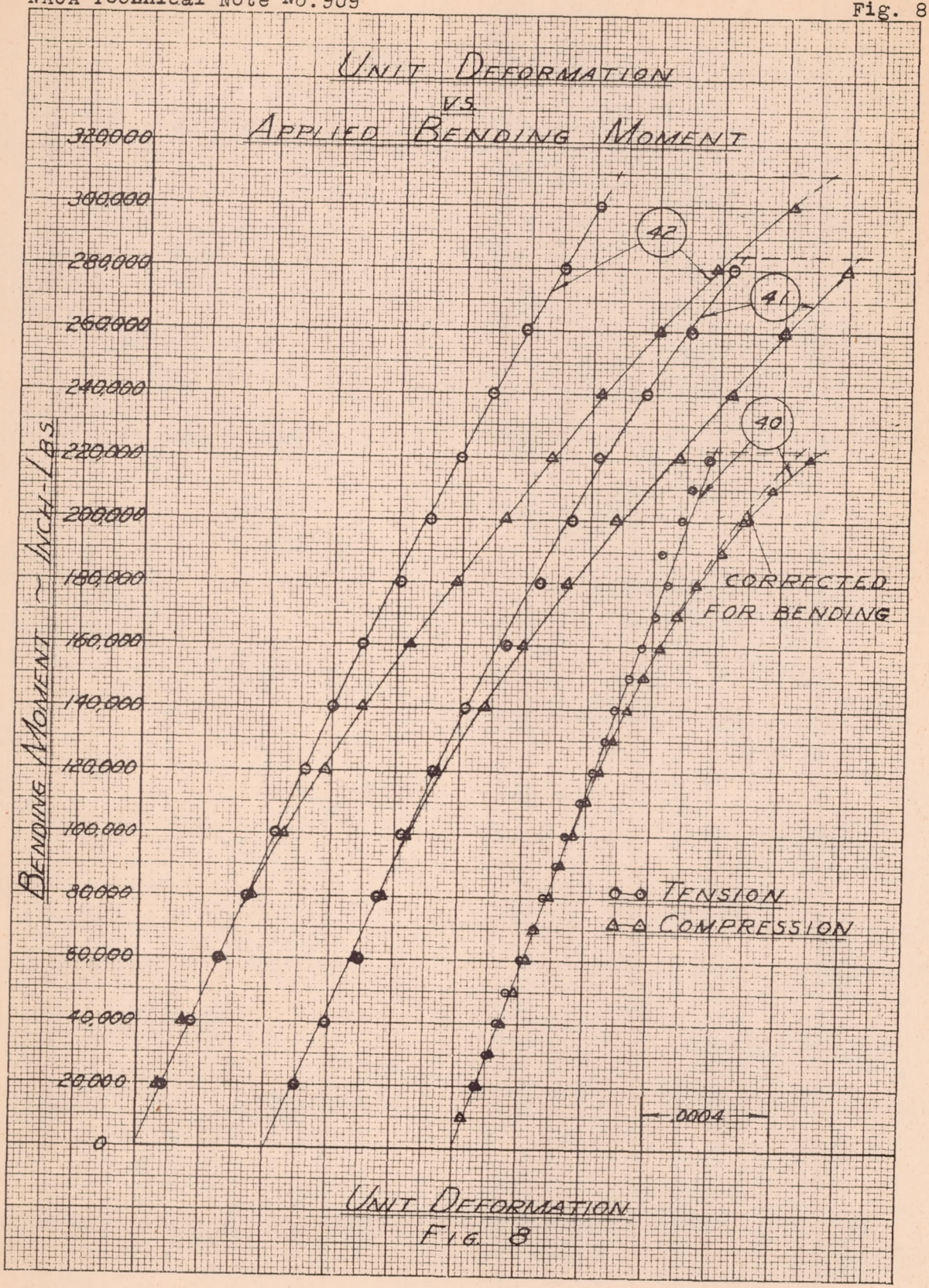
UNIT DEFORMATION
VS.
APPLIED BENDING MOMENT
BENDING MOMENT ~ INCH-LBS.
320,000
300,000
280,000
260,000
240,000
220,000
200,000
180,000
160,000
140,000
120,000
100,000
80,000
60,000
40,000
20,000
0
42
41
40
CORRECTED FOR BENDING
TENSION
COMPRESSION
.0004
UNIT DEFORMATION

FIG. 8

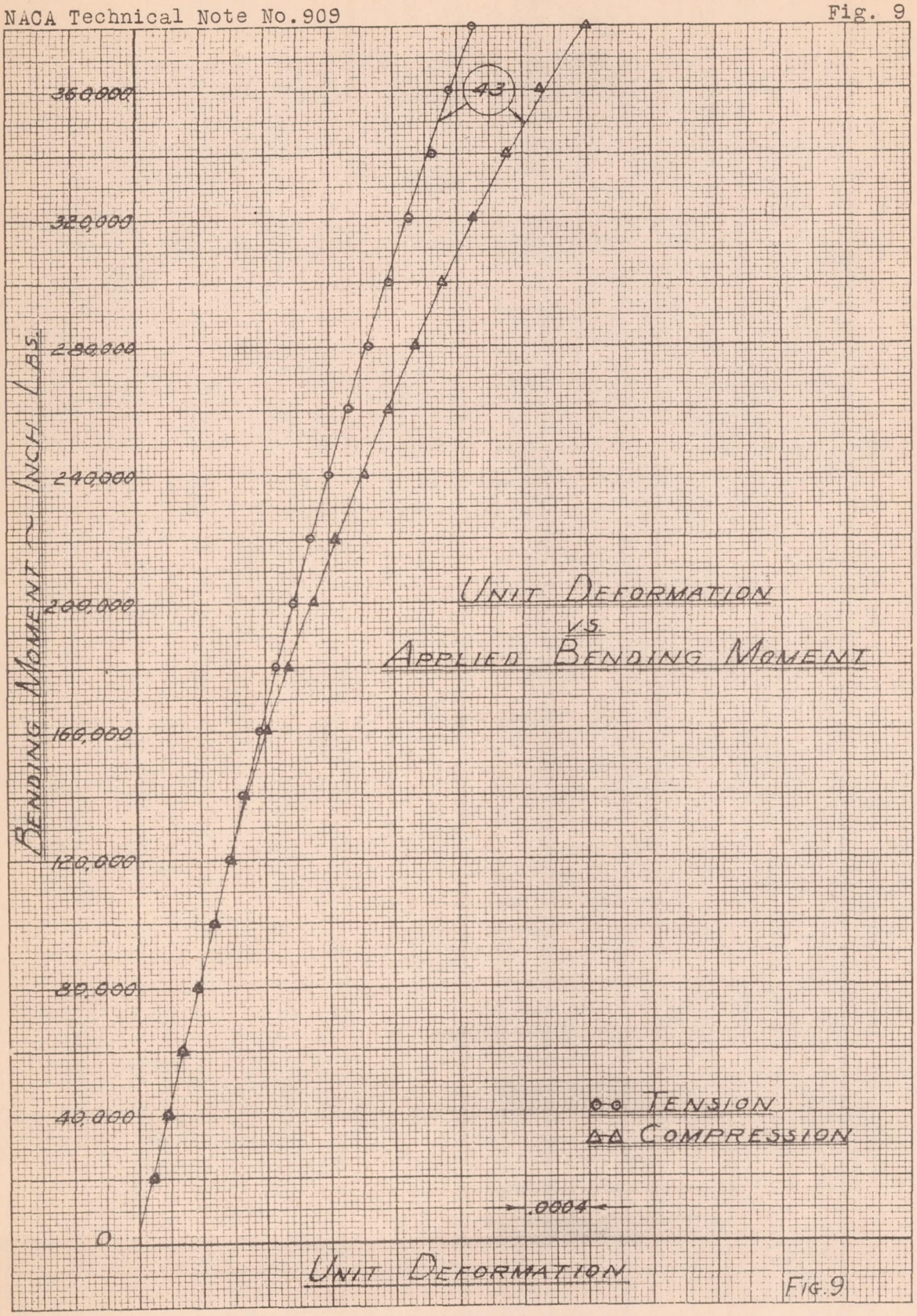
360,000
320,000
280,000
240,000
200,000
160,000
120,000
80,000
40,000
0
BENDING MOMENT ~ INCH LBS.
43
UNIT DEFORMATION
VS.
APPLIED BENDING MOMENT
o-o TENSION
Δ-Δ COMPRESSION
.0004
UNIT DEFORMATION
FIG. 9

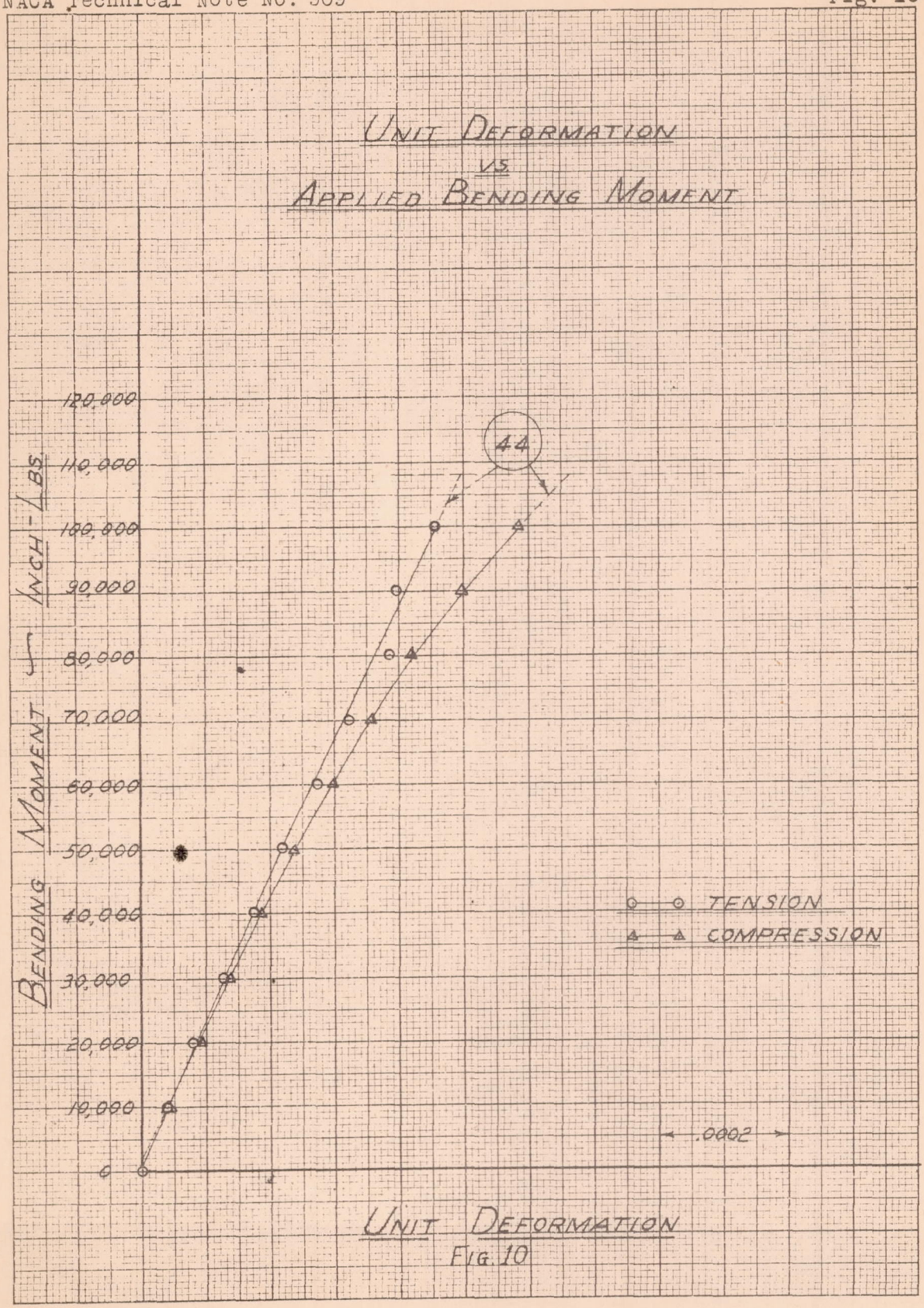
UNIT DEFORMATION
VS
APPLIED BENDING MOMENT
BENDING MOMENT - INCH-LBS.
120,000
110,000
100,000
90,000
80,000
70,000
60,000
50,000
40,000
30,000
20,000
10,000
0
44
TENSION
COMPRESSION
.0002
UNIT DEFORMATION

FIG. 10

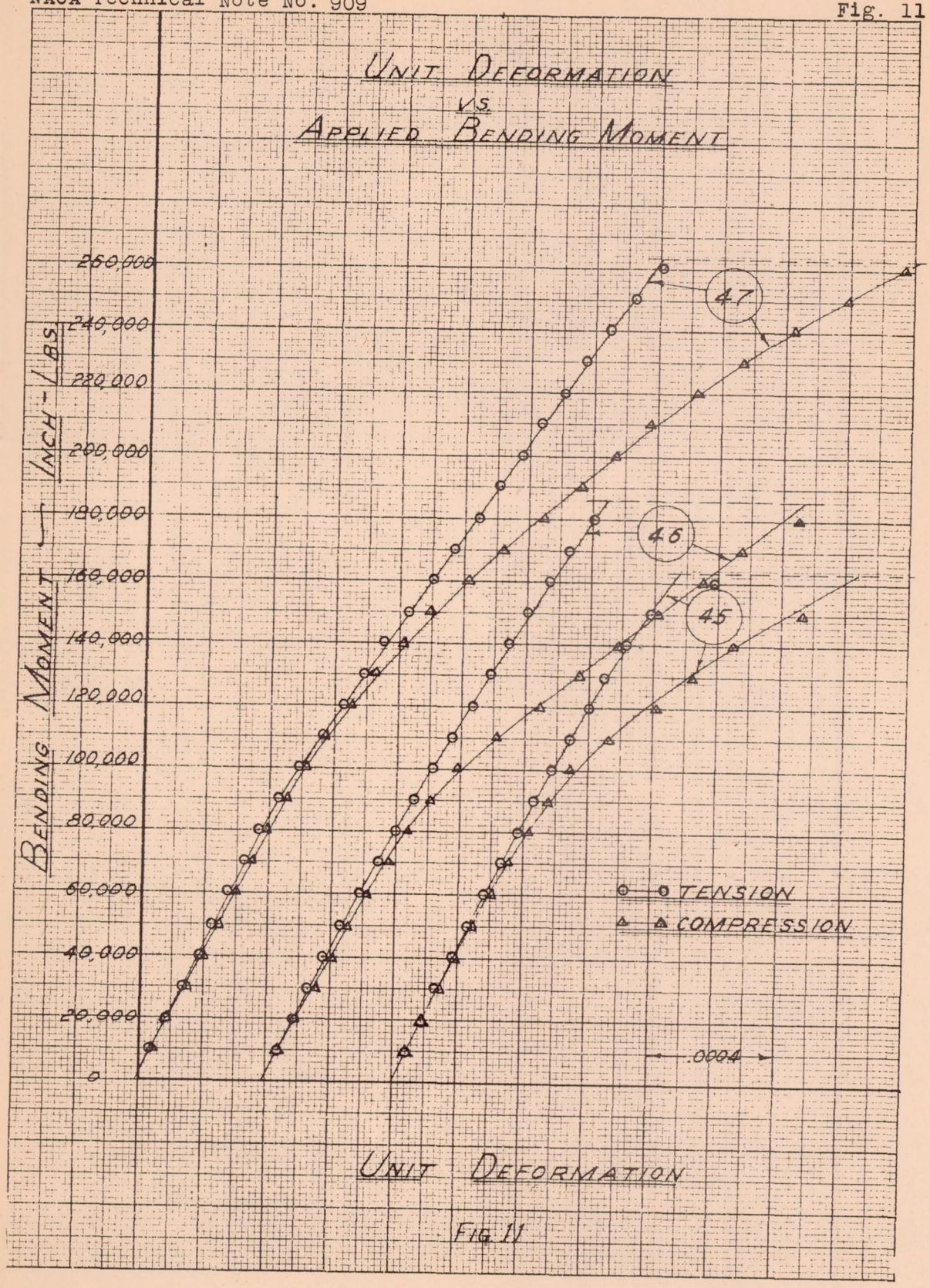
UNIT DEFORMATION
VS.
APPLIED BENDING MOMENT
BENDING MOMENT — INCH-LBS.
260,000
240,000
220,000
200,000
180,000
160,000
140,000
120,000
100,000
80,000
60,000
40,000
20,000
0
47
46
45
TENSION
COMPRESSION
.0004
UNIT DEFORMATION

FIG. 11

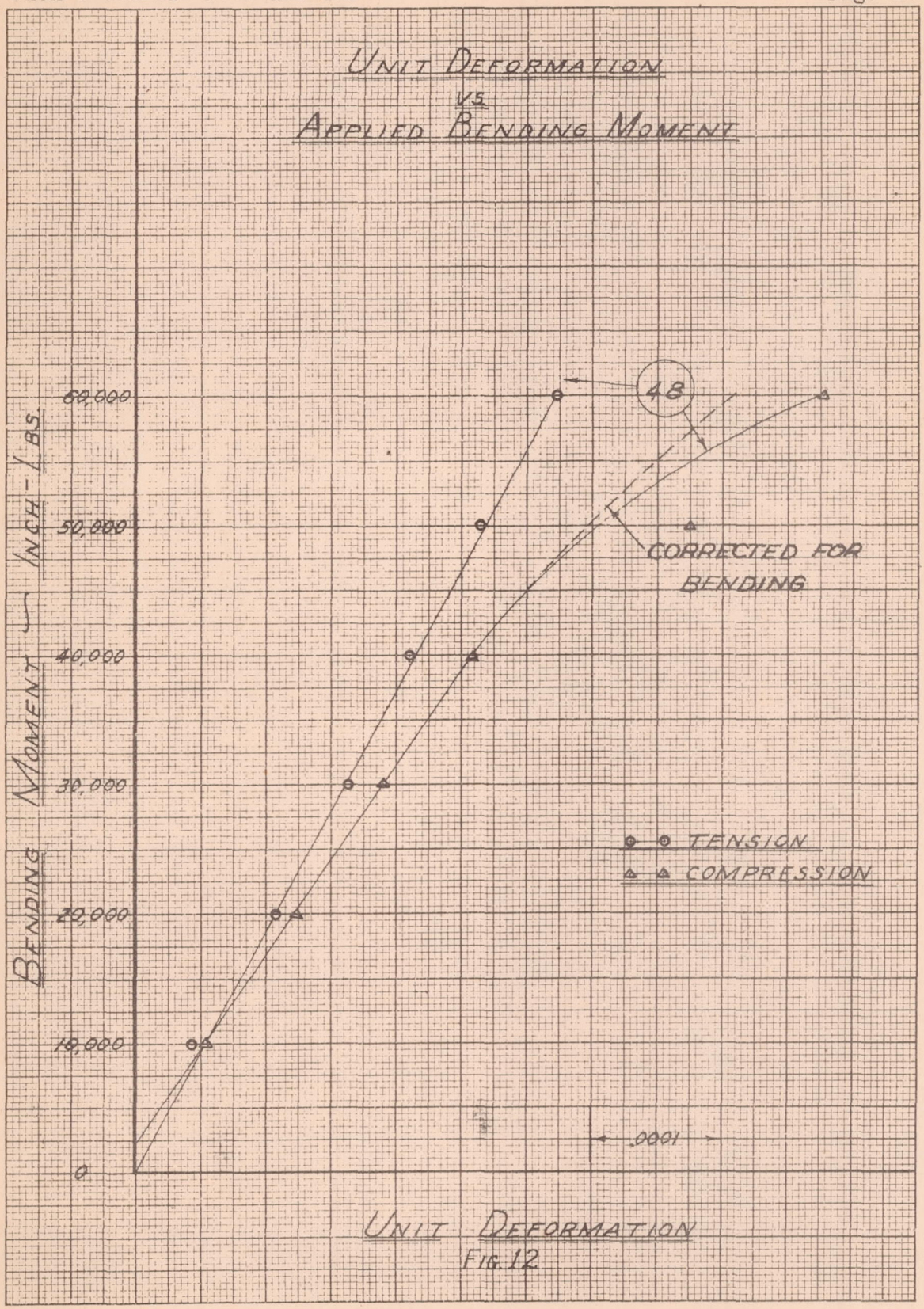
UNIT DEFORMATION
VS.
APPLIED BENDING MOMENT
BENDING MOMENT - INCH - LBS.
60,000
50,000
40,000
30,000
20,000
10,000
0
48
CORRECTED FOR BENDING
TENSION
COMPRESSION
.0001
UNIT DEFORMATION

FIG. 12

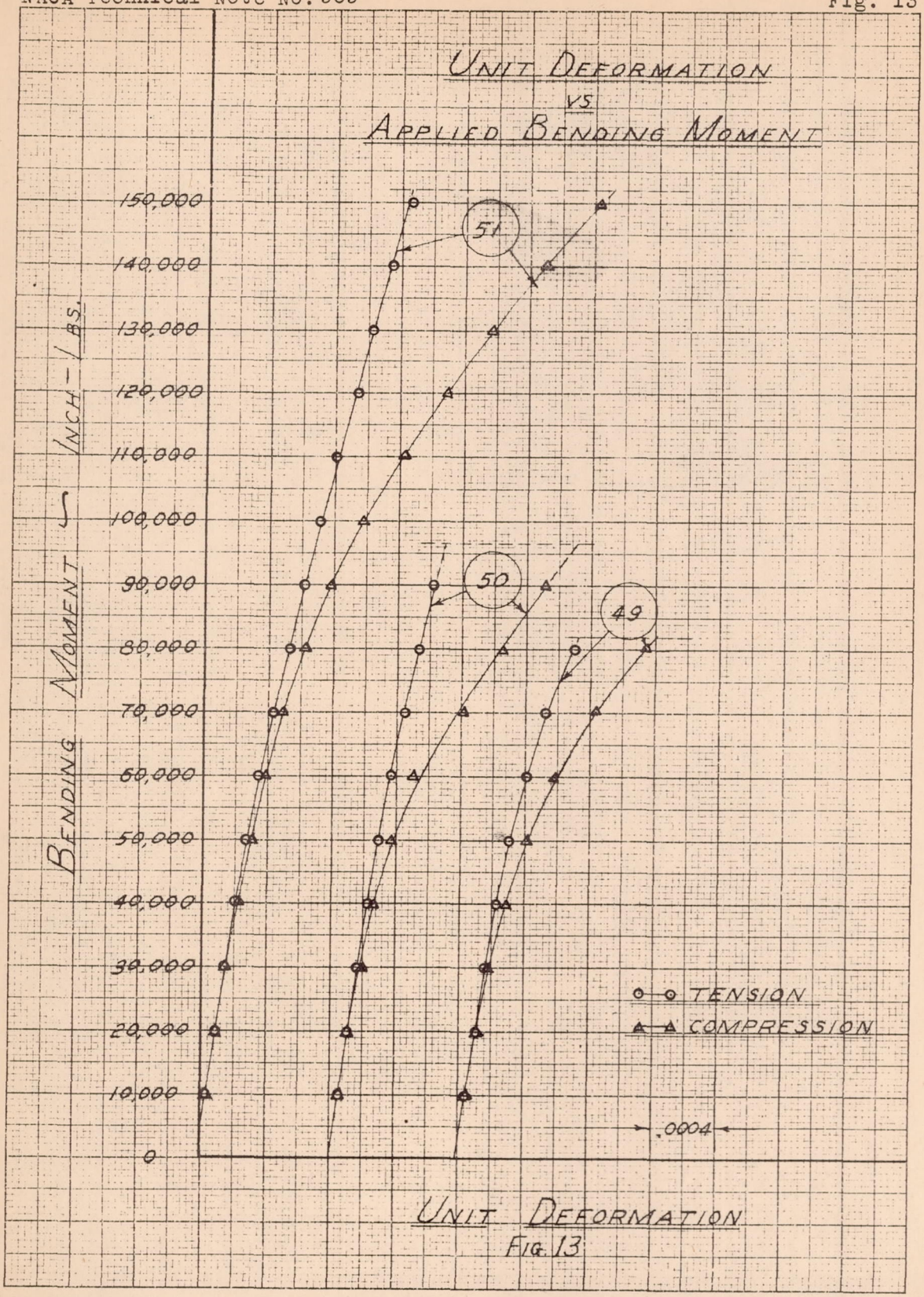
UNIT DEFORMATION
VS
APPLIED BENDING MOMENT
BENDING MOMENT - INCH - LBS.
150,000
140,000
130,000
120,000
110,000
100,000
90,000
80,000
70,000
60,000
50,000
40,000
30,000
20,000
10,000
0
51
50
49
TENSION
COMPRESSION
.0004
UNIT DEFORMATION

FIG. 13

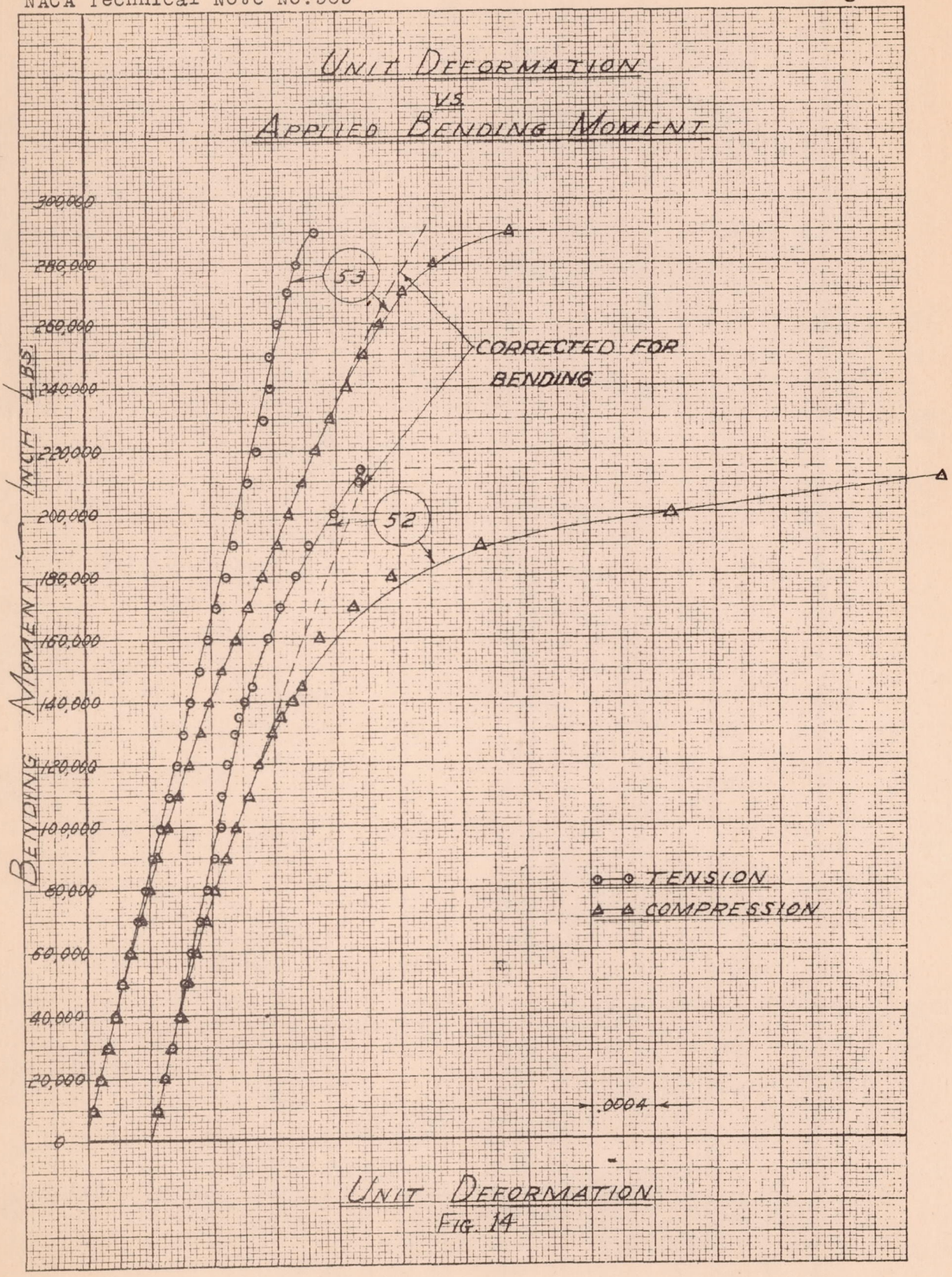
UNIT DEFORMATION
VS.
APPLIED BENDING MOMENT
BENDING MOMENT, INCH LBS.
300,000
280,000
260,000
240,000
220,000
200,000
180,000
160,000
140,000
120,000
100,000
80,000
60,000
40,000
20,000
0
53
52
CORRECTED FOR BENDING
TENSION
COMPRESSION
.0004
UNIT DEFORMATION

FIG. 14

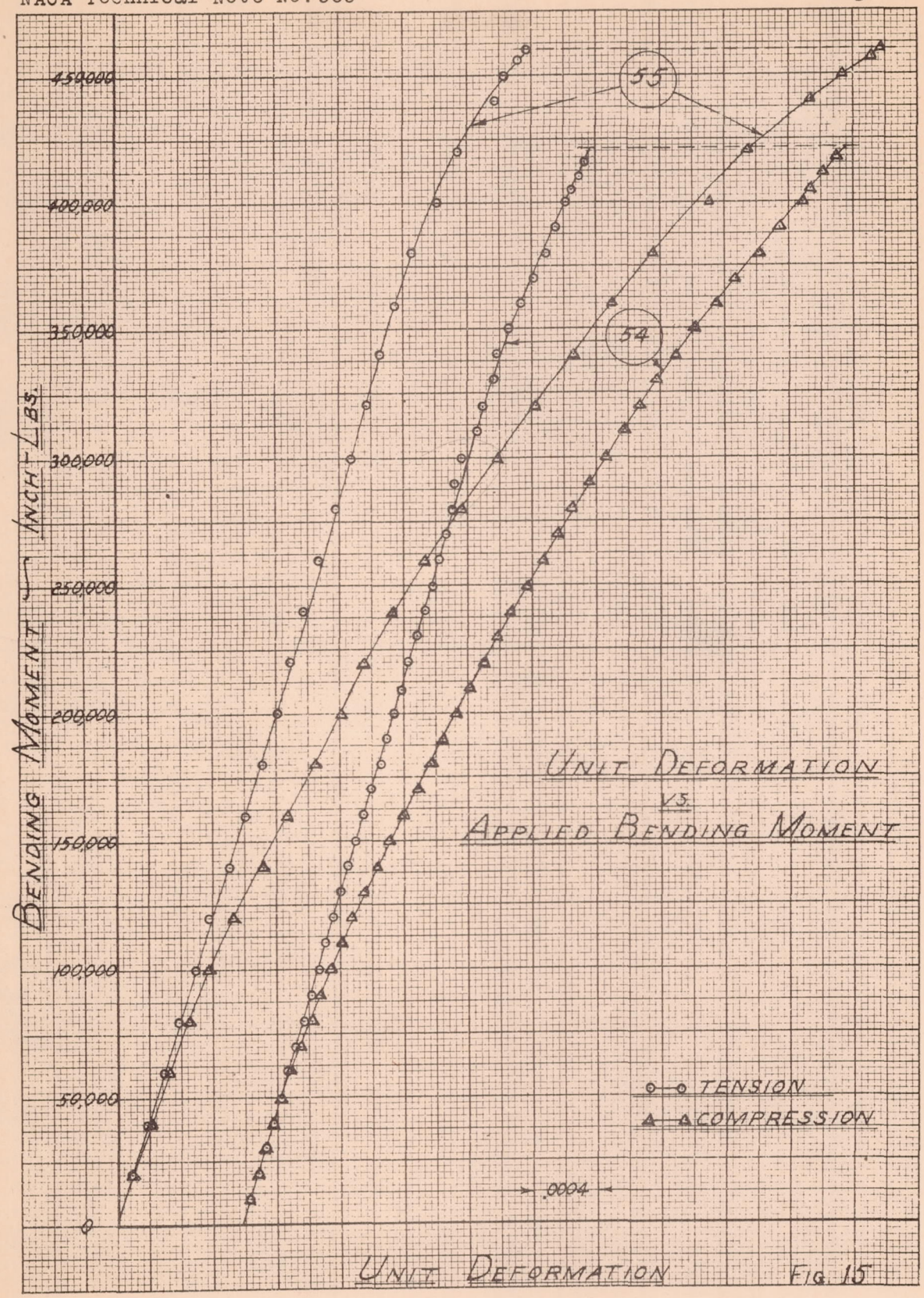
450,000
400,000
350,000
300,000
250,000
200,000
150,000
100,000
50,000
0
BENDING MOMENT — INCH-LBS.
55
54
UNIT DEFORMATION
VS.
APPLIED BENDING MOMENT
TENSION
COMPRESSION
.0004
UNIT DEFORMATION

FIG. 15

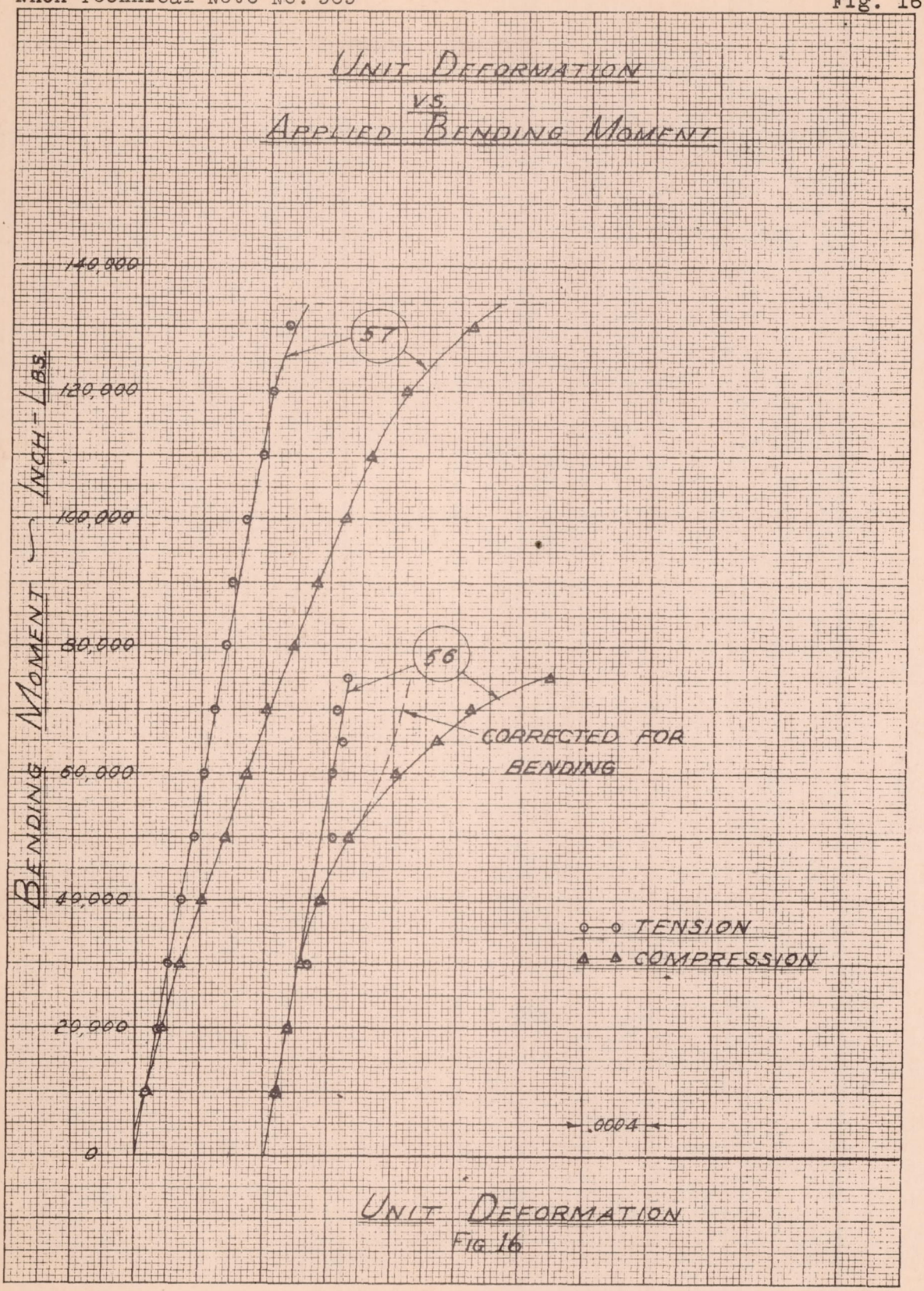
UNIT DEFORMATION
VS.
APPLIED BENDING MOMENT
BENDING MOMENT — INCH - LBS.
140,000
120,000
100,000
80,000
60,000
40,000
20,000
0
57
56
CORRECTED FOR BENDING
TENSION
COMPRESSION
.0004
UNIT DEFORMATION
FIG 16

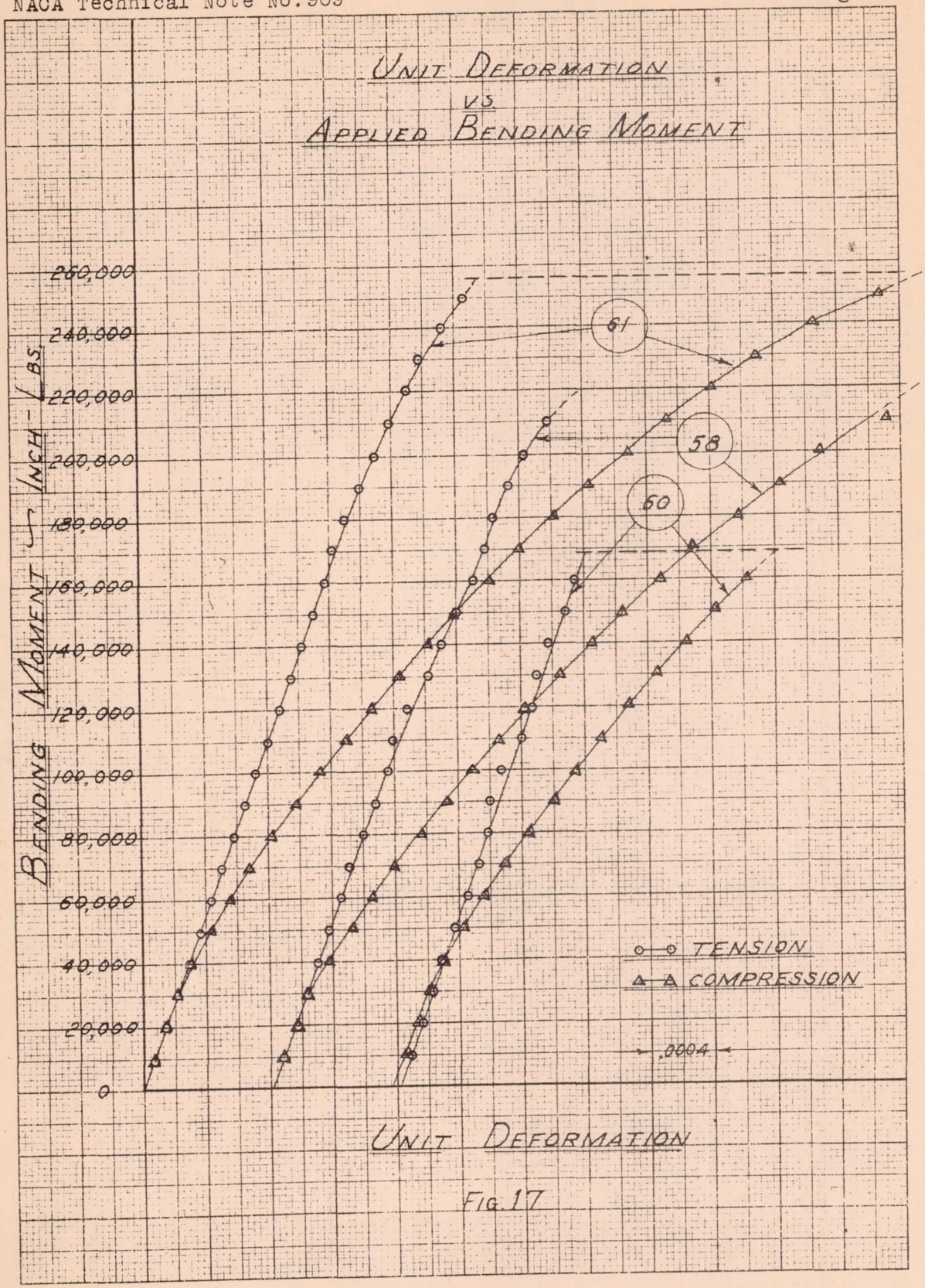
UNIT DEFORMATION
VS.
APPLIED BENDING MOMENT
BENDING MOMENT - INCH - LBS.
260,000
240,000
220,000
200,000
180,000
160,000
140,000
120,000
100,000
80,000
60,000
40,000
20,000
0
61
58
60
TENSION
COMPRESSION
.0004
UNIT DEFORMATION

FIG. 17

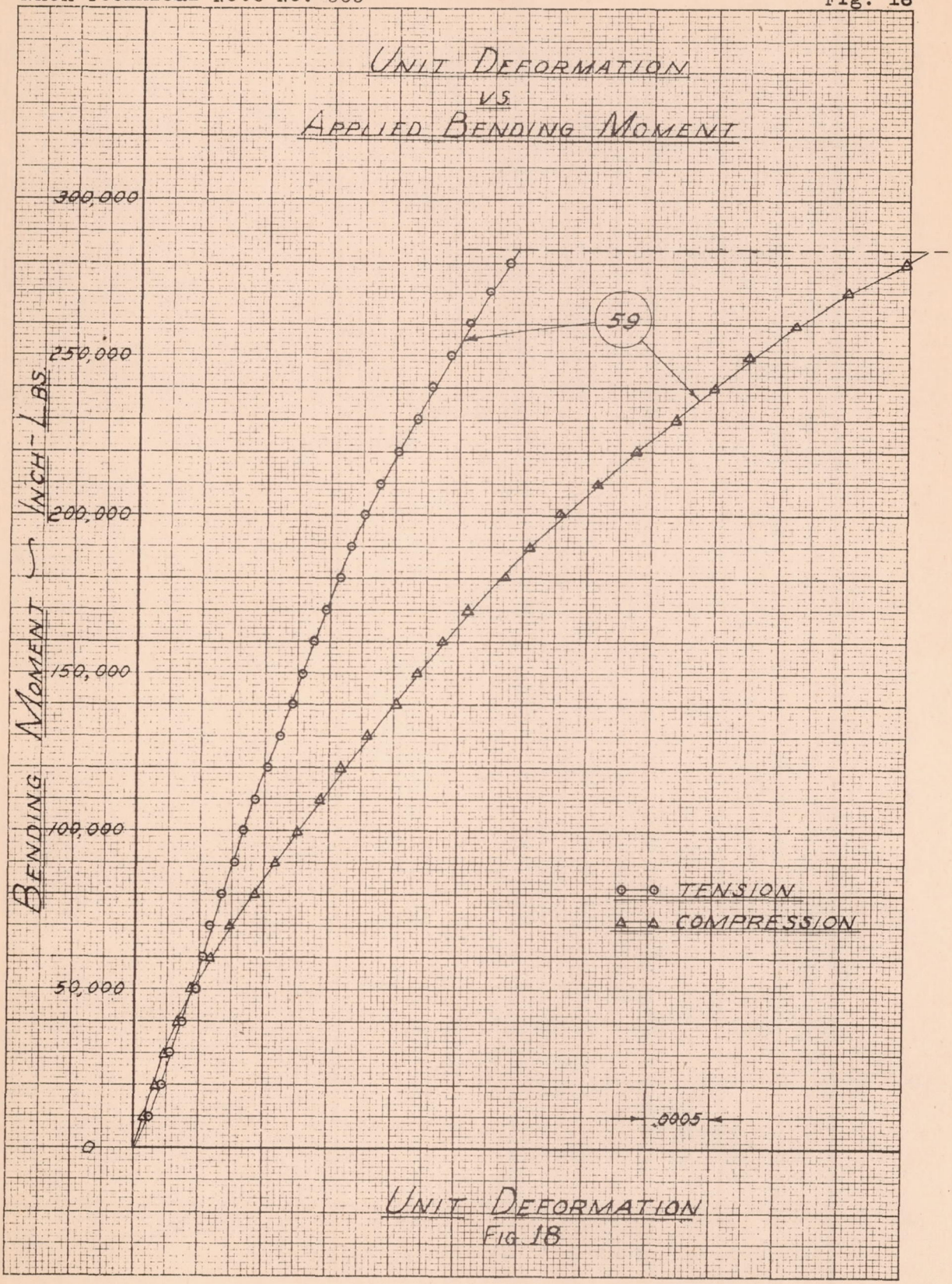
UNIT DEFORMATION
VS
APPLIED BENDING MOMENT
300,000
250,000
200,000
150,000
100,000
50,000
0
BENDING MOMENT - INCH-LBS.
59
TENSION
COMPRESSION
.0005
UNIT DEFORMATION

FIG. 18

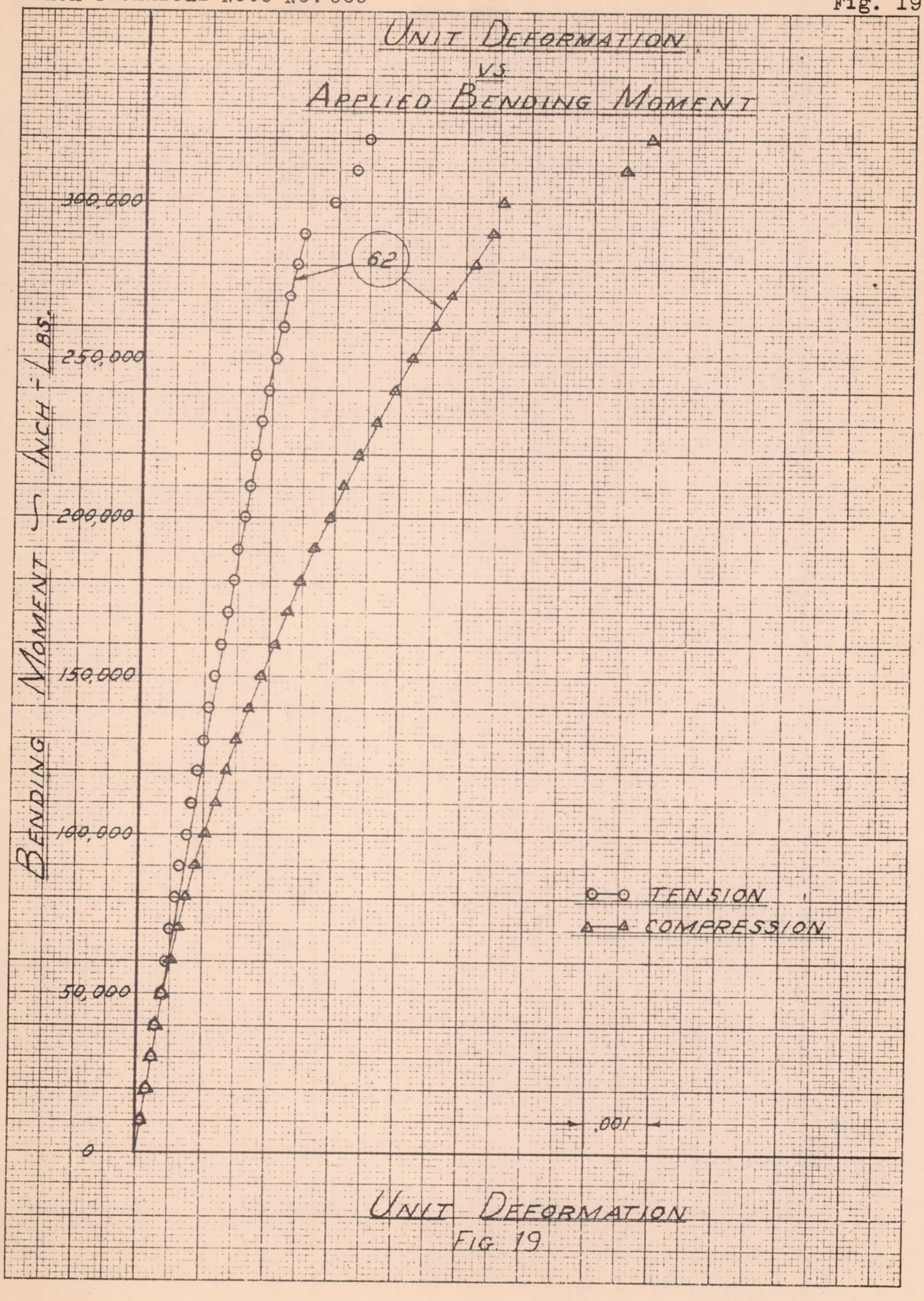
UNIT DEFORMATION
VS
APPLIED BENDING MOMENT
BENDING MOMENT IN INCH-LBS.
300,000
250,000
200,000
150,000
100,000
50,000
0
62
TENSION
COMPRESSION
.001
UNIT DEFORMATION

FIG. 19

Fig. 20

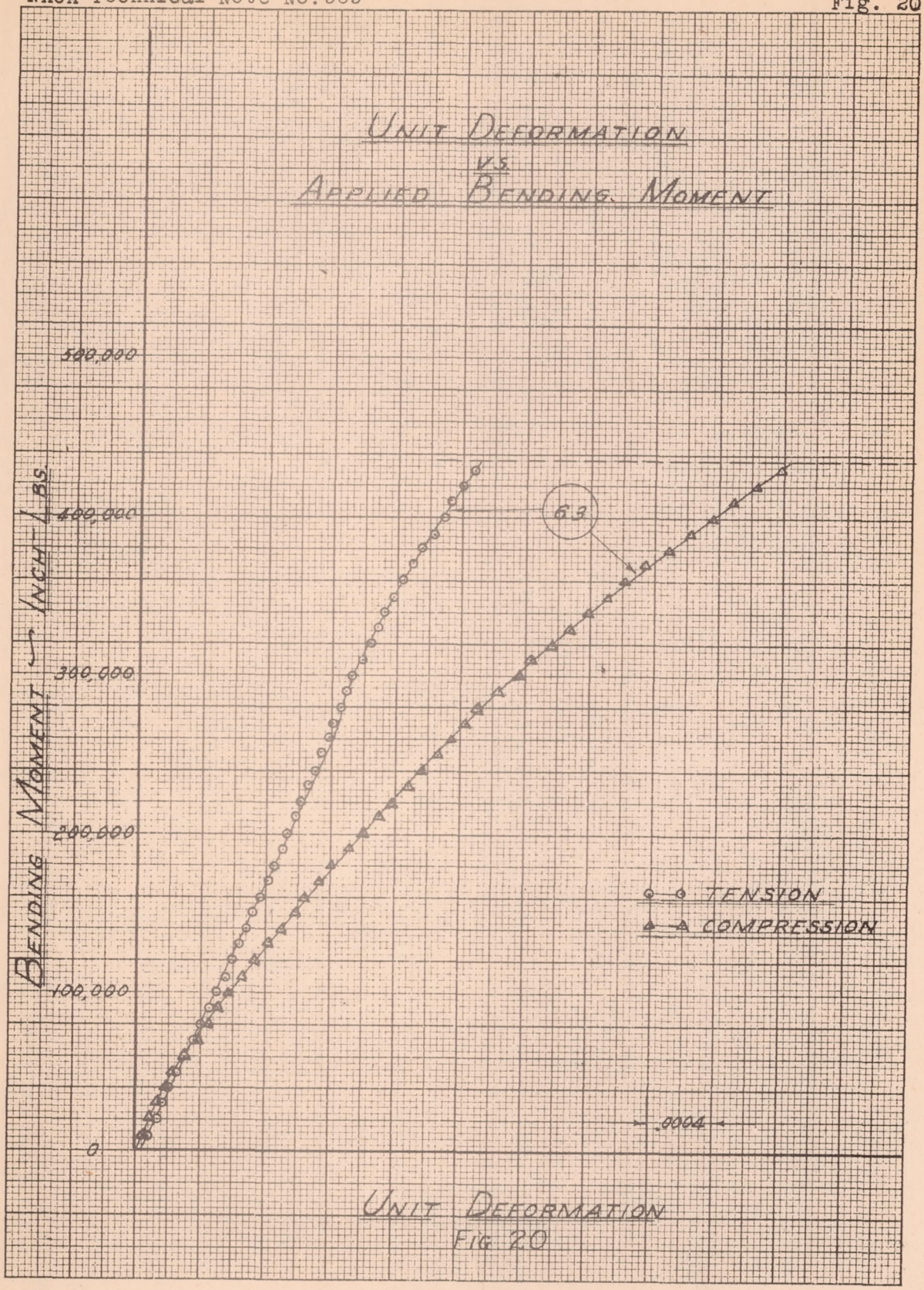
UNIT DEFORMATION
VS.
APPLIED BENDING MOMENT
500,000
400,000
300,000
200,000
100,000
0
BENDING MOMENT → INCH-LBS
63
TENSION
COMPRESSION
.0004
UNIT DEFORMATION

FIG 20

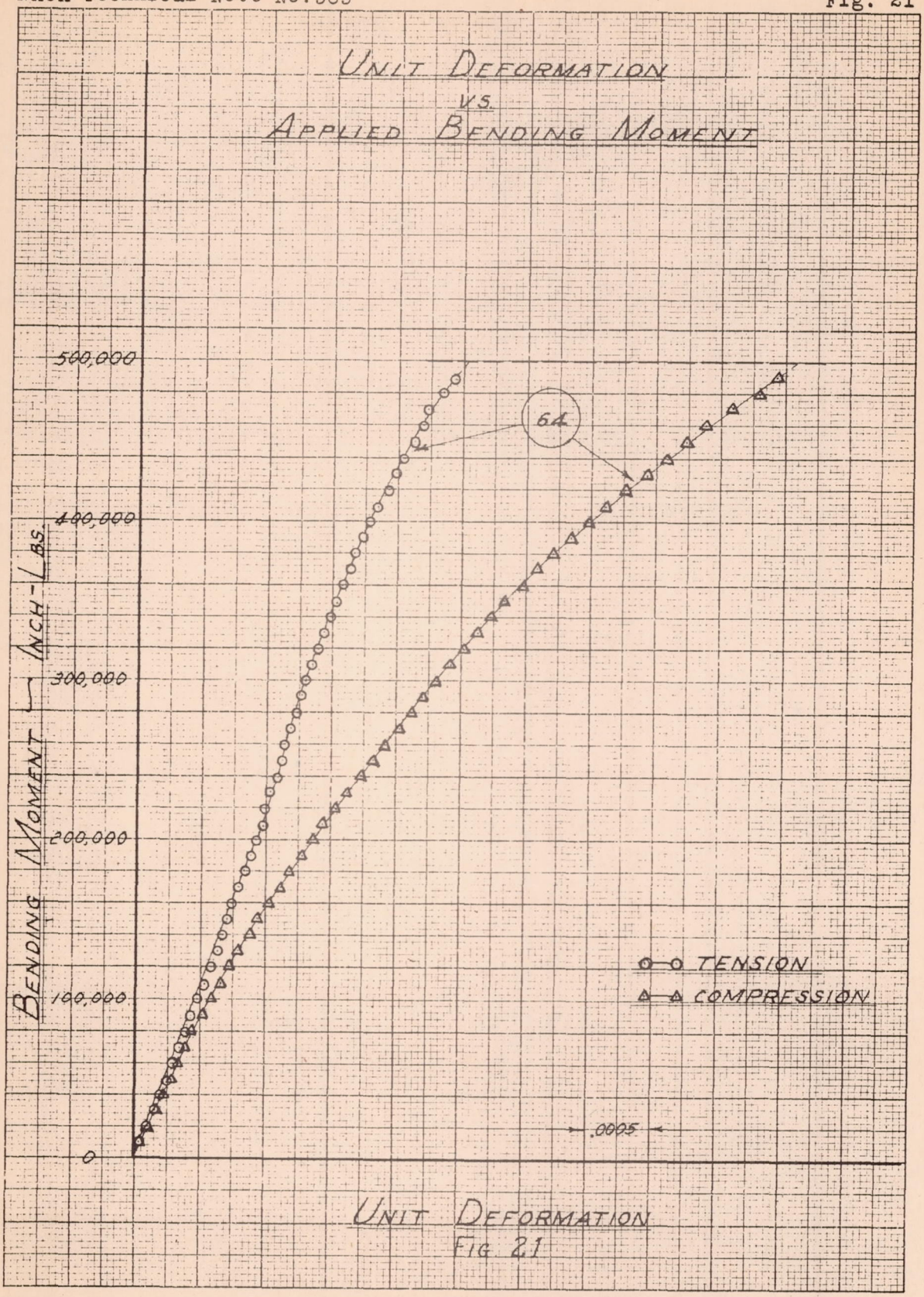
UNIT DEFORMATION
VS.
APPLIED BENDING MOMENT
BENDING MOMENT — INCH-LBS.
500,000
400,000
300,000
200,000
100,000
0
64
TENSION
COMPRESSION
.0005
UNIT DEFORMATION

FIG 21

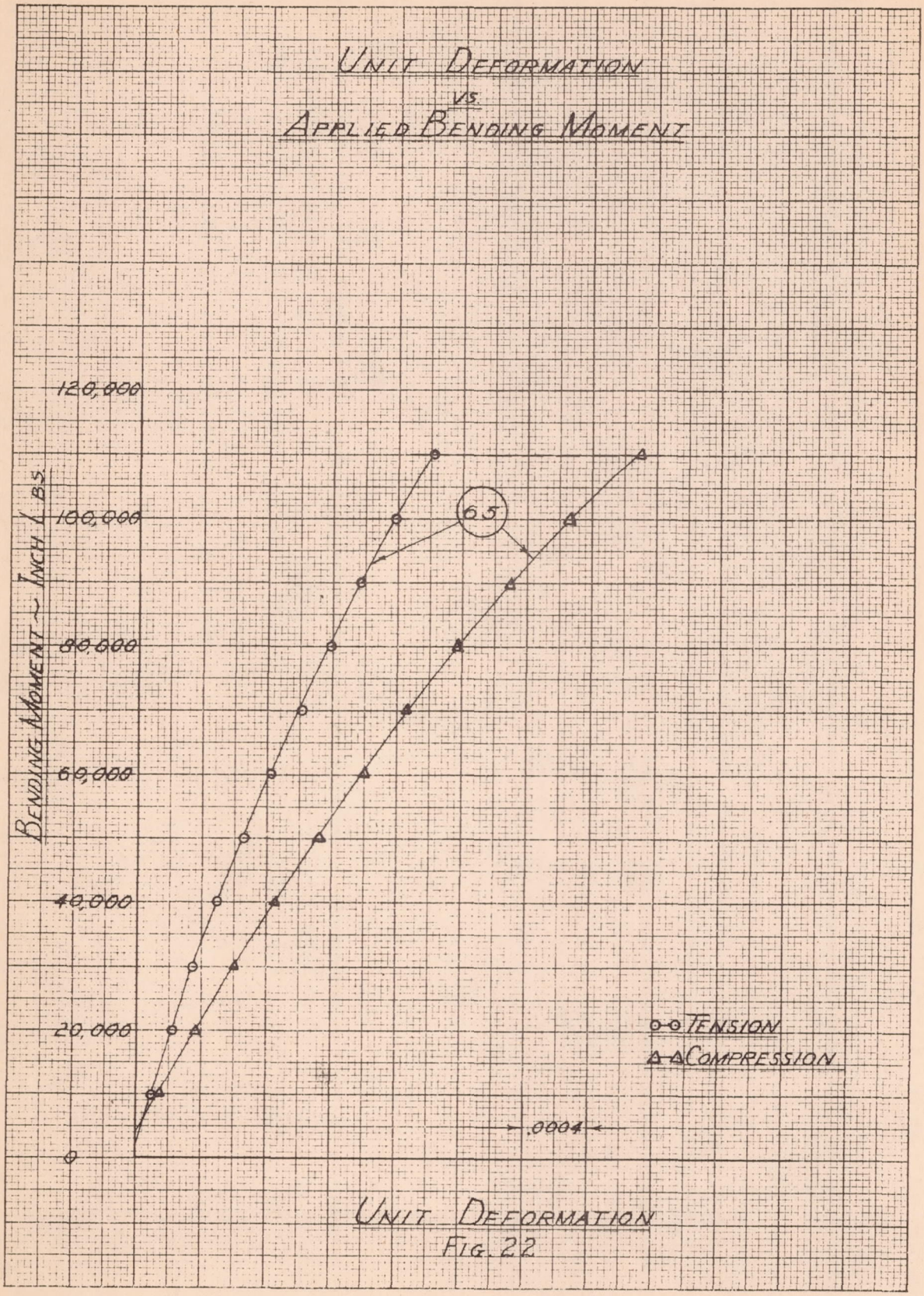
UNIT DEFORMATION
VS.
APPLIED BENDING MOMENT
BENDING MOMENT ~ INCH LBS.
120,000
100,000
80,000
60,000
40,000
20,000
0
65
.0004
TENSION
COMPRESSION
UNIT DEFORMATION

FIG. 22

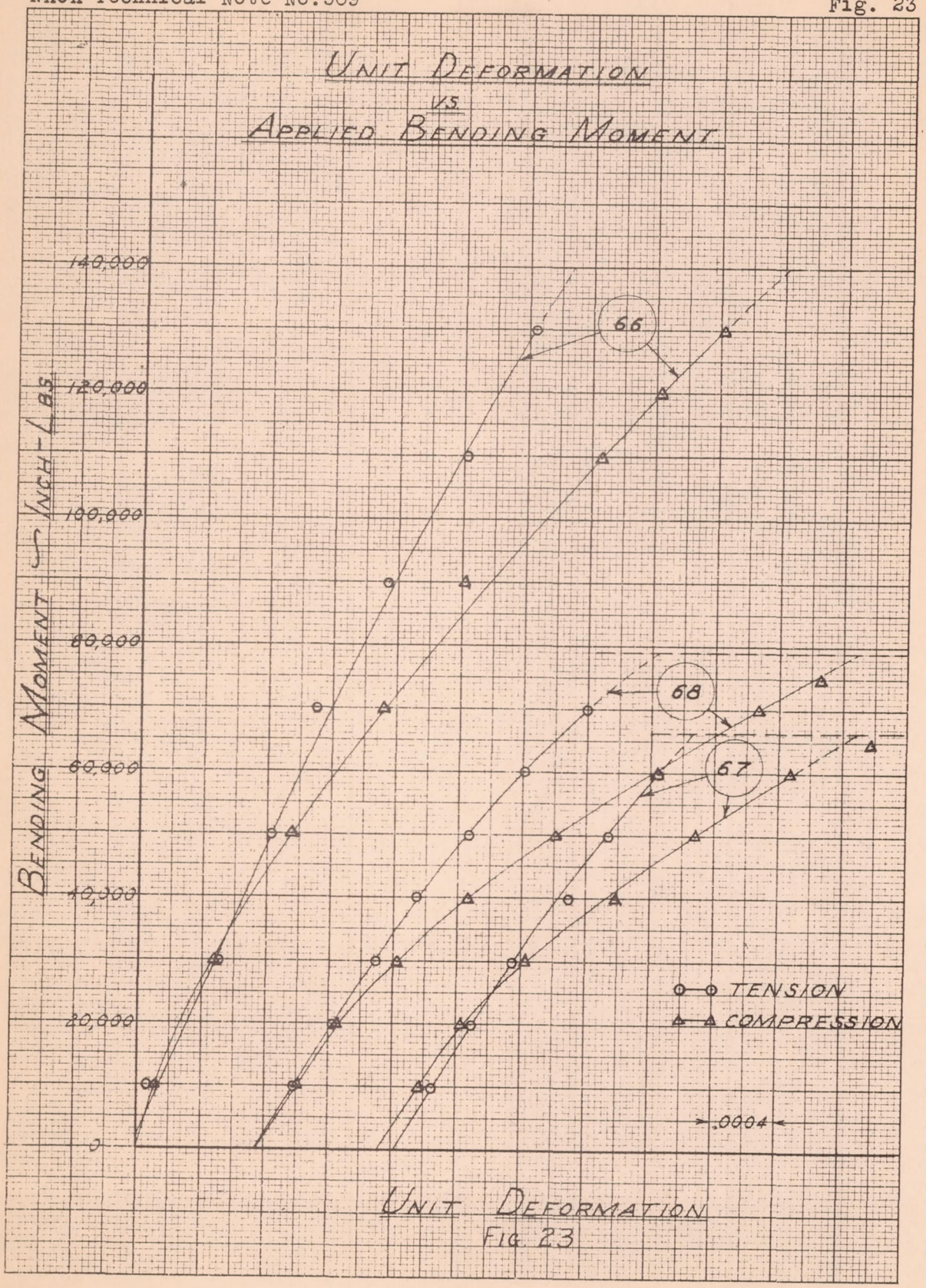
UNIT DEFORMATION
VS.
APPLIED BENDING MOMENT
BENDING MOMENT - INCH-LBS.
140,000
120,000
100,000
80,000
60,000
40,000
20,000
0
66
68
67
TENSION
COMPRESSION
.0004
UNIT DEFORMATION

FIG 23

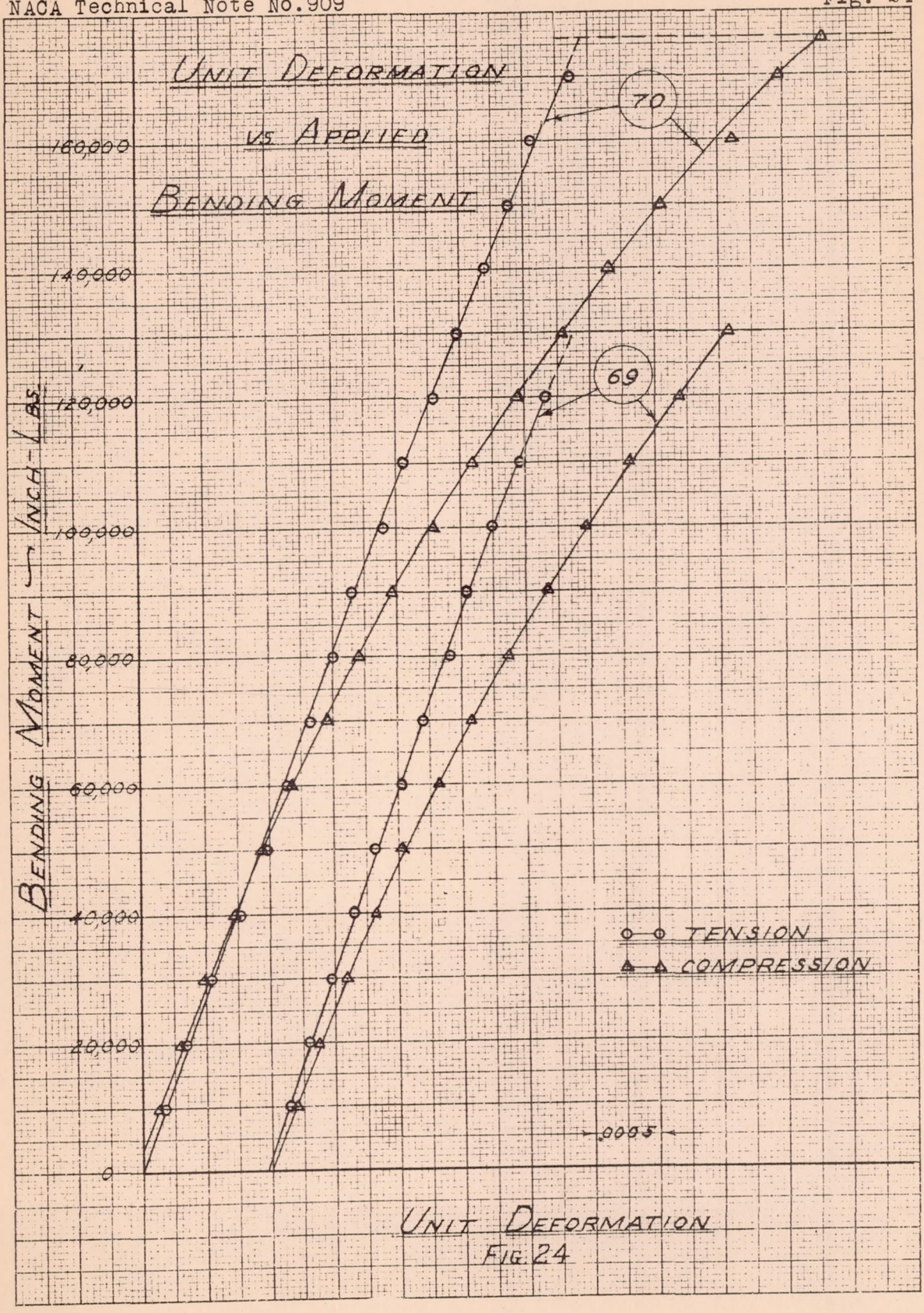
UNIT DEFORMATION
VS APPLIED
BENDING MOMENT
70
69
160,000
140,000
120,000
100,000
80,000
60,000
40,000
20,000
0
BENDING MOMENT IN INCH-LBS.
TENSION
COMPRESSION
.0005
UNIT DEFORMATION

FIG. 24

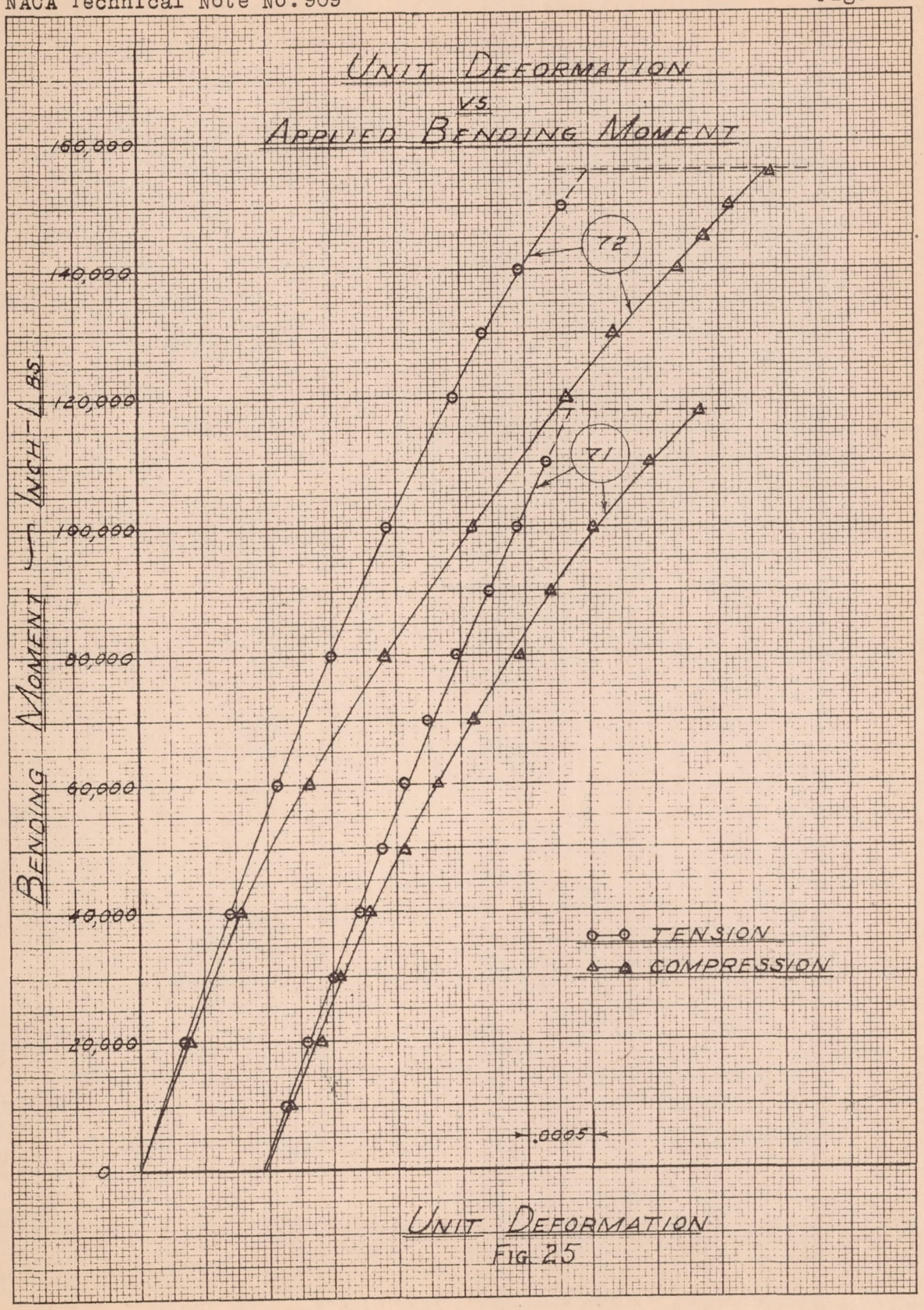
UNIT DEFORMATION
VS.
APPLIED BENDING MOMENT
BENDING MOMENT - INCH-LBS.
160,000
140,000
120,000
100,000
80,000
60,000
40,000
20,000
0
72
71
TENSION
COMPRESSION
.0005
UNIT DEFORMATION

FIG. 25

Fig. 26

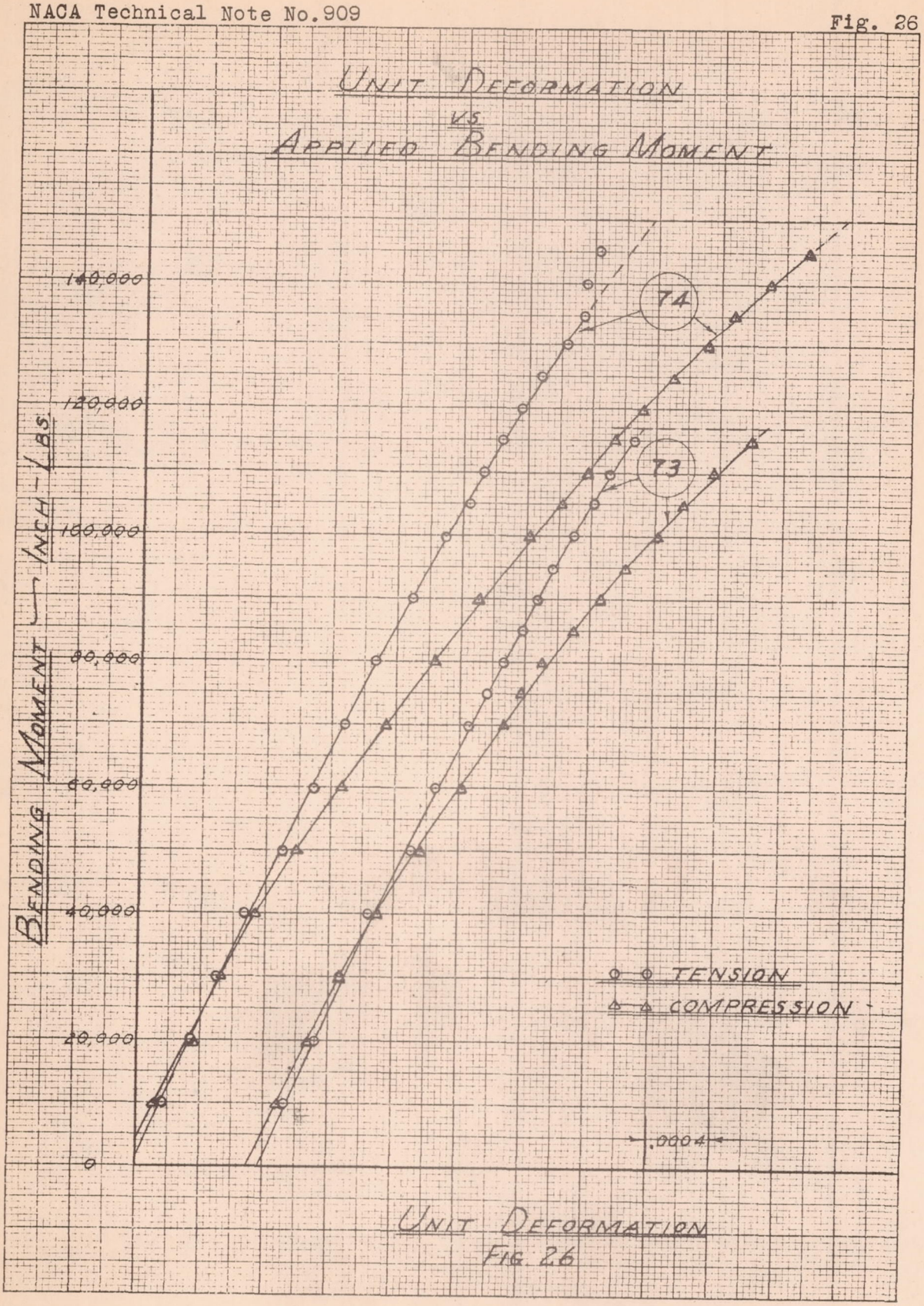
UNIT DEFORMATION
VS
APPLIED BENDING MOMENT
BENDING MOMENT - INCH-LBS
140,000
120,000
100,000
80,000
60,000
40,000
20,000
0
74
73
TENSION
COMPRESSION
.0004
UNIT DEFORMATION

FIG. 26

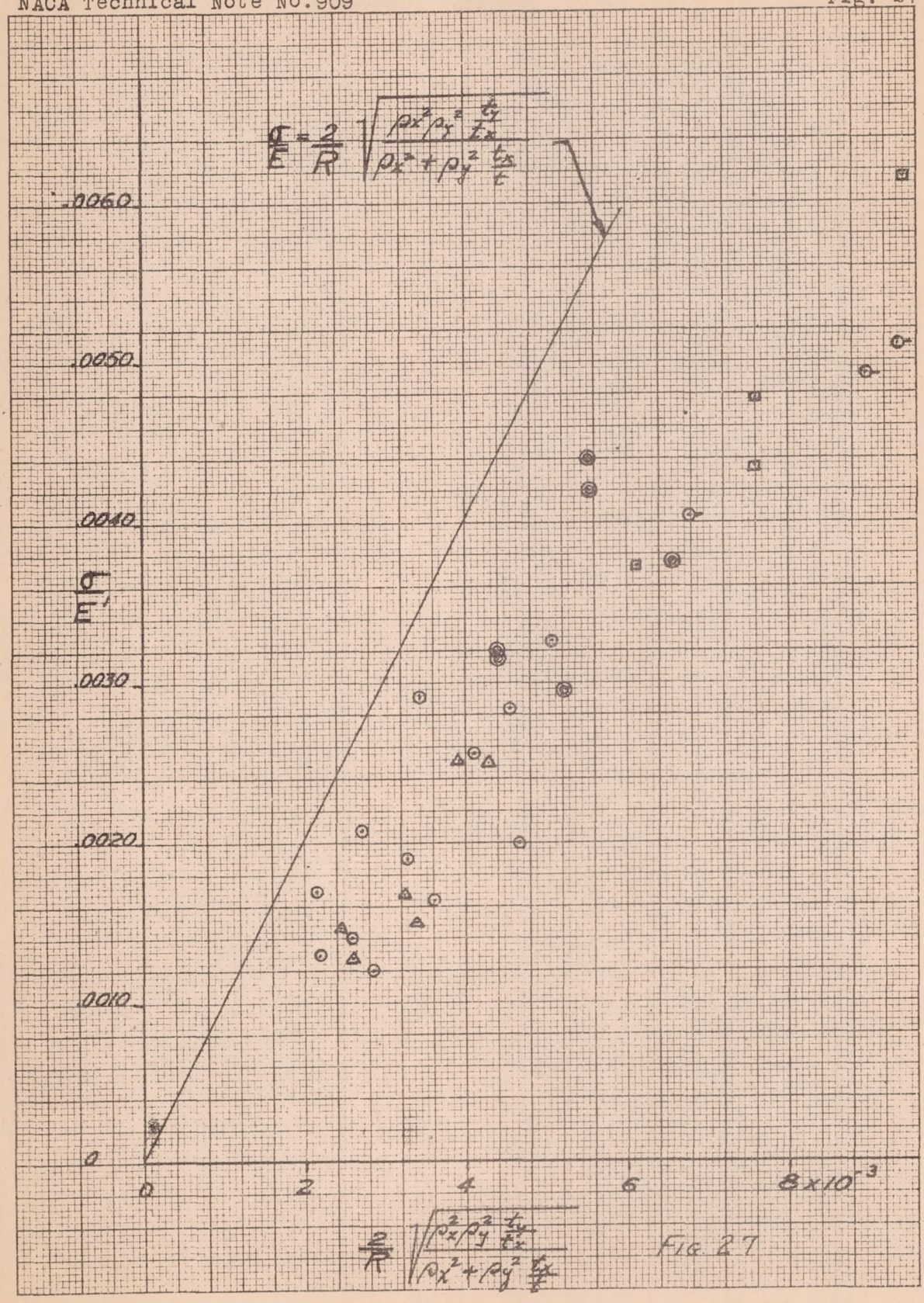
$\frac{\sigma}{E} = \frac{2}{R}\sqrt{\frac{\rho_x^2 \rho_y^2 \frac{t_y}{t_x}}{\rho_x^2 + \rho_y^2 \frac{t_x}{t}}}$
.0060
.0050
.0040
$\frac{\sigma}{E}$
.0030
.0020
.0010
0
0
2
4
6
8×10^{-3}
$\frac{2}{R}\sqrt{\frac{\rho_x^2 \rho_y^2 \frac{t_y}{t_x}}{\rho_x^2 + \rho_y^2 \frac{t_x}{t}}}$

Fig. 27

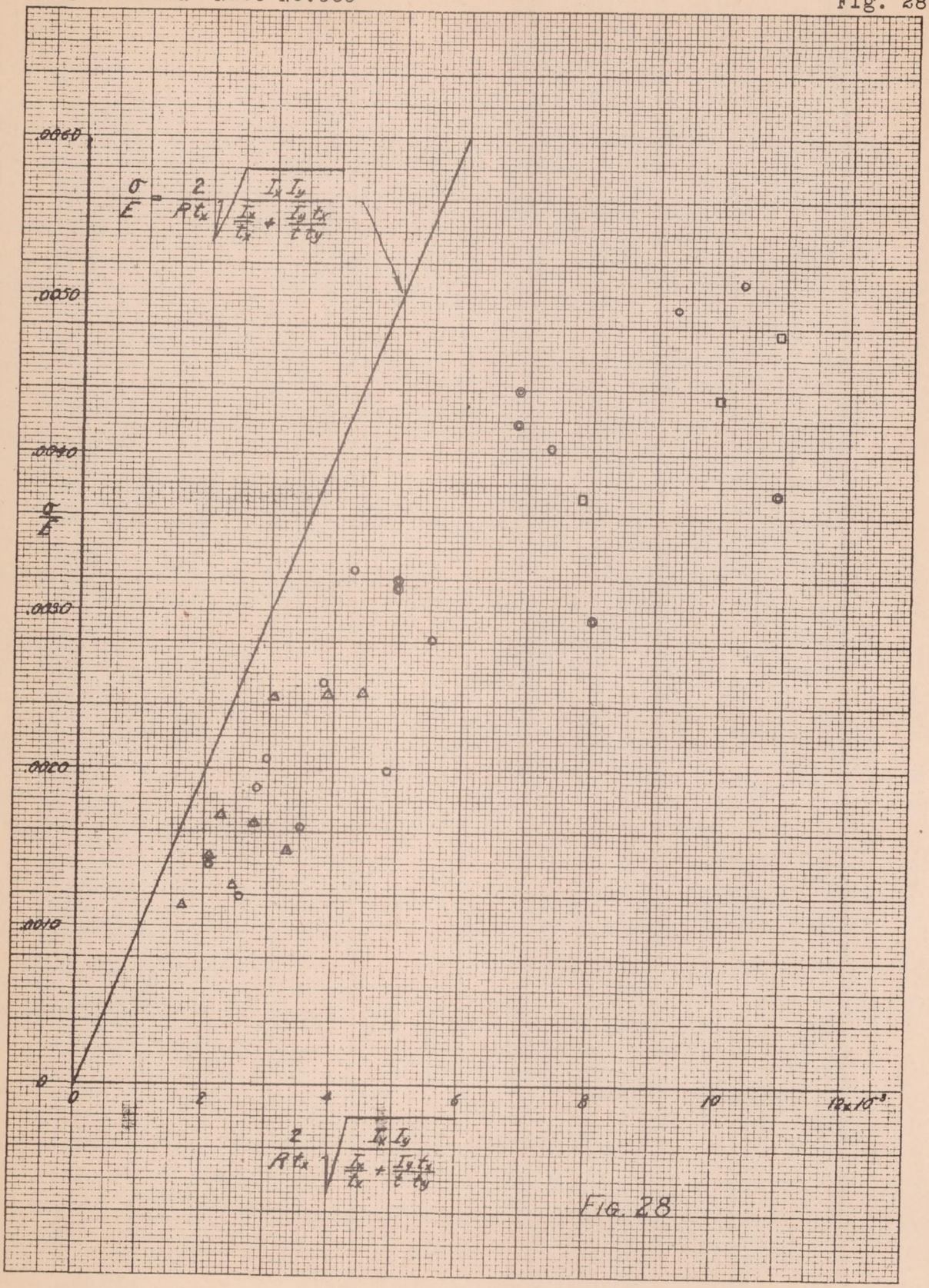
.0060
.0050
.0040
.0030
.0020
.0010
0
0
2
4
6
8
10
$R_x \times 10^{-3}$
$\frac{\sigma}{E} = \frac{2}{R t_x} \sqrt{\frac{I_x I_y}{\frac{I_x}{t_x} + \frac{I_y}{t} \frac{t_x}{t_y}}}$
$\frac{\sigma}{E}$
$\frac{2}{R t_x} \sqrt{\frac{I_x I_y}{\frac{I_x}{t_x} + \frac{I_y}{t} \frac{t_x}{t_y}}}$

FIG. 28

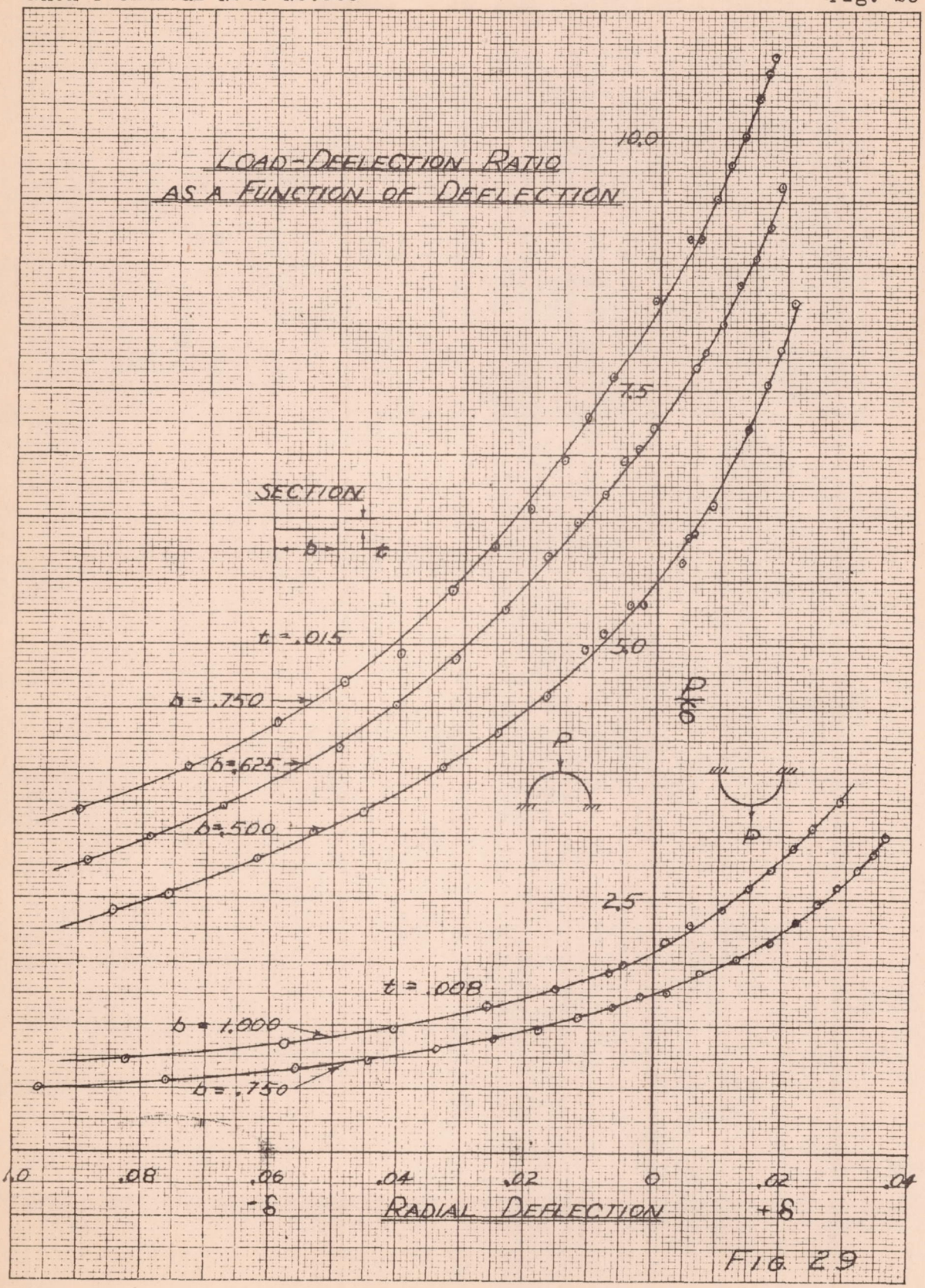
LOAD-DEFLECTION RATIO
AS A FUNCTION OF DEFLECTION
10.0
7.5
5.0
2.5
P/δ
SECTION
b
t
t = .015
b = .750
b = .625
b = .500
t = .008
b = 1.000
b = .750
P
P
.10
.08
.06
.04
.02
0
.02
.04
-δ
RADIAL DEFLECTION
+δ

FIG 29

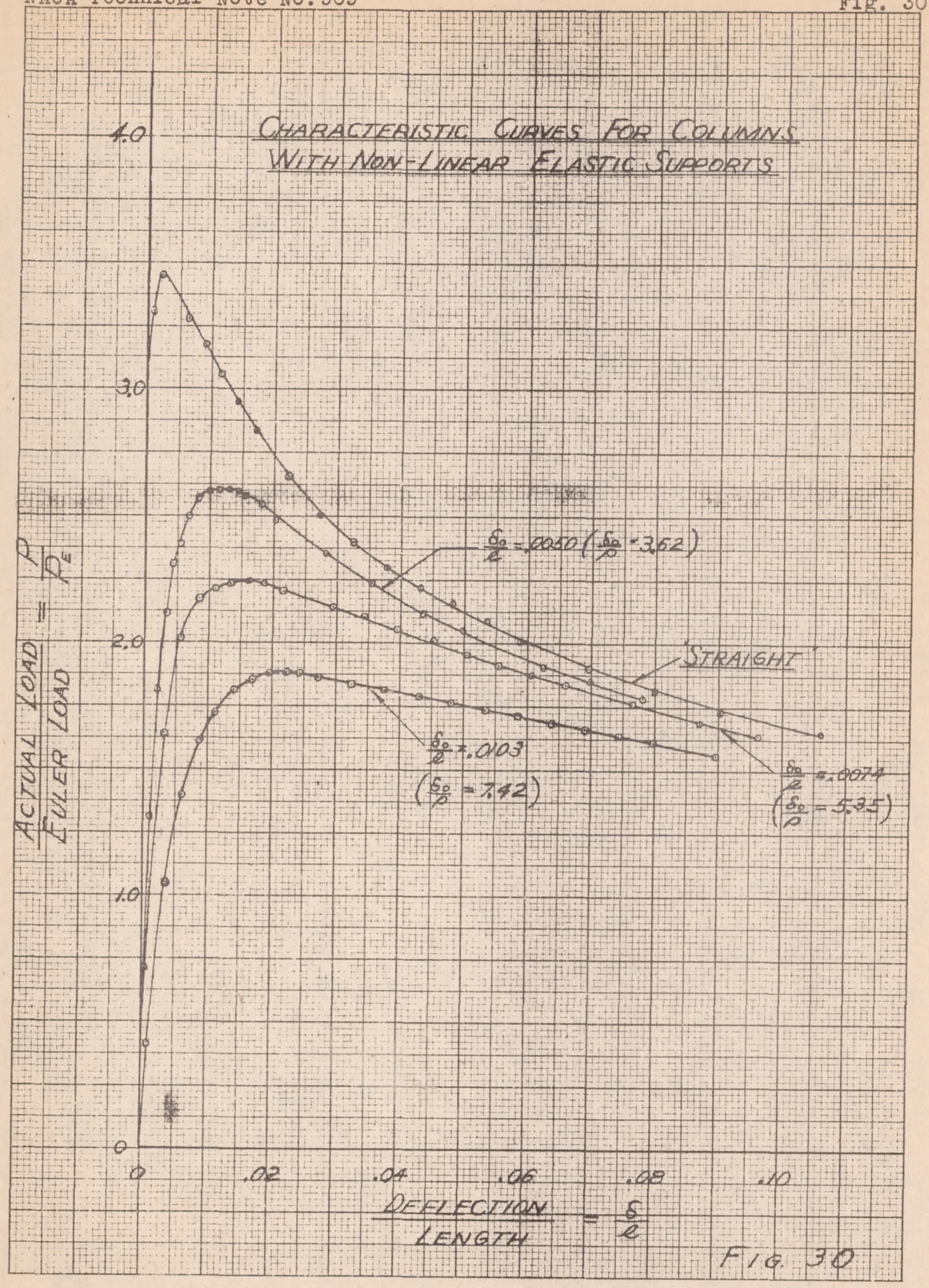
CHARACTERISTIC CURVES FOR COLUMNS WITH NON-LINEAR ELASTIC SUPPORTS
4.0
3.0
2.0
1.0
0
ACTUAL LOAD / EULER LOAD = P/Pe
δo/ℓ = .0050 (δo/ρ = 3.62)
STRAIGHT
δo/ℓ = .0103 (δo/ρ = 7.42)
δo/ℓ = .0074 (δo/ρ = 5.35)
0
.02
.04
.06
.08
.10
DEFLECTION / LENGTH = δ/ℓ

FIG. 30

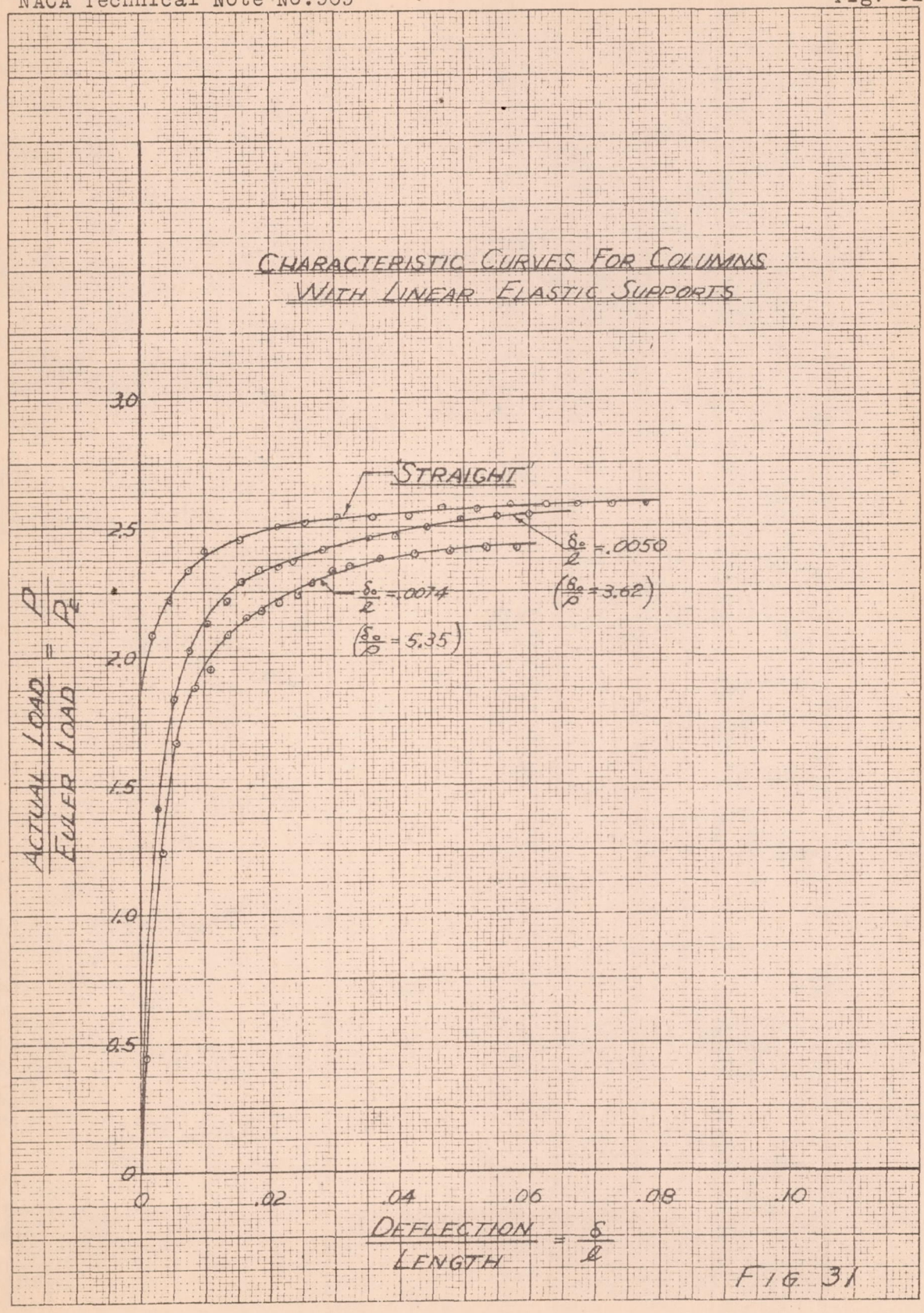
CHARACTERISTIC CURVES FOR COLUMNS
WITH LINEAR ELASTIC SUPPORTS
STRAIGHT
$\frac{\delta_0}{\ell} = .0050$
$\left(\frac{\delta_0}{\rho} = 3.62\right)$
$\frac{\delta_0}{\ell} = .0074$
$\left(\frac{\delta_0}{\rho} = 5.35\right)$
ACTUAL LOAD / EULER LOAD = $\frac{P}{P_E}$
3.0
2.5
2.0
1.5
1.0
0.5
0
0
.02
.04
.06
.08
.10
DEFLECTION / LENGTH = $\frac{\delta}{\ell}$
FIG 31

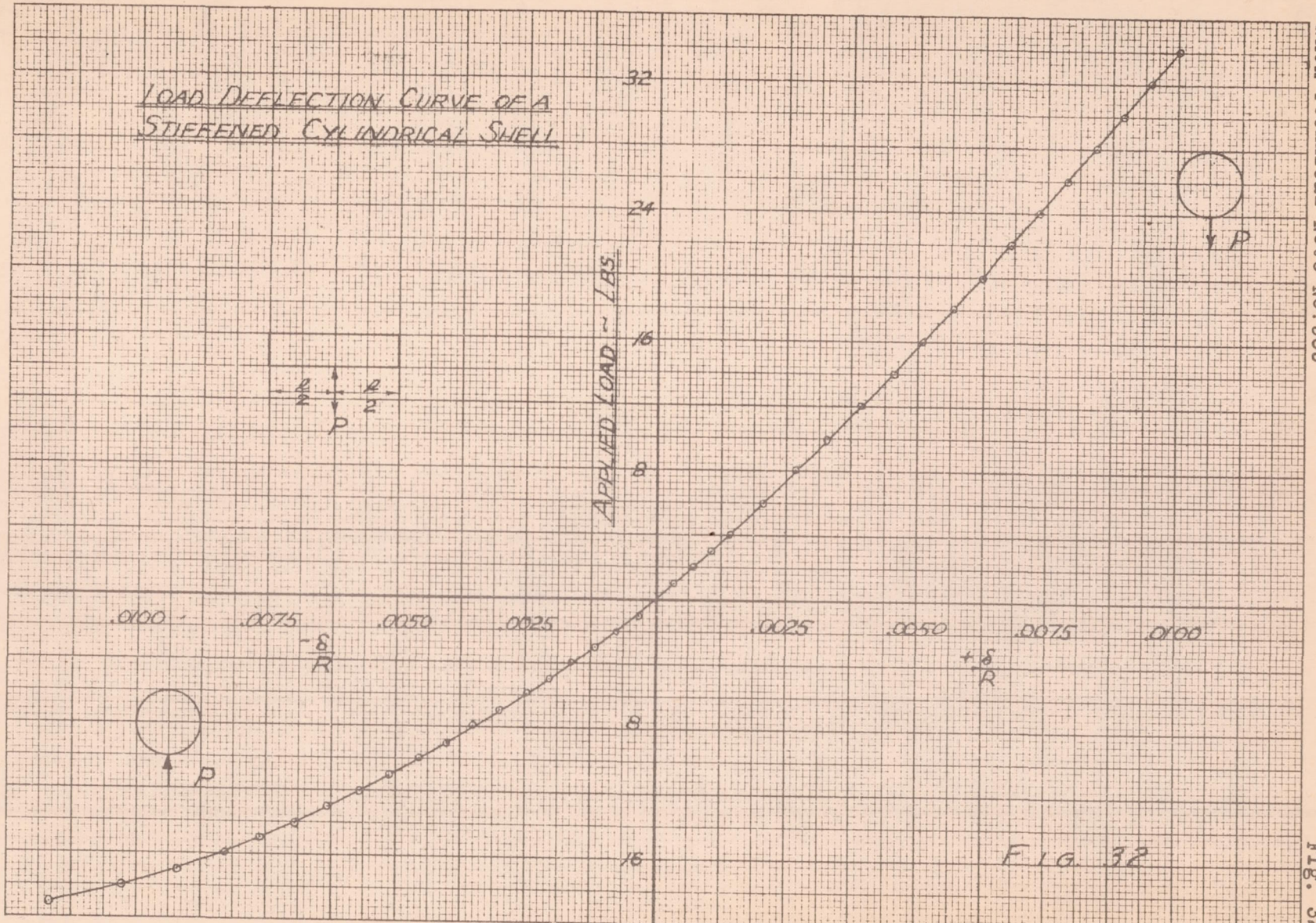
LOAD DEFLECTION CURVE OF A STIFFENED CYLINDRICAL SHELL
APPLIED LOAD ~ LBS.
32
24
16
8
8
16
.0100
.0075
.0050
.0025
-δ/R
.0025
.0050
.0075
.0100
+δ/R
P
P
P

FIG. 32

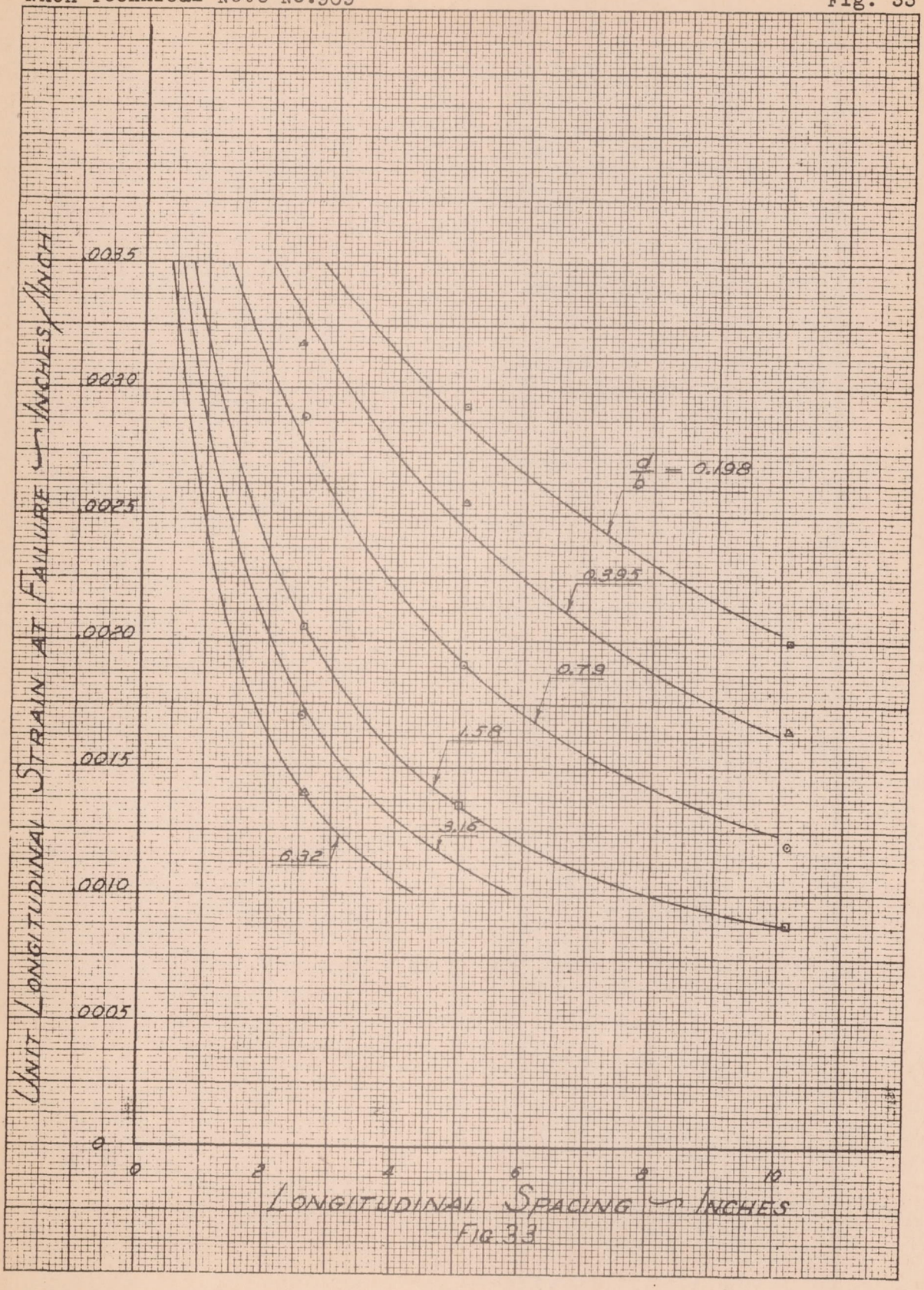
Unit Longitudinal Strain at Failure ~ Inches/Inch
.0035
.0030
.0025
.0020
.0015
.0010
.0005
0
0
2
4
6
8
10
Longitudinal Spacing ~ Inches
d/b = 0.198
0.395
0.79
1.58
3.16
6.32

Fig. 33

Fig. 34

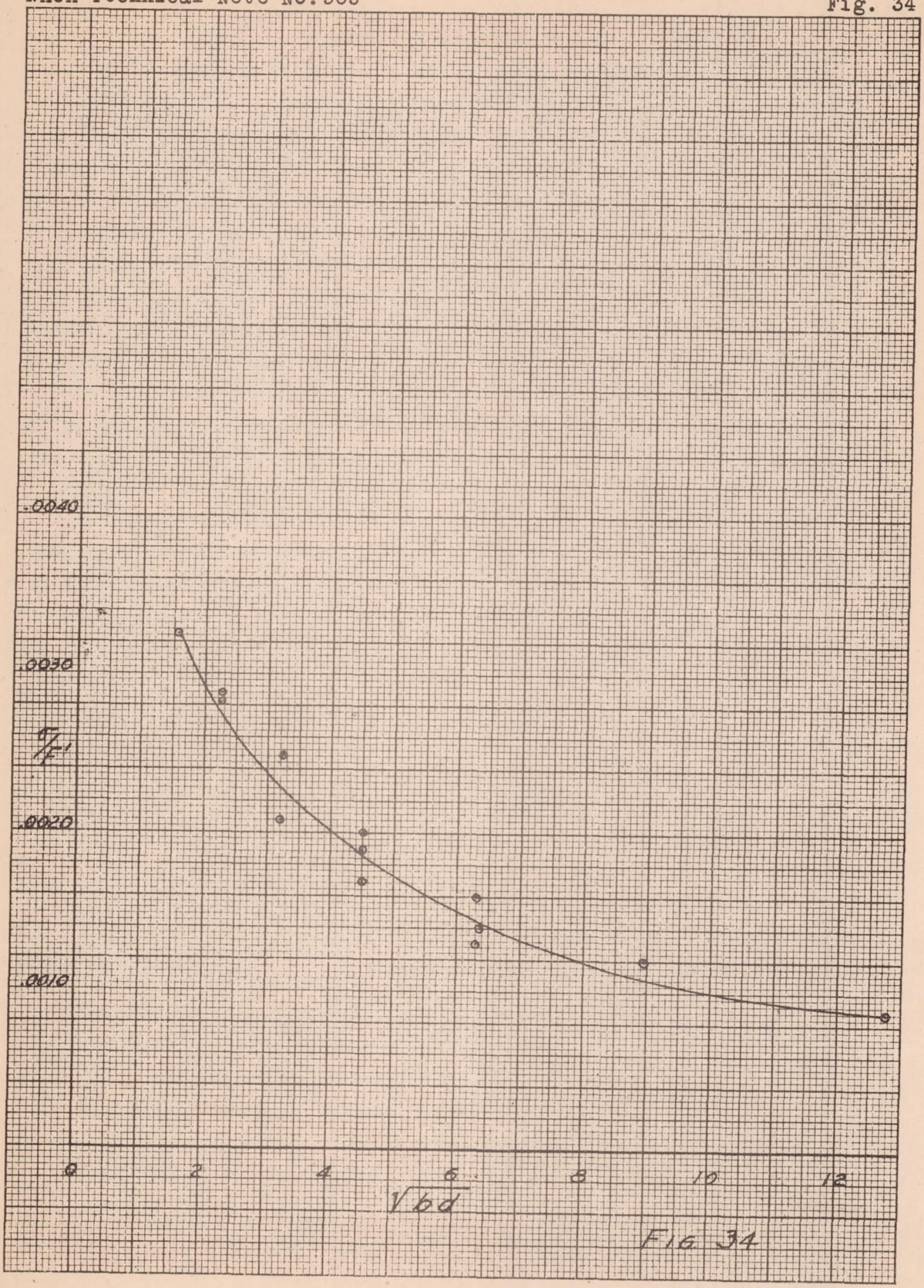

FIG. 34

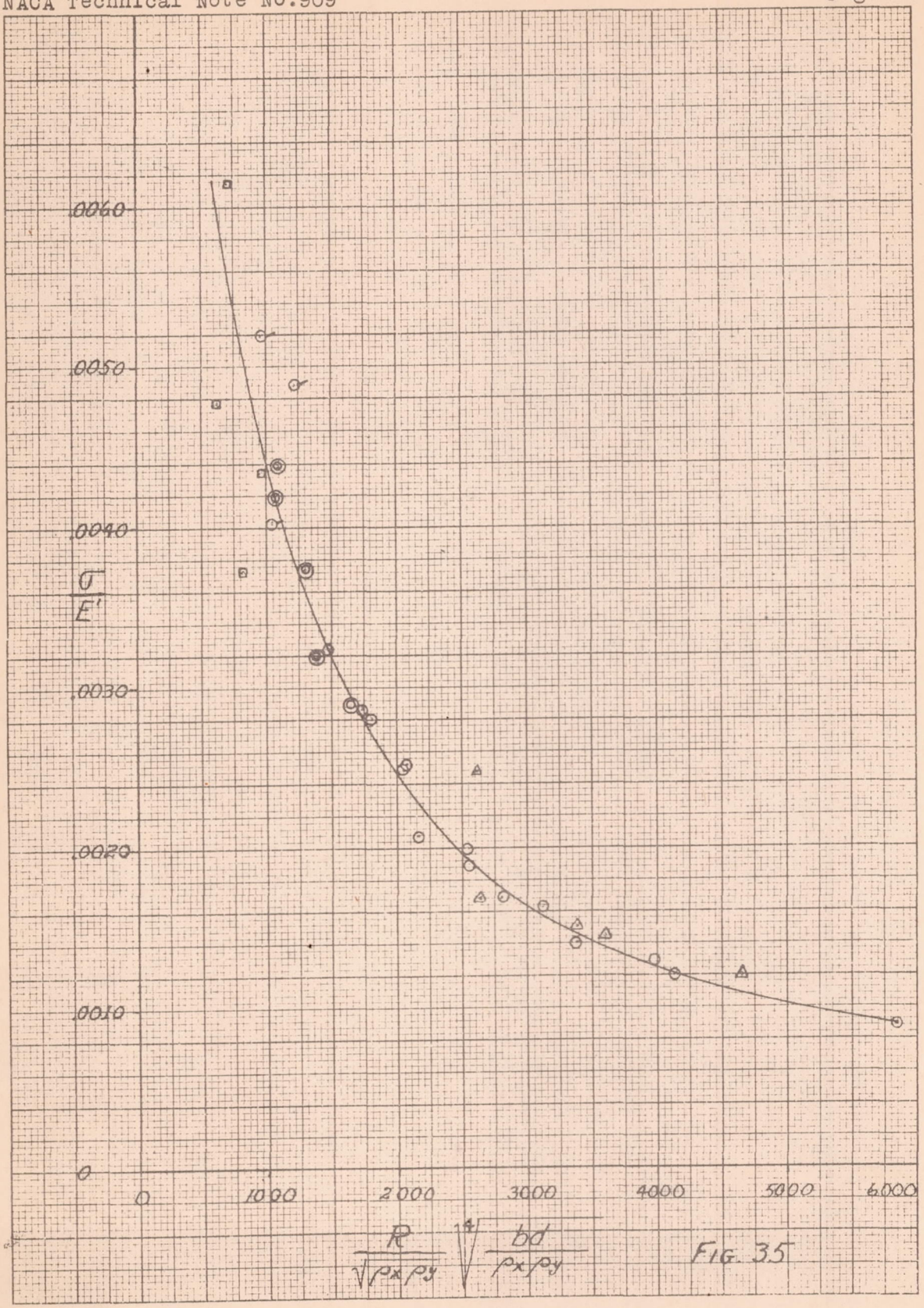
.0060
.0050
.0040
$\frac{\sigma}{E'}$
.0030
.0020
.0010
0
0
1000
2000
3000
4000
5000
6000
$\frac{R}{\sqrt{p_x p_y}} \sqrt{\frac{bd}{p_x p_y}}$

FIG. 35

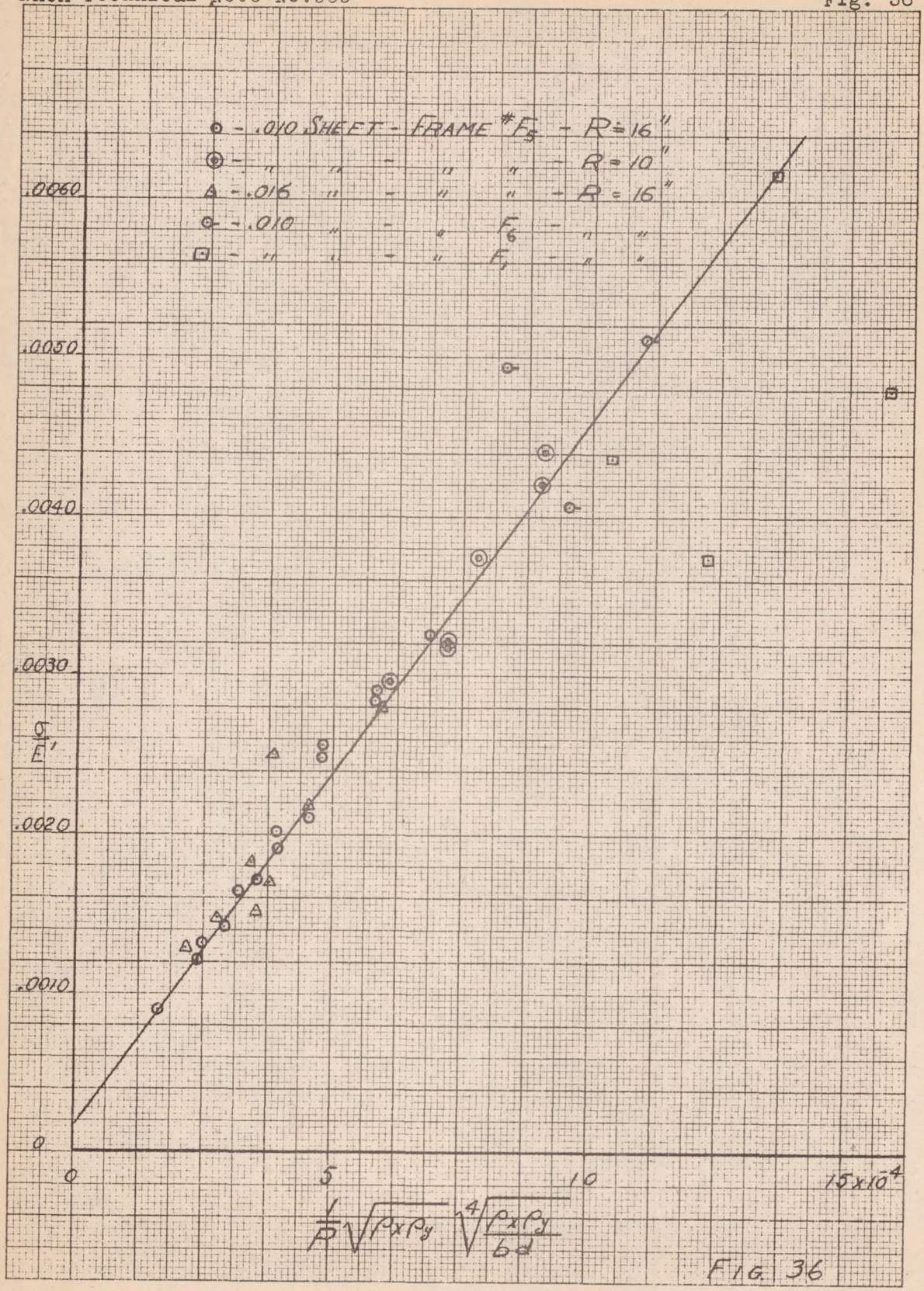
○ - .010 SHEET - FRAME *F5 - R = 16"
◎ - " " - " " - R = 10"
△ - .016 " - " " - R = 16"
⊙ - .010 " - " F6 - " "
⊡ - " " - " F7 - " "
.0060
.0050
.0040
.0030
σ/E'
.0020
.0010
0
0
5
10
15x10⁻⁴
1/P √(Px Py) ⁴√(Px Py / bd)

FIG. 36

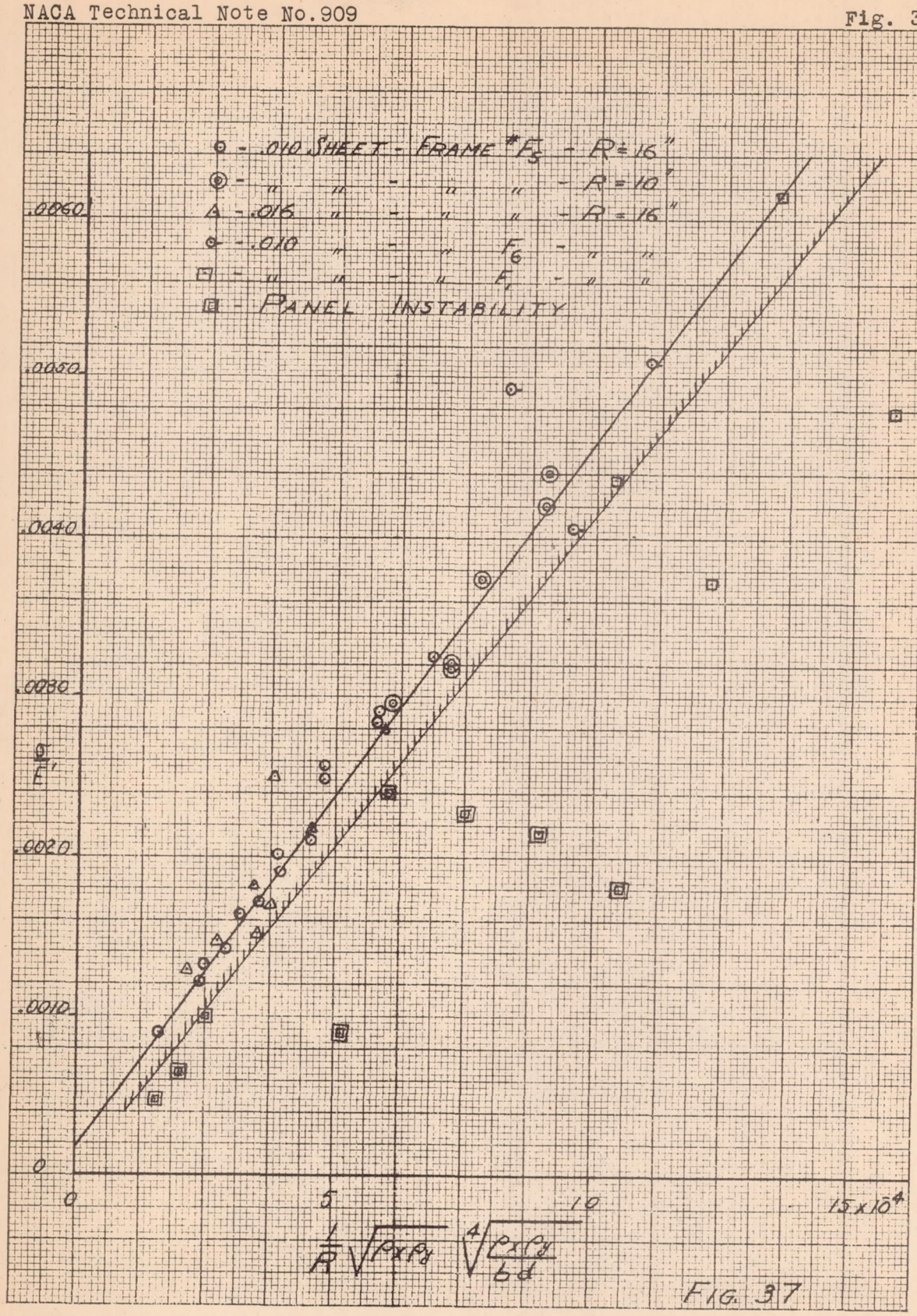
⊙ - .010 Sheet - Frame #F5 - R=16"
◎ - " " - " " - R=10"
Δ - .016 " - " " - R=16"
⊙ - .010 " - " F6 - " "
□ - " " - " F7 - " "
▣ - Panel Instability
.0060
.0050
.0040
.0030
.0020
.0010
0
0
5
10
15 x 10⁴
σ/E'
1/P √(ρx ρy) ⁴√(ρx ρy / b d)

FIG. 37

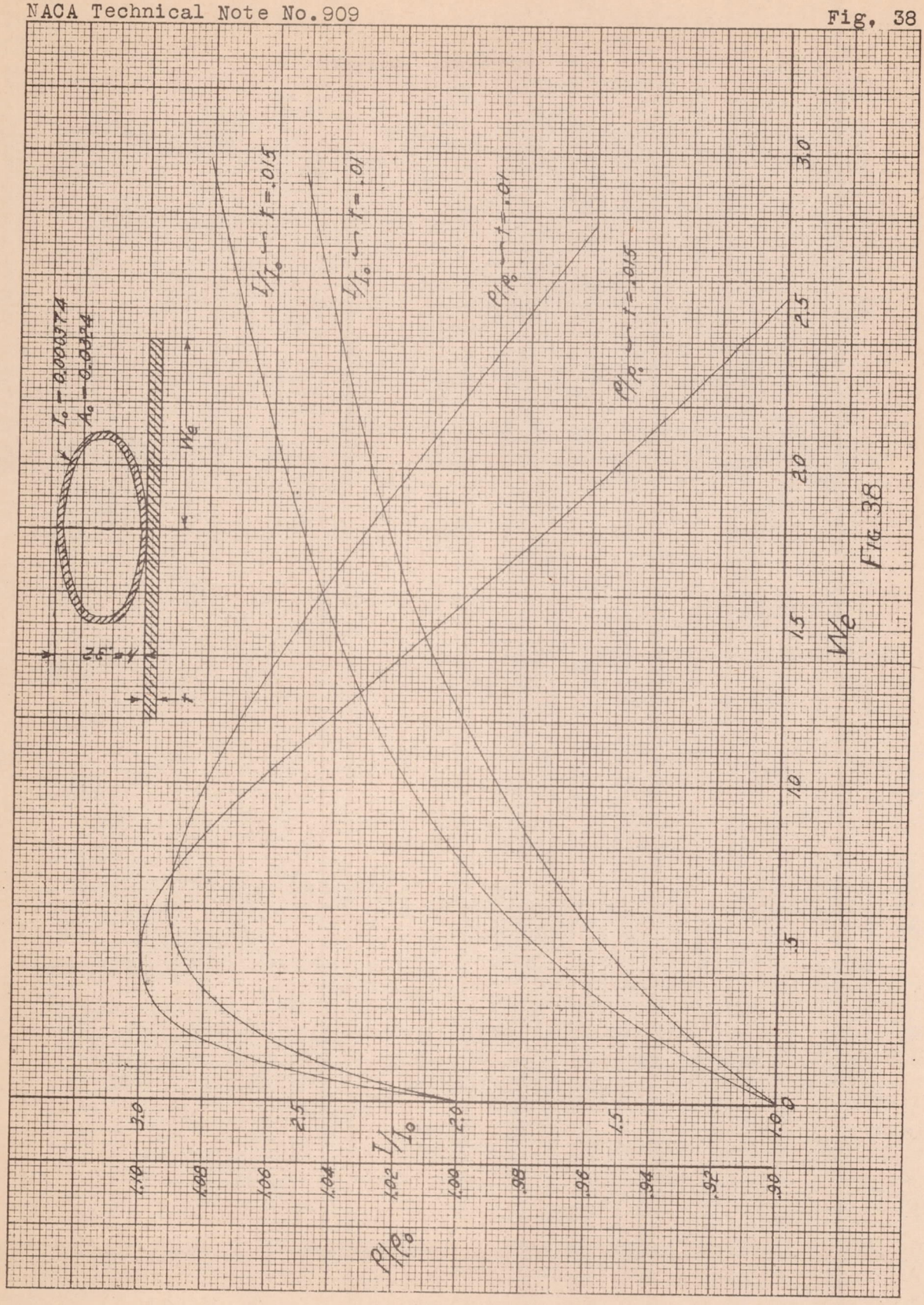
$I_o = 0.000372$
$A_o = 0.0274$
W_o
t
I/I_o t=.015
I/I_o t=.01
P/P_o t=.01
P/P_o t=.015
P/P_o
I/I_o
W_o
0
.5
1.0
1.5
2.0
2.5
3.0
.90
.92
.94
.96
.98
1.00
1.02
1.04
1.06
1.08
1.10
Fig. 38

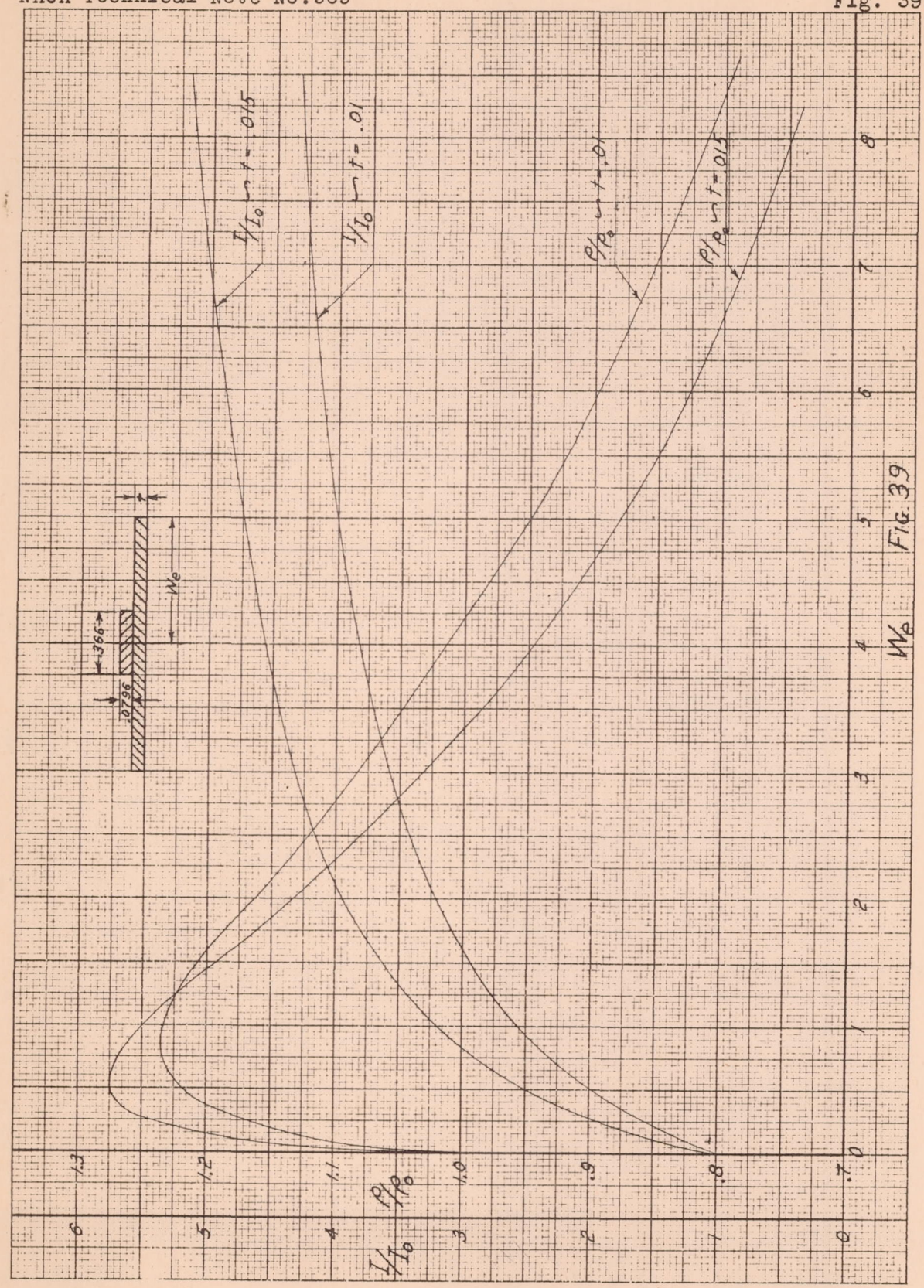
I/I₀ — t = .015
I/I₀ — t = .01
p/p₀ — t = .01
p/p₀ — t = .015
We
.366
.0796
t
I/I₀
p/p₀
We
Fig. 39

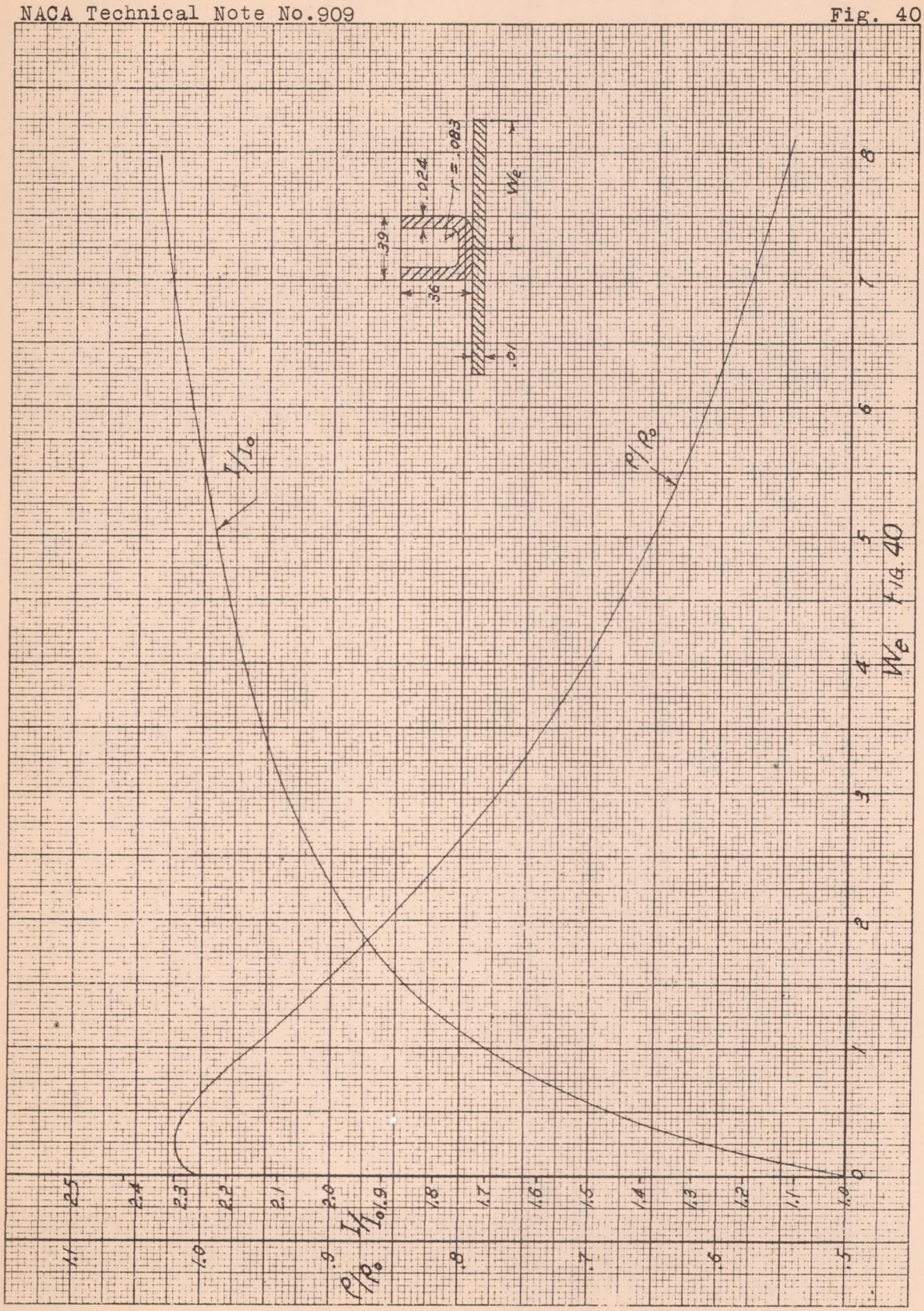
I/I0
p/p0
We
Fig. 40
.083
.024
.39
.36
.01
We

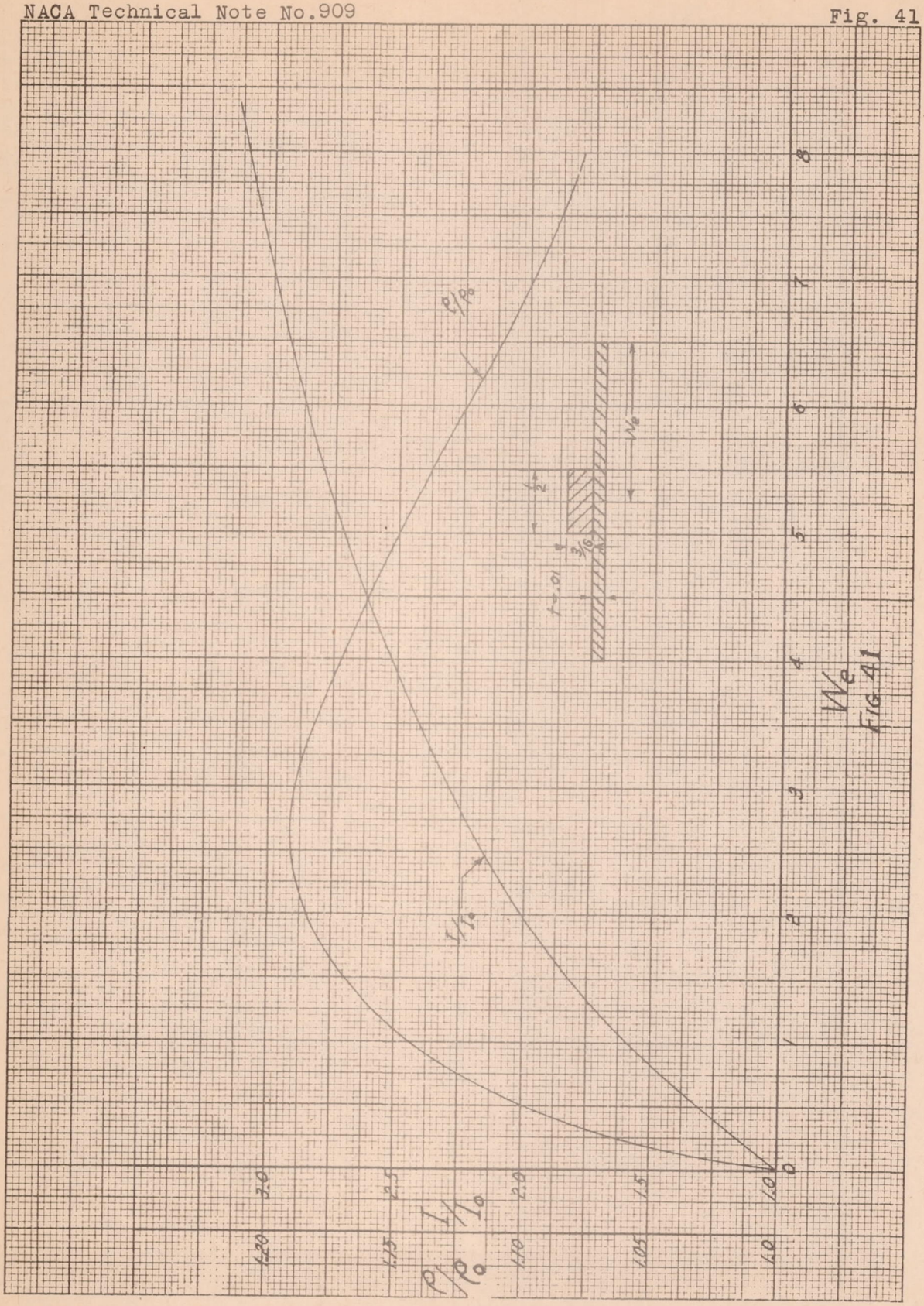
ρ/ρ0
T/T0
V/Ve
Fig. 41
t=.01
3/16
1/2
Ve
2.0
1.20
1.5
1.10
1.0
1.05
1.0
0
1
2
3
4
5
6
7
8

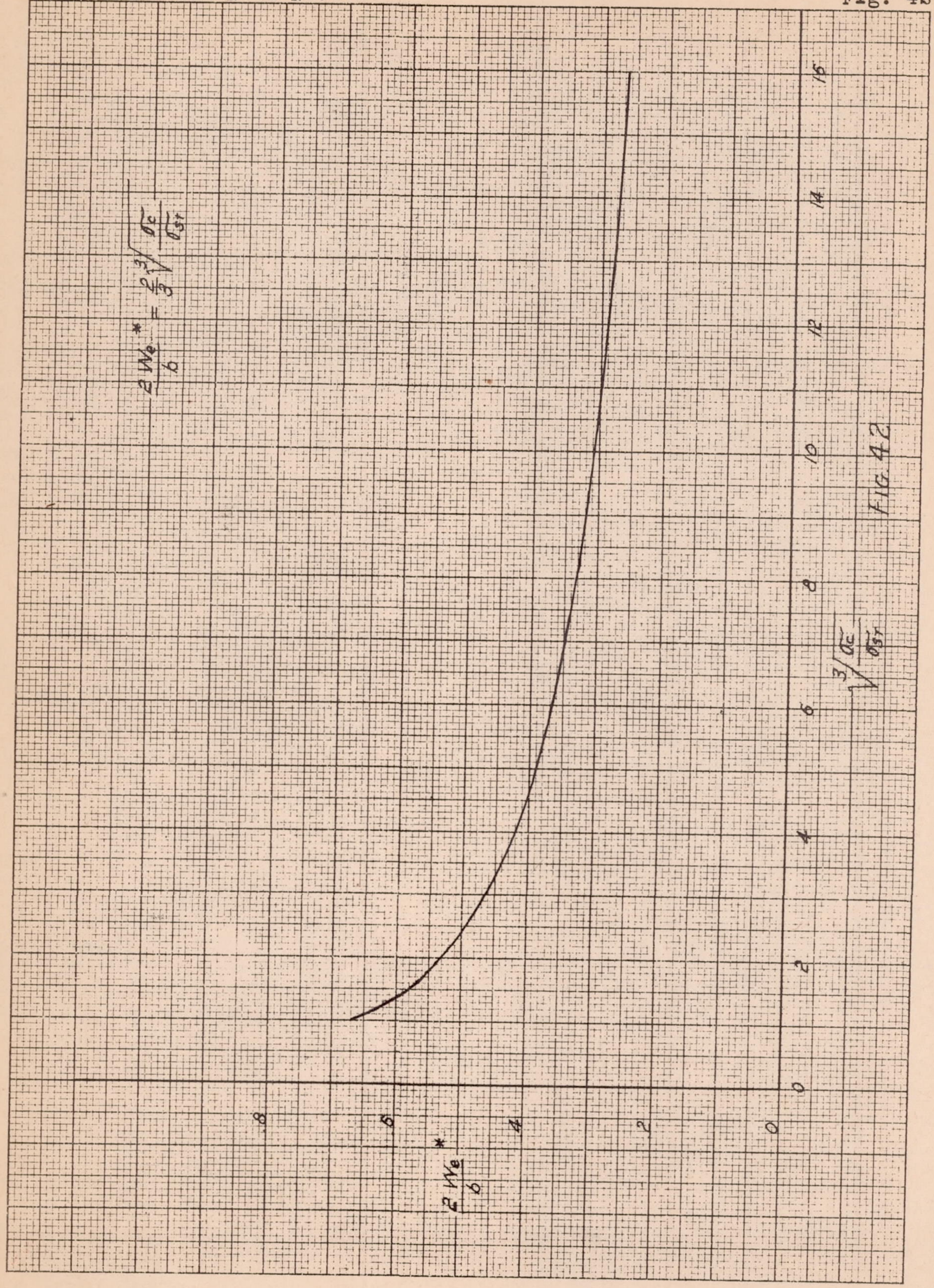
2We*/b = 2/3 ∛(σc/σst)
0
2
4
6
8
10
12
14
16
∛(σc/σst)
0
2
4
6
8
2We*/b
FIG. 42

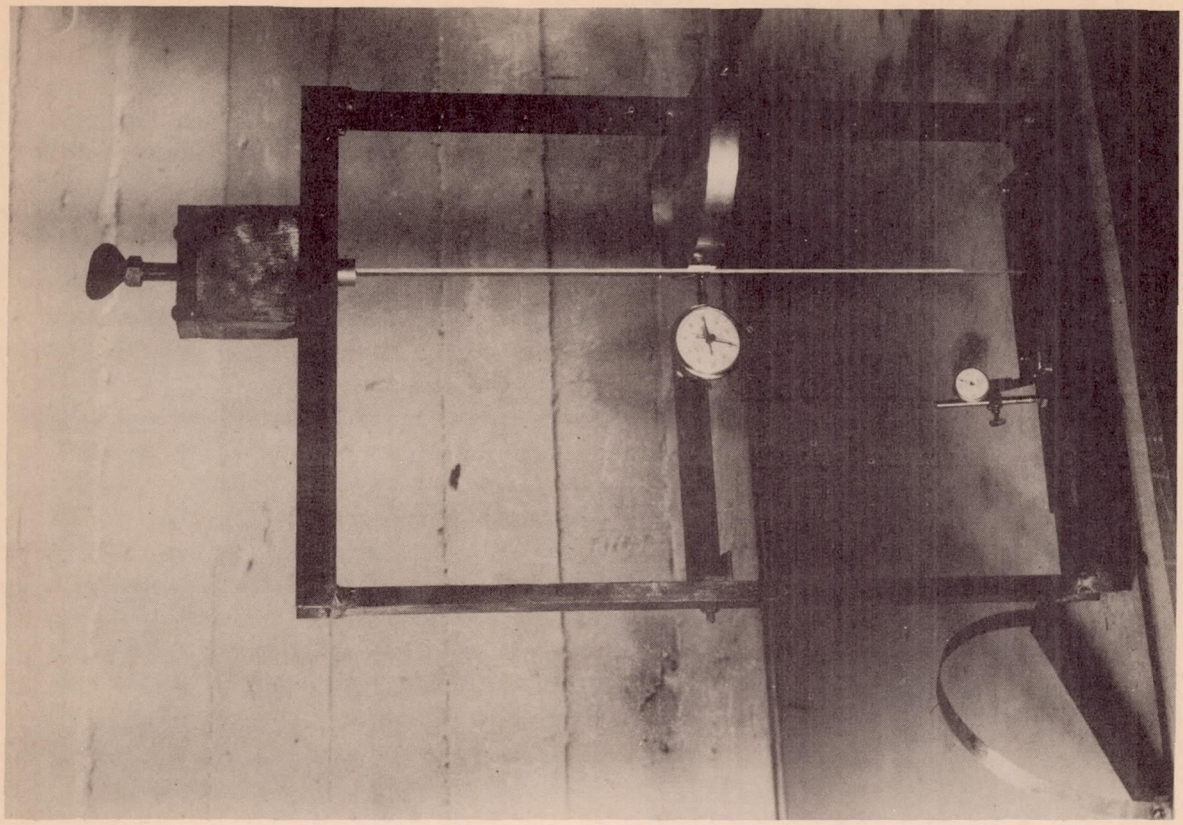

Figure 43. Test apparatus

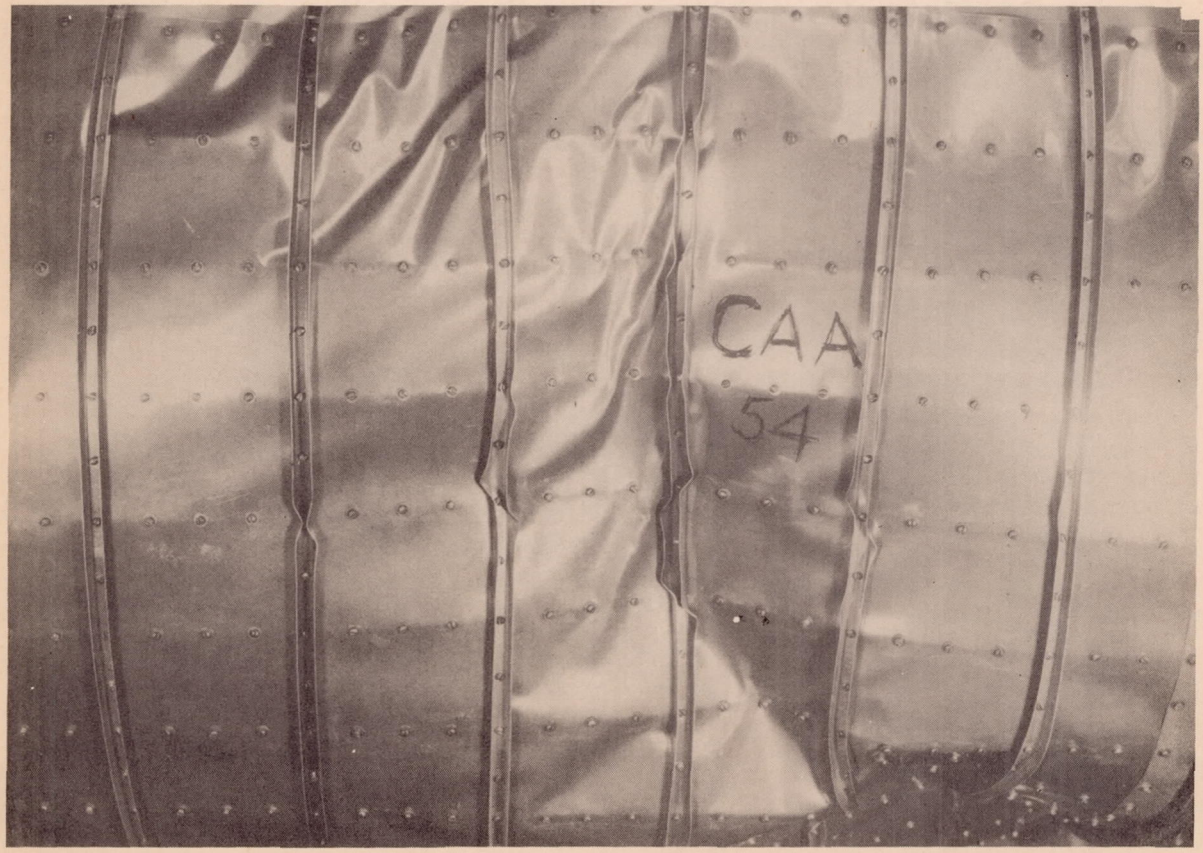

Figure 44. Local instability failure of the channel section frames.

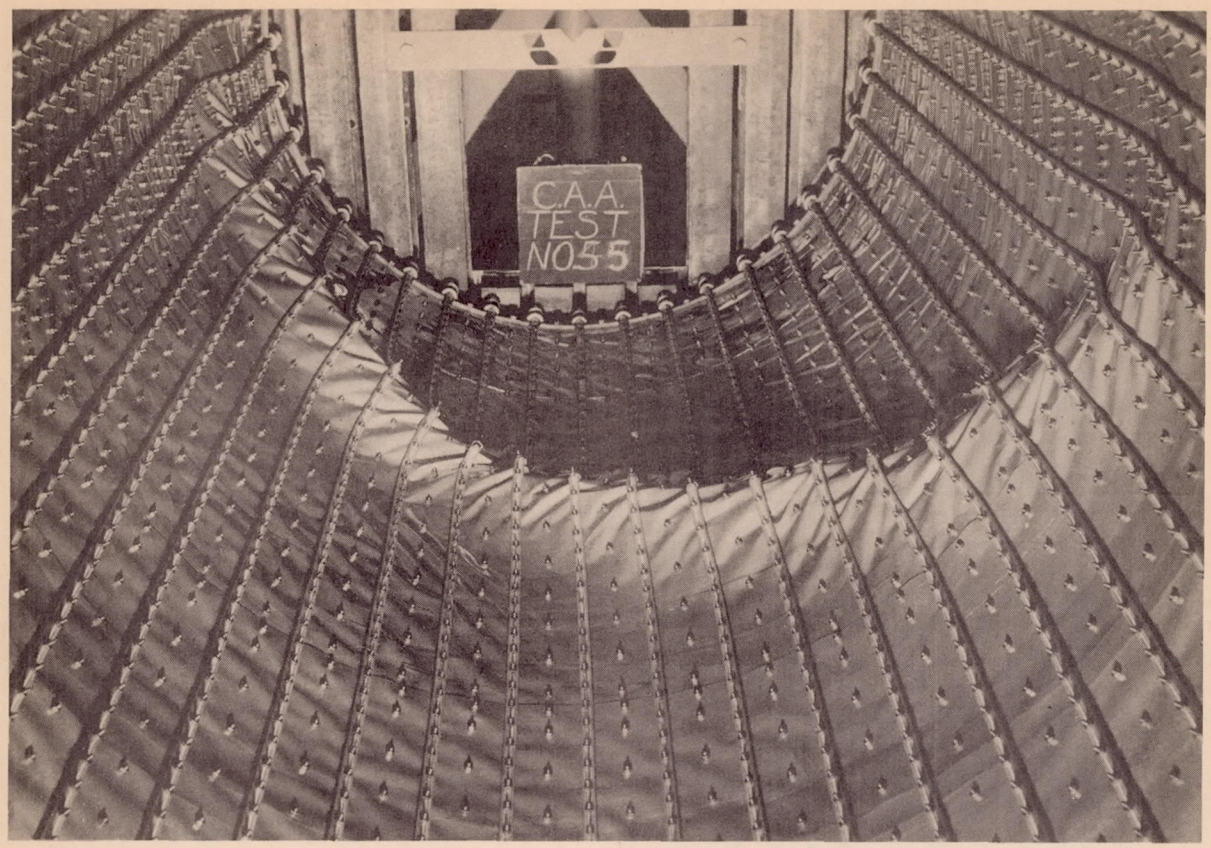

Figure 45. Characteristic wave form of the specimens with channel section frames.

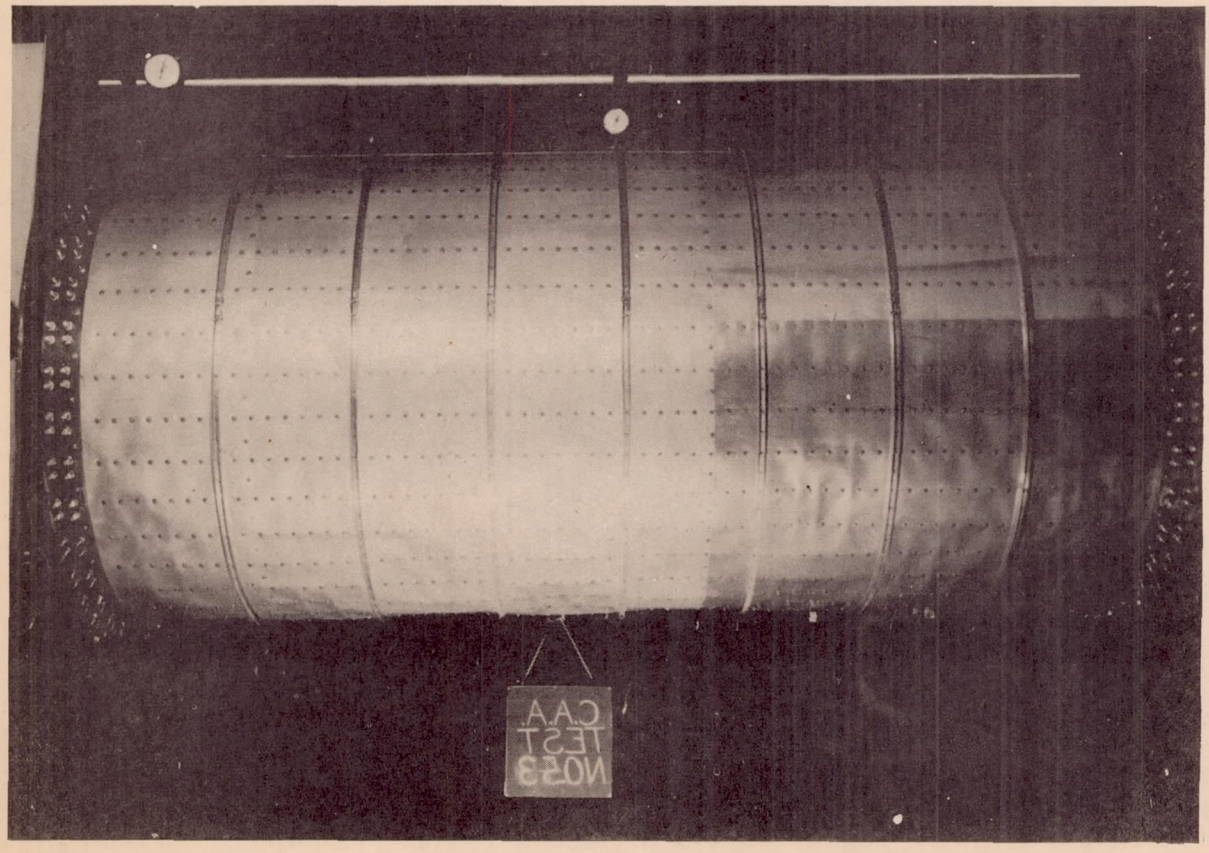

Figure 46. Typical panel instability type failure.

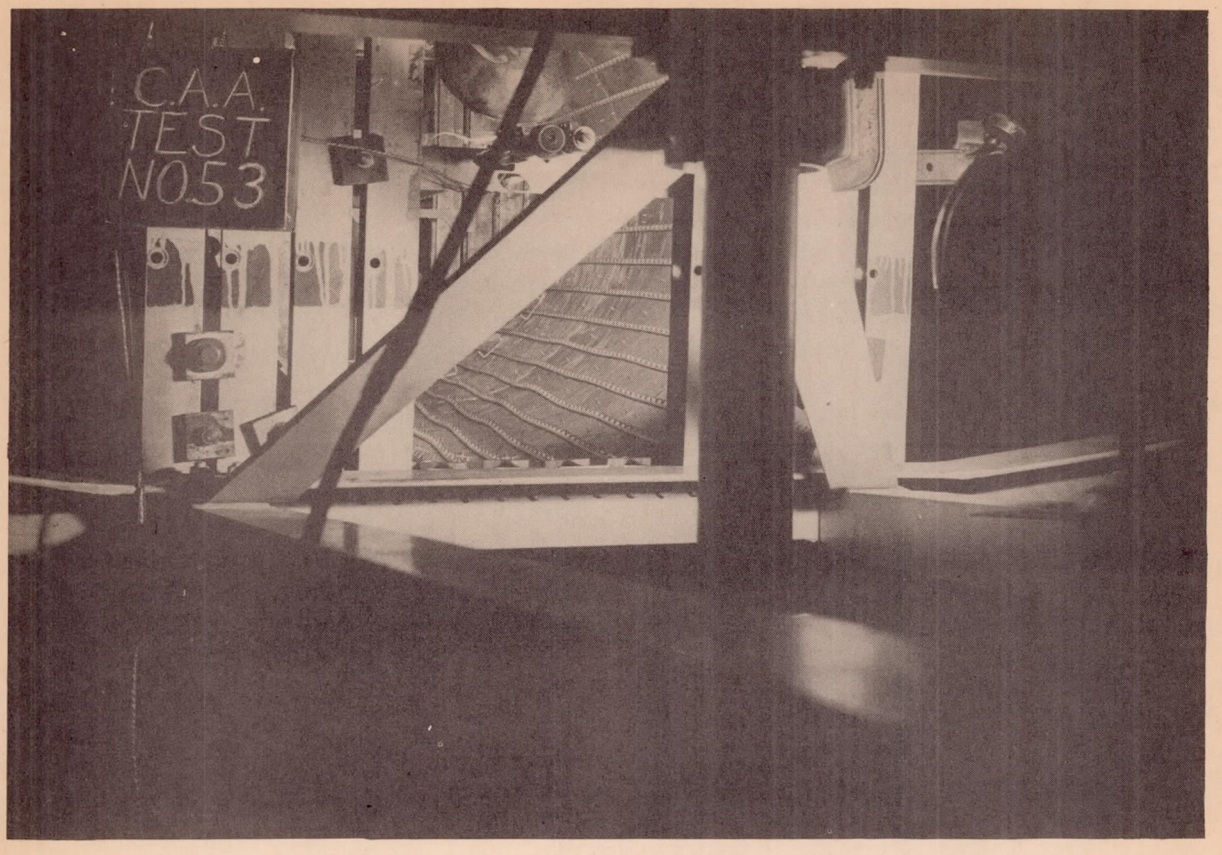

Figure 47. Panel instability.

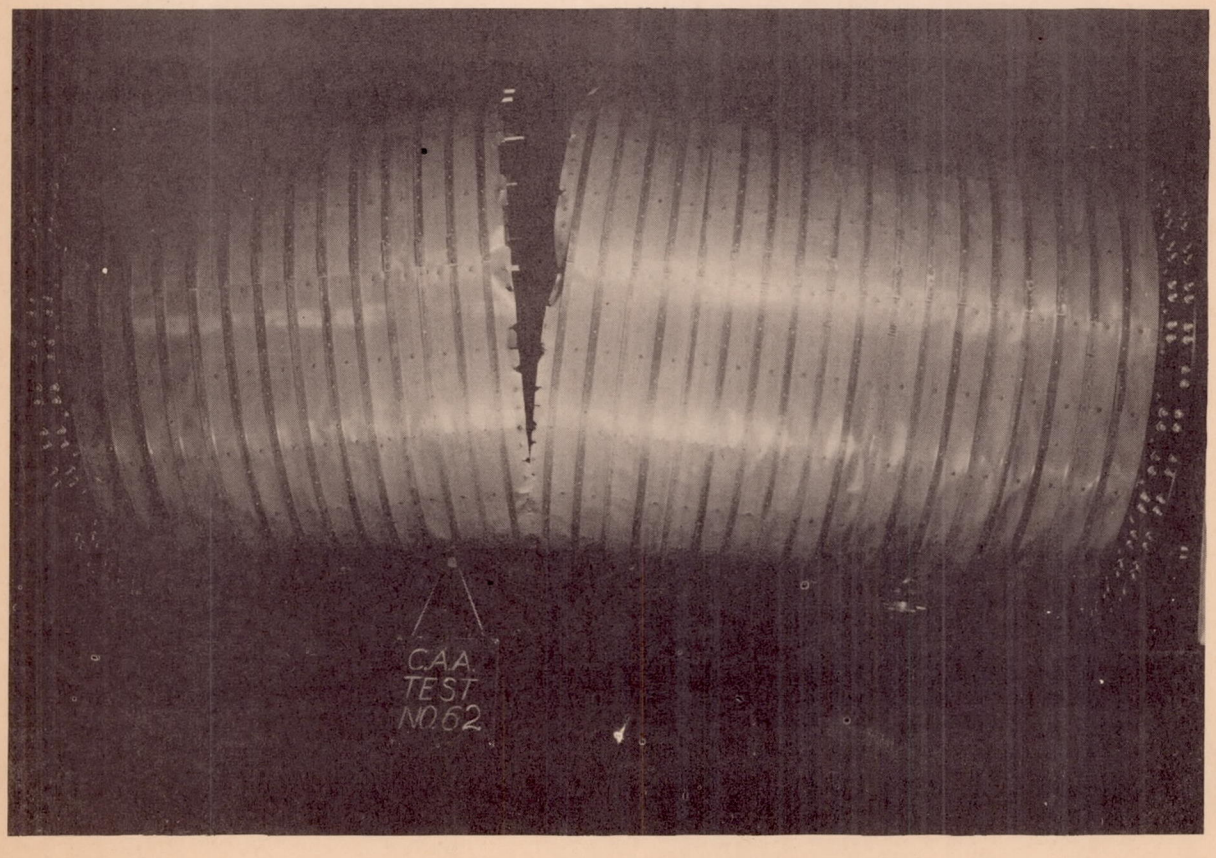

Figure 48. Tension failure.